THE *IN VITRO* AND *IN VIVO* EVALUATIONS OF NEWLY FORMULATED OSTEOPROTEGERIN-CHITOSAN GEL IN BONE REGENERATION

SOHER NAGI MOHAMMED JAYASH

**FACULTY OF DENTISTRY
UNIVERSITY OF MALAYA
KUALA LUMPUR**

2017

THE *IN VITRO* AND *IN VIVO* EVALUATIONS OF NEWLY FORMULATED OSTEOPROTEGERIN-CHITOSAN GEL IN BONE REGENERATION

SOHER NAGI MOHAMMED JAYASH

THESIS SUBMITTED IN FULFILMENT OF THE REQUIREMENTS FOR THE DEGREE OF DOCTOR OF PHILOSOPHY

FACULTY OF DENTISTRY
UNIVERSITY OF MALAYA
KUALA LUMPUR

2017

UNIVERSITY OF MALAYA
ORIGINAL LITERARY WORK DECLARATION

Name of Candidate: Soher Nagi Mohammed Jayash

Matric No: DHA120009

Name of Degree: Doctor of Philosophy

Title of thesis:

The *in vitro* and *in vivo* evaluations of newly formulated osteoprotegerin-chitosan

gel   in bone regeneration

Field of Study: Oral Medicine

 I do solemnly and sincerely declare that:

(1) I am the sole author/writer of this Work;
(2) This Work is original;
(3) Any use of any work in which copyright exists was done by way of fair dealing and for permitted purposes and any excerpt or extract from, or reference to or reproduction of any copyright work has been disclosed expressly and sufficiently and the title of the Work and its authorship have been acknowledged in this Work;
(4) I do not have any actual knowledge nor do I ought reasonably to know that the making of this work constitutes an infringement of any copyright work;
(5) I hereby assign all and every rights in the copyright to this Work to the University of Malaya ("UM"), who henceforth shall be owner of the copyright in this Work and that any reproduction or use in any form or by any means whatsoever is prohibited without the written consent of UM having been first had and obtained;
(6) I am fully aware that if in the course of making this Work I have infringed any copyright whether intentionally or otherwise, I may be subject to legal action or any other action as may be determined by UM.

Candidate's Signature   Date:

Subscribed and solemnly declared before,

Witness's Signature   Date:

Name:

Designation:

ABSTRACT

The receptor activator of nuclear factor kappa-B (RANK)/RANK ligand/osteoprotegerin (OPG) system plays a critical role in bone remodelling by regulating osteoclast formation and activity. OPG has been used systemically in the treatment of bone diseases that has many side effects. Therefore, in searching for more effective and safer treatment for bone diseases, we have investigated newly formulated OPG-chitosan complexes, which is prepared as a local application for its osteogenic potential to remediate bone defects. This study was designed to develop a new OPG-chitosan gel for bone tissue engineering applications and to evaluate the biocompatibility, sustained release ability and biodegradability of gel *in vitro*. The cytotoxicity of OPG in chitosan and its proliferation in vitro was evaluated using normal, human periodontal ligament (NHPL) fibroblast cell culture. The cytotoxicity of these combinations was compared by measuring cell survival with a tetrazolium salt reduction (MTT) assay. The cellular morphological changes were observed under an inverted microscope. A propidium iodide and acridine orange double-staining assay was used to evaluate the morphology and quantify the viable and nonviable cells. The present study also evaluated the effectiveness of new formulated OPG- chitosan gel *in vivo*. In this study, the OPG-chitosan gel was formulated using human OPG protein and three different molecular weights (MW) of water-soluble chitosan i.e. 10, 25 and 50 kDa. The physicochemical properties were determined using the fourier transform infra-Red (FTIR) spectroscopy, thermogravimetric analysis (TGA) and the differential scanning calorimetry (DSC). The formulation gel was subjected to protein release assay and biodegradability test. *In vitro* cytotoxicity test of OPG-chitosan gel was carried out on NHPL fibroblast and NH osteoblast using the Alamar blue (AB) assay. The morphology of fabricated OPG-chitosan gels and attachment of cells on the gel was observed and compared using scanning electron microscope (SEM). The osteogenic

potential of the OPG-chitosan gel was evaluated in 18 female rabbits which involved creating critical-sized defects on the calvarial bone, filled with the OPG-chitosan gel and sacrificed at 6 and 12 weeks. This study showed that the OPG-chitosan gel showed more thermally stable material with biodegradability rate (28 days). Chitosan could withstand temperatures of 200 °C before decomposing. The OPG-chitosan gel water uptake exhibited similarity of the fluid contents percentage with those of living tissues. The gel was able to enhance a favorable condition for cell viability and tissue growth *in vitro*. The AB assay result revealed that the OPG-chitosan gel has no critical cytotoxic effect on fibroblast and osteoblast cells and a clear cell layer covering the entire outermost surface of the gel was observed by scanning electron microscopy at 72 hours of incubation. The *in vivo* results showed bone growth in the OPG-chitosan gel filled defects with the mean values that statistically higher than that of the control defects (unfilled defects) ($p < 0.05$). In a nutshell, the results have suggested the newly developed OPG-chitosan gel has the ability to extend the release pattern, support the growing of cells, specific degradation by lysozyme, and the effectiveness of OPG-chitosan gel in bone healing. It can be concluded that the OPG-chitosan gel has many characteristics beneficial to tissue engineering applications.

ABSTRAK

Pengaktif reseptor faktor nuklear kappa-B (RANK)/ RANK ligan/ sistem osteoprotegerin (OPG) memainkan peranan yang penting dalam pembentukan semula tulang dengan mengawal pembentukan osteoklas dan aktiviti. OPG telah digunakan secara sistemik dalam rawatan penyakit tulang yang mempunyai banyak kesan sampingan. Oleh itu, dalam mencari rawatan yang lebih berkesan dan lebih selamat untuk penyakit-penyakit tulang, kami telah menyiasat baru digubal kompleks OPG-kitosan disformulasikan terbaru, yang disediakan sebagai aplikasi setempat untuk potensi osteogenik untuk mengatasinya kecacatan tulang. Kajian ini bertujuan untuk membangunkan gel osteoprotegerin-kitosan baru untuk aplikasi kejuruteraan tisu tulang dan untuk menilai biokompatibiliti, keupayaan kelegaan berterusan dan biodegradabiliti gel *in vitro*. Kajian ini juga menilai keberkesanan dirumuskan gel OPG-kitosan baru dalam *in vivo*. Dalam kajian ini, gel OPG-kitosan itu digubal menggunakan protein OPG manusia dan tiga berat molekul yang berbeza (MW) larut air kitosan iaitu 10, 25 dan 50 kDa. Sifat-sifat fizikokimia ditentukan menggunakan fourier transform infra-red (FTIR) spektroskopi, analisis Termogravimetri (TGA) dan kalorimeter pengimbasan pembezaan (DSC). Gel ini tertakluk kepada asai pelepasan protein dan ujian biodegradabiliti. Dalam ujian citotoksisiti *in vitro* telah dijalankan ke atas NHPL fibroblast dan NH osteoblast menggunakan cerakin alamar biru (AB). Morfologi gel OPG-chitosan direka dan lampiran sel pada gel diperhatikan dan dibandingkan menggunakan mikroskop elektron pengimbas (SEM). Potensi osteogenik gel OPG-kitosan yang dinilai dalam arnab yang melibatkan mewujudkan kecacatan kritikal bersaiz pada tulang kalvarial, penuh dengan gel OPG-kitosan itu, dan dihorbankan pada 6 dan 12 minggu. Kajian ini menunjukkan bahawa gel kitosan yang OPG- menunjukkan bahan stabil lebih haba dengan kadar biodegradabiliti (28 hari). Ia boleh menahan suhu 200 ° C sebelum mengurai. Pengambilan gel air OPG-kitosan dipamerkan persamaan

kandungan peratusan cecair dengan tisu-tisu hidup. Gel dapat meningkatkan keadaan yang baik untuk daya maju sel dan pertumbuhan tisu dalam *in vitro*. Hasil asai AB mendedahkan bahawa gel OPG-kitosan tidak mempunyai kesan sitotoksik kritikal fibroblas dan sel-sel osteoblas dan lapisan sel yang jelas meliputi permukaan paling luar keseluruhan gel diperhatikan dalam imbasan mikroskop elektron di 72 jam pengeraman. Dalam Hasil kajian *in vivo* menunjukkan pertumbuhan tulang pada kecacatan gel OPG-kitosan yang penuh dengan nilai-nilai purate yang secara statistik lebih tinggi daripada kecacatan kawalan (kecacatan unfiled) (p <0.05). Secara ringkas, keputusan telah mencadangkan gel OPG-kitosan yang baru dibangunkan mempunyai keupayaan untuk memanjangkan corak pelepasan itu, menyokong penanaman sel, kemerosotan tertentu dengan lisozim, degradasi gel OPG-kitosan dalam penyembuhan tulang. Ia boleh membuat kesimpulan bahawa gel OPG-chitosan ini mempunyai banyak ciri-ciri manfaat kepada aplikasi kejuruteraan tisu.

ACKNOWLEDGEMENTS

TABLE OF CONTENTS

LIST OF FIGURES

LIST OF TABLES

LIST OF SYMBOLS AND ABBREVIATIONS

°C	degree Celsius
µL	Microliter
AB	Alamar Blue
AOPI	Acridine orange and propidium iodide staining
ATR	Attenuated total reflectance
BMPs	Bone morphogenic proteins
DcR	Decoy receptor
DMEM	Dulbecco's modified eagle medium
DMSO	Dimethyl sulfoxide
DR	Death receptor
DSC	Differential scanning calorimetry
EWC%	Percentage equilibrium water content
FBS	Fetal bovine serum
FTIR	Fourier transform infrared spectroscopy
GCF	Gingival crevice fluid
H and E	Hematoxylin and Eosin
HMW	High molecular weight
IGF	Insulin-like growth factor
IHC	Immunohistochemistry
IL	Interleukins
kDa	kilodalton
Kg	Kilogram
kGy	kilogray
LMW	Low molecular weight

M_0	Mass of the dry gel at time 0
MMW	Medium molecular weight
M_s	Mass of the gel in equilibrium
MTT	3-(4, 5-dimethylthiazol-2-yl)-2, 5-diphenyltetrazolium bromide
MWs	Molecular weights
NH	Normal human
NHPL	Normal human periodontal ligament
Nm	Nanometer
OC	Osteocalcin
OPG	Osteoprotegerin
OPN	Osteopontin
PBS	phosphate buffered saline
PGE	prostaglandin E
PTH	Parathyroid hormone
RANK	Receptor activator of nuclear factor κB
RANKL	Nuclear factor κB ligand
S%	Percentage of water absorption
SEM	Scanning electron microscope
TGA	Thermogravimetric analyses
TGF	transforming growth factor
TNF	tumour necrosis factor
TRAIL	TNF-related apoptosis inducing ligand
TRAP	tartrate-resistant acid-phosphatase
W_0	Initial weight of the gels
W_{24}	Wet weight of gels after 24 hours
X	Absorbance of treated cell

X_c Absorbance of the control group

LIST OF APPENDICES

CHAPTER 1: INTRODUCTION

Background

The discovery of nuclear factor κB ligand (RANKL)/ RANK/OPG signaling pathway that has a role in the pathogenesis of bone loss by modulating RANK-induced osteoclastogenesis have provided the rationale for the development of drugs to treat bone diseases (Liu & Zhang, 2015).

OPG is a secretory glycoprotein of the tumour necrosis factor (TNF) receptor and plays a key role in the regulation of bone resorption (Theoleyre et al., 2006). OPG has one ligand namely RANKL. RANKL is a Type 2 transmembrane glycoprotein that belongs to the TNF family of cytokines. RANKL is expressed on the surface of osteoblasts, stromal cells, and T cells. The binding of RANKL to RANK stimulates differentiation of monocyte/macrophage progenitor cells into active and matured osteoclasts via numerous signaling pathways (Theoleyre, et al., 2006; Baud'huin et al., 2013). The role of OPG in the pathological aspects of bone diseases, such as osteoporosis associated with estrogen deficiency and periodontal disease, has been well established (Bostanci et al., 2007; Koide et al., 2013; Balli et al., 2015; Hassan et al., 2015). The OPG therapy has been used to reduce bone resorption and to enhance osseous healing (Bekker et al., 2001; Kostenuik et al., 2001; Fili et al., 2009), the therapeutic strategies are based on OPG's potent inhibitory action on osteoclast differentiation and function.

Since the discovery of OPG as an inhibitor of osteoclast activity and maturation, it has opened up a new research exploration using OPG as a potential therapeutic agent for treatment of bone diseases (Hofbauer et al., 2001). To our knowledge, there is no study investigating the use of a drug delivery system using a polymer/polysaccharide matrix, such as chitosan as a transporter, to deliver OPG locally.

Various matrix materials are available in the market for drug delivery such as ceramics, liposomes, and polymers (Mouriño et al., 2013; Gentile et al., 2015; Gentile et al., 2016). Polymers are attractive materials for biomedical applications such as orthopaedic applications, proliferation of various soft tissues, drug delivery systems and conjugated to small drugs and proteins for the treatment of osteoporosis, osteoarthritis, and bone cancer (Mouriño, et al., 2013; Gentile, et al., 2015; Gentile, et al., 2016). Localized delivery of drugs or bioactive factors can be achieved using polymeric hydrogels. Polymer hydrogels can be designed with a wide range of polymers and crosslinking schemes to make materials that have controlled and sustained drug release. Natural polymers (chitosan) is derived from chitin (Ilium, 1998), with ideal properties for biomedical applications such as antimicrobial activity, biocompatible, biodegradable, mucoadhesive material and accentuated affinity to proteins (Coimbra et al., 2011a). The chitosan-based biomaterials are being tested in the treatment of bone defect (Florczyk et al., 2013; Jung et al., 2013). Clinically, chitosan also has dental applications as it can be used to repair socket after dental extraction (Ezoddini-Ardakani et al., 2011b). It has been applied as a biodegradable dental chip containing chlorhexidine or thymoquinone for the management of chronic periodontitis in patients (Jothi et al., 2009; Al-Bayaty et al., 2013). Therefore, in this study, we attempt to formulate a new gel comprising OPG and chitosan for bone tissue regeneration which OPG is released over a prolonged period of time to inhibit bone resorption.

Aim and objectives

The aim of this study was to formulate OPG-chitosan gel and evaluate its biocompatibility and osteogenic potential. The objectives were as following:

- To assess cell proliferation and morphological effects of OPG and chitosan raw materials on normal human periodontal ligament (NHPL) fibroblast cells by using 3-(4, 5-dimethylthiazol-2-yl)-2, 5-diphenyltetrazolium bromide (MTT) and acridine orange and propidium iodide (AOPI) assays.

- To evaluate biocompatibility of OPG-chitosan gels on NHPL fibroblast cells and normal human (NH) osteoblast cells *in vitro* by using AB assay and SEM.

- To formulate the OPG-chitosan gels from different molecular weights of water-soluble chitosan and determine physicochemical properties of gels by using Fourier Transform Infra-Red (FTIR) spectroscopy, Thermogravimetric Analyses (TGA) and Differential Scanning Calorimetry (DSC).

- To evaluate *in vitro* biodegradation and drug release of OPG-chitosan gel.

- To evaluate the efficacy of the OPG-chitosan gel in bone regeneration in rabbit model by means of clinical evaluation, radiographical (XtremeCT) evaluation and Hematoxylin and Eosin stain (H&E) and immunohistochemistry (IHC)

- To evaluate toxicity effects of OPG-chitosan gel by biochemical assays (liver and kidney function tests).

CHAPTER 2: LITERATURE REVIEW

An overview of bone

General structure

Bone is a specialized form of connective tissue that consists of cells and extracellular matrix. The major component of the bone matrix proteins is collagen that constitutes about 90% of the total weight. The most abundant of proteins is type I collagen followed by type V collagen. Trace amounts of other types such as III, XI, and XIII collagen have also been found in the bone matrix (Ross & Pawlina, 2011).

The matrix also contains non-collagenous proteins that form the ground substance of the bone. They are essential to the bone development, growth, remodeling, and repair. The four main groups of non-collagenous proteins found in the bone are proteoglycan macromolecules, multi-adhesive glycoproteins, bone-specific vitamin K-dependent proteins, and growth factors and cytokines (Ross & Pawlina, 2011).

Proteoglycan macromolecules contribute to the compressive strength of bone and are also responsible for binding growth factors and may inhibit mineralization. Multiadhesive glycoproteins which include osteonectin, sialoproteins such as Osteopontin, and Sialoprotein I and II, are responsible for attachment of the cells and collagen fibers to the mineralized ground substance (Egerbacher et al., 2006; Ross & Pawlina, 2011).

Bone-specific vitamin K-dependent proteins include osteocalcin which captures calcium from the circulation and stimulates osteoclast in the bone remodeling, protein S which aid to remove the apoptotic cells and matrix Gla-protein which assists in the development of vascular calcifications (Ross & Pawlina, 2011).

Growth factors and cytokines include insulin-like growth factors, tumor necrosis factor-α, transforming growth factor β, platelet-derived growth factors, bone morphogenic proteins (BMPs) and interleukins (IL1, IL6). BMPs induce the differentiation of mesenchymal cells into the osteoblast (Ross & Pawlina, 2011). The inorganic components of the bone are the crystal of calcium hydroxyapatite, which composed mostly of calcium and phosphorus(Gartner & Hiatt, 2012).

The bone is classified according to its density i.e. either compact or spongy. The bone can also be classified according to shape; the location of spongy and compact bone varies with the shape of the bone of long bones, short bones, flat bones, irregular bones (Hage & Hamade, 2015). Mature bone is composed of structural units called osteons (Haversian systems) which consist of concentric lamellae of the bone matrix surrounding a central canal called Haversian canal. Between the osteons are the remnants of previous concentric lamella called interstitial lamellae. Immature bone differs from the mature bone in several aspects such as immature bone is nonlamellar also known as a bundle or woven bone, contain more cells per unit which are randomly arranged and more ground substance in immature bone. (Ross & Pawlina, 2011).

Cells of bone tissues

There are five cell types associated with the bone tissue: osteoprogenitor cells, osteoblasts, osteocytes, osteoclast and bone lining cells. Each of these cells is regarded as a different form of the basic cell type except the osteoclast which originates from a different cell line.

Osteoprogenitor cells are derived from the mesenchymal stem cells in the bone marrow that have the potential for differentiation into different cell types including fibroblast, osteoblast, adipocytes, chondrocytes and muscle cells (Galli et al., 2014). These cells are found in the internal and external layer of the bones and also reside in the

microvasculature supplying bone. They comprise of endosteal cells that line the marrow cavities, Haversian canals and Volkmann's canals and the periosteal cells that form the innermost layer of the periosteum. The morphology of these cells is consistent but its stimulation leads to differentiation into more active cells, the osteoblasts (Humber, 2010; Ross & Pawlina, 2011).

Osteoblast cell is a secretory cell that retains the ability to divide. It secretes type I collagen and bone matrix proteins that form the initial non mineralized bone or osteoid. Osteoblast secreted osteoclast stimulating factor and bone matrix proteins such as osteocalcin and osteonectin, bone sialoproteins I and II, osteopontin, thrombospondin, alkaline phosphatase and various proteoglycans (Florencio-Silva et al., 2015). The cells are a cuboidal or polygonal shape in the light microscope and their aggregation into a single layer in apposition to the forming bone. The inactive osteoblast that differs from the secretory osteoblast found in an active matrix deposition is flat and attenuated cells that cover the bone surface. The osteoblast is surrounded by osteoid matrix and then become an osteocyte (Ross & Pawlina, 2011). Osteoblasts have expressed the receptor for activation of RANKL on their surface. When this ligand contacts with preosteoclast's surfaces RANK-induced preosteoclast to differentiate into the osteoclast (Gartner & Hiatt, 2012).

The osteocyte is the mature cell that is responsible for maintaining the bone matrix. They can synthesise new matrix, also participate in matrix degradation and help to maintain calcium homeostasis. Each cell occupied the space called lacuna and from the cell, cytoplasmic processes extended through the canaliculi in the matrix to contact process of the neighboring osteocyte and bone-lining cells (Mescher, 2013). Formative osteocyte deposits new matrix that exhibits certain characteristic similar to those of osteoblasts. Also, the osteocyte has a resorptive function but isn't precisely defined. The

observed changes can be explained by enzymatic degradation of collagen by osteocyte-secreted matrix metalloproteinases (Thompson et al., 2015).

Bone lining cells are derived from the osteoblasts and cover bone that is not remodeling. They are thought to function in the maintenance and nutritional support of the osteocytes and regulate the movement of calcium and phosphate into and out of the bone (Ross & Pawlina, 2011).

Osteoclasts are large, multinucleated cells that are responsible for the bone resorption. They are derived from the fusion of mononuclear hemopoietic progenitor under influence of multiple cytokines. Osteoclast precursors expressed initially two important transcription factors, c-*f*os and later RANK on their surface. The RANK receptors interact with RANKL produced and expressed on the stromal cell surface. The RANK- RANKL mechanism is essential for the osteoclast differentiation and maturation (Soysa et al., 2012). Lysosomal enzymes such as tartrate-resistant acid phosphatase and cathepsin K are actively synthesized by the osteoclast and are secreted into the bone-resorbing compartment. Its function is regulated both by locally acting cytokines and by systemic hormones. Calcitonin, androgens, insulin, thyroid hormone, insulin-like growth factors-1, IL1, Macrophage colony-stimulating factor (CSF)-1, and platelet-derived growth factor are osteoclastic receptors (Hadjidakis & Androulakis, 2006).

Bone remodeling

Frost (1990) defined bone remodeling as a process results from the action of osteoblasts and osteoclasts whereby old bone is continuously replaced by new tissue as a result of balanced bone resorption and formation. Remodeling process results from the action of the tissue-forming osteoblasts and the tissue-resorbing osteoclasts which work together in certain cell units called basic multicellular units.

The remodeling cycle consists of three consecutive phases: resorption, reversal, and formation. Resorption begins with the migration of mononuclear preosteoclasts to the bone surface, where they form multinucleated osteoclasts. After the completion of osteoclastic resorption, there is a reversal phase when mononuclear cells appear on the bone surface. These cells provide signals for osteoblast differentiation and migration that initiate bone formation. The formation phase performed with osteoblasts laying down bone until the resorbed bone is completely replaced by new bone. At the end of this phase, the surface is covered with flattened lining cells and a prolonged resting period begins until a new remodeling cycle is initiated (Frost, 1990).

There is both systemic and local regulation of bone cell function. The systemic regulation includes parathyroid hormone, vitamin D, calcitonin, growth hormone, glucocorticoids, thyroid hormones, estrogens, and androgens. Parathyroid hormone (PTH) is an important player in bone mass homeostasis. Intermittent injections of PTH in rats have been shown to increase bone mass through increased synthesis of local growth factors such as insulin-like growth factor I which stimulate bone cell proliferation and matrix synthesis. There were synergistic effects of combined PTH and mechanical stimulation of the trabecular bone formation rate so that it was suggested for treatment of osteoporosis (Kim et al., 2003). Also, elevation of PTH in response to calcium stress increased circulating 1, 25 (OH) 2D3, which acted on the immature osteoblasts to stimulate osteoclastogenesis through the RANKL/OPG regulatory system (Suda et al., 1999).

These different pathways may be central to the site-specific regulation of bone remodeling. Vitamin D-mediated osteoclastogenesis is regulated locally by OPG production in mature osteoblasts (Baldock et al., 2006).

Calcitonin suppresses osteoclast secretory activity particularly of tartrate-resistant acid phosphatase (TRAP). It also inhibits both basal and stimulated resorption of organ cultured intact bone directly causes a loss of the ruffled border of osteoclasts and reduces osteoclast number over time (Carter & Schipani, 2006).

The growth hormone and insulin-like growth factor signaling pathways are important regulators of muscle and bone cell survival and function. The decline in circulating growth hormone and insulin-like growth factor 1 levels that is associated with aging may contribute to reduction in trabecular bone mass and muscle strength (Perrini et al., 2010).

Glucocorticoids induce bone resorption and stimulated RANKL and macrophage colony-stimulating factor expression and prolonged osteoclast lifespan. The suppression of the resorptive phase of remodeling contributes to the retarded bone formation central to glucocorticoids -induced osteoporosis (Kim et al., 2006).

Excess thyroid hormones would decrease the amount of mineralized tissue as well as the degree of bone mineralization. This suggested an accelerated bone turnover that is confirmed by an increase in serum concentrations of bone formation and bone resorption markers in hyperthyroidism (Monfoulet et al., 2011).

Estrogen has an osteoprotective function by regulating the life span of mature osteoclasts via the induction of the Fas/FasL system (Nakamura et al., 2007). Estrogen also stimulates proliferation of osteoblastic cells via estrogen receptor α (Galea et al., 2013). Estrogen also affects gene coding for enzymes, bone matrix proteins, hormone receptors, transcription factors, and up-regulates the local production of OPG, insulin-like growth factor (IGF) I, IGF II and transforming growth factor (TGF) β (Hadjidakis & Androulakis, 2006).

Androgen has been shown to affect bone cells e.g. stimulating osteoblast proliferation and also stimulating osteoblast and osteocyte apoptosis through an increased in Bax/Bcl-2 ratio even in anabolic settings. Androgens thus play a distinct role in skeletal homeostasis (Wiren et al., 2006).

The local regulation of the bone cell function includes the OPG/RANKL/RANK system. These molecules are the key factors in linking bone formation to resorption during bone remodeling process. The expression of bone formation markers is activated in the bone formation phase, followed by the stimulation of RANKL/OPG expression in the bone resorption phase (Tanaka et al., 2011).

Bone regeneration

Non-critical bone defect can repair spontaneously without intervention. However, the critical bone defect will require reconstructive surgery and bone transplantation. Autogenous bone graft would be the best and safest strategy for bone repair. Autogenous bone graft is acquired from the patient's own body e.g. mandibular symphyseal region and iliac crest bone (Park et al., 2004). The disadvantages of the autogenous graft are operative time for graft harvest, donor site morbidity, graft resorption, molding challenges. Due to these disadvantages, numerous alternatives to autogenous bone graft are available to address these limitations (Rogers & Greene, 2012).

Allograft bone is graft transplanted from one individual to another individual of a different genetic background. It may be used to repair large bone defects, but this bone graft also exhibits several limitations, which include the possibility of disease transmission, graft rejection, problems with graft integration and viability at the recipient site (Catanzariti & Karlock, 1996).

Recently, the interest for alloplastic bone substitute materials has increased as an alternative to autogenous bone graft and xenogenic materials, especially in oral surgery. The use of chitosan in bone regeneration is controversial. Spin-Neto and co-workers study (2010; 2012) revealed that there was no significant bone formation following chitosan and chitosan hydrochloride gel application in critical size bone defects and defects repaired by connective tissue, with variable degrees of inflammation. On the other hand, another study report that chitosan has a high degree of biocompatibility and osteoconductivity (Bojar et al., 2014).

Other approaches based on gene therapy that have revealed high promise in experimental studies. Before these approaches become a clinical reality, significant efficacy and safety concerns will require being overcome (Lienemann et al., 2012).

Growth factor delivery for effective bone tissue engineering is considered as progenitor cell proliferation and differentiation which is induced by the pro-osteogenic growth factors e.g. IGF, and members of the BMP family. BMP-2 to BMP-9 is the most potent growth factors known to induce ectopic bone formation. A major limitation to growth factor therapy is that significant quantities of growth factors, more than physiological levels, are needed to induce the formation of bone. For example, 3.5 mg of recombinant BMP-7 is used for the treatment of a bone defect, which corresponds to 2-fold of the entire amount of BMP-7 found in a human being. This is may lead to very high treatment costs and a significant risk for adverse side effects such as an ectopic bone formation or osteolysis (Lienemann, et al., 2012).

Osteoprotegerin (OPG)

OPG has been identified by Simonet and co-workers (1997) as a secretory glycoprotein form of the superfamily of TNF receptors. It inhibits osteoclast maturation

and protects the bone from both normal osteoclast remodeling and ovariectomy-associated bone loss.

The name osteoprotegerin derived from Latin OS for bone and protegere for to protect (Holen & Shipman, 2006). It is also named OCIF (osteoclastogenesis inhibitory factor), TR-1 (TNF receptor-related molecule-1), TNF receptor superfamily member and FDCR-1 (follicular dendritic cell receptor-1).

OPG mRNA is expressed in bone, skin, liver, lung, stomach, placenta, brain and the range of other tissues. The site of its expression does not necessarily predict the site(s) at which it exerts its biological function as OPG is a secreted protein (Simonet, et al., 1997).

OPG has no transmembrane and cytoplasmic domain as the most of the TNF superfamily receptors and is secreted as a soluble protein. OPG is synthesized by osteoblast as a propeptide from which the signal peptide (with 21 amino acids) separates, generating a 380-amino acid matures peptide. It has two terminals, N and C-terminus and has seven major domains (domains 1–7). At the N-terminus of OPG is death domains (D1–D4) which are cysteine-rich structures with a characteristic of the extracellular domains of the TNFR family proteins, these domains are essential for biological activity. At the C-terminus, it has two death domains (D5-D6) that share structure feature with the death domains of the TNF receptor p55, Fas, and TNF-related apoptosis-inducing ligand (TRAIL) receptor, all of which mediate apoptosis signals. Also in the C- terminus, it has domain 7 which contains the heparin binding site. Binding to heparin or heparin-like molecules is important for such growth factors as basic fibroblast growth factor to function. Despite it did not correlate with the biological activity but changes in heparin-binding with some proteins affect stability, rate of clearance, and target cell specificity. Domain 7 is also responsible for the dimerization

of OPG by a disulfide bond and the dimer TNF protein is a more potent inhibitor (Simonet, et al., 1997; Yamaguchi et al., 1998; Yasuda et al., 1998; Holen & Shipman, 2006).

OPG exists as monomeric and homodimeric forms, and these two forms have either similar potency for inhibiting osteoclastogenesis in vitro as reported in Tomoyasu and co-workers study (1998) or the dimeric form of OPG is a more potent RANKL inhibitor than the monomeric form as OPG homodimer has greater affinity for RANKL than the monomeric form, this reported in Schneeweis and co-workers study (2005).

OPG production is stimulated by 1α, 25-dihydroxyvitamin D3, estrogens, pro-inflammatory cytokines such as IL-1 and TNF-α as well as TGF-β whereas parathyroid hormone and glucocorticoids suppress OPG production (Thirunavukkarasu et al., 2001; Bronner et al., 2005).

Biological functions of osteoprotegerin

OPG has almost one ligand, RANKL. RANKL is a type 2 transmembrane glycoprotein that belongs to the TNF family of cytokines. It expressed on the surface of osteoblasts, stromal cells and T cells (Yasuda, et al., 1998). This ligand is encoded as a monomer structural and is functionally active as a homotrimer. A trimeric RANKL can be expressed in two forms: as a membrane-anchored form and as a soluble form released from the plasma membrane through enzymatic cleavage by membrane metalloprotease–disintegrin TNF-alpha convertase or a related metalloprotease. These two forms can function as potential ligands which can interact with RANK and/or OPG receptors with the same biological activity (Lum et al., 1999).

The stimulation of RANKL production is by the same factors that stimulate bone resorption, i.e. PTH, parathyroid hormone-related protein, vitamin D3, interleukin-1

(IL-1), IL-11, IL-17, TNF-alpha, prostaglandin E (PGE) 2 and CD40L (Drugarin et al., 2003).

In bone, RANKL specifically binds the RANK receptors which are a type I transmembrane protein of the TNF receptor superfamily (Anderson et al., 1997). RANK receptor expressed on the surface of hematopoietic osteoclast progenitors, mature osteoclasts, chondrocytes, mammary gland epithelial cells, trophoblast cells, dendritic cells, mature T cells, and hematopoietic precursors (Hsu et al., 1999; Fata et al., 2000; Neumann et al., 2005).

RANKL is a heterotrimer containing 3 molecular intracellular domains (I, II, and III) and interact with three monomers of RANK, linked by disulfide bonds. The RANK/RANKL binding stimulate the differentiation the monocyte/macrophage progenitor cells to osteoclasts through the activation of numerous signaling pathways involved in the osteoclast differentiation, activation , and survival (Theoleyre, et al., 2006; Baud'huin, et al., 2013). It has been reported that mice with a disrupted RANKL gene showed complete lack osteoclasts that caused severe osteopoterosis and a defect in tooth eruption as a result of an inability of osteoblasts to support osteoclastogenesis (Kong et al., 1999b).

As the binding of RANKL to RANK on pre-osteoclasts and osteoclasts is essential for their maturity and activity, OPG that is a soluble decoy receptor for RANKL prevents binding of RANKL to RANK and subsequent activation of osteoclast and inhibit osteoclastogensis and bone resorption.

Moreover, OPG seems also to play a key role in cell survival, via its interaction with TRAIL. TRAIL was identified by Wiley and co-workers (1995) as a type 2 membrane protein of the TNF superfamily, produced by most of human tissues. There are five

TRAIL receptors, two death receptors (DR4 and DR5) which stimulate and support apoptosis, and the other three decoy receptors, DcR1, DcR2 , and OPG, are decoy receptors unable to induce apoptosis and thus binding block TRAIL-induced apoptosis of Jurkat cells (Emery et al., 1998). The binding of the OPG to the TRAIL and RANKL has similar affinities. As a result of the TRAIL/OPG interaction, TRAIL-induced apoptosis in several types of cells and numerous cancer cells is inhibited (Neville-Webbe et al., 2004). This could explain the reason of the phenomena of the stimulation of OPG production by tumor cells (Reid et al., 2009). Pritzker and co-workers (2004) reported that OPG acts as a survival factor for human microvascular endothelial cell survival due to its ability to bind and block TRAIL-induced apoptosis.

Role of osteoprotegerin in the pathogenesis of bone diseases

Various studies suggest that different bone diseases are related to alterations in OPG/RANKL/RANK system. Here we summarize several bone diseases associated with OPG/RANKL/RANK abnormalities that are estrogen secretion deficiency associated with osteoporosis, drug-induced osteoporosis, hyperparathyroidism, Paget's disease, chronic inflammatory diseases, autoimmune diseases, osteopetrosis, bone tumors and metastases and Cushing syndrome and periodontal disease.

Osteoporosis

Osteoporosis associated with estrogen deficiency and drug-induced osteoporosis are conditions related to abnormalities in OPG/RANKL/RANK system. Estrogens and androgens have direct effects on osteoclasts and these hormones inhibit *in vitro* bone resorption as well as inhibit the production of the pro-resorptive cytokine and IL-6 (Bellido et al., 1995; Pederson et al., 1999). The estrogen has an important role in the bone anti resorbing activity by stimulating OPG expression in osteoblasts. Estrogens induce the *in vitro* expression of OPG gene and stimulate OPG production from

osteoblasts and thus inhibit RANKL production (Hofbauer et al., 1999). The decrease of estrogen secretion associated with decreasing the ovarian function leads to the decrease of the OPG production in the source cells. The estrogen has an important role in the bone anti resorbing activity by stimulating OPG expression in osteoblasts (Bord et al., 2003).

Glucocorticoid-induced osteoporosis is the most frequent secondary form of osteoporosis. Glucocorticoids downregulate OPG expression and increase the RANKL expression (Wang et al., 2011). Following glucocorticoid exposure, an increase in the osteoblastic RANKL/OPG ratio is associated with enhanced osteoclastogenesis (von Tirpitz et al., 2003).

Immunosuppressants such as cyclosporine A, rapamycin, and tacrolimus (Hofbauer, et al., 2001; Stein et al., 2007) have also been implicated in the pathogenesis of post-transplant osteoporosis. These drugs have been found to significantly decrease OPG mRNA levels and protein secretion by osteoblast precursor cells in a dose-dependent manner. It also stimulates RANKL mRNA levels in marrow stromal cells, thus substantially increasing the RANKL/OPG ratio and induce osteoclastogenesis (Hofbauer, et al., 2001). OPG serum levels were positively correlated with serum levels of osteocalcin, parathyroid hormone, and creatinine. After renal transplantation, patients who received cyclosporine and glucocorticoids after 2 weeks have shown significant reduction in serum levels of OPG compared to baseline levels while creatinine clearance also increased (Sato et al., 2001; Hofbauer et al., 2004).

Hyperparathyroidism (PTH)

Parathyroid hormone stimulates RANKL expression and inhibits OPG remain production by osteoblasts, and thus promotes osteoclastogenesis (Tsukii et al., 1998).

The effects of PTH on the production of OPG remain controversial. Most *in vitro* studies indicated that PTH decreases OPG secretion by the osteoblasts (Lee & Lorenzo, 1999; Onyia et al., 2000). The results of *in vivo* studies were conflicting. Rats treated with PTH have been reported to suffer reduction in OPG mRNA levels in rat femur metaphyseal and diaphyseal bone (Onyia, et al., 2000). However, another study reported hyperparathyroidism is accompanied by a high serum concentration of OPG and RANKL as well as a low OPG/RANKL ratio. Both treatments with alendronate or parathyroidectomy reduce bone resorption and increase the OPG / RANKL ratio. Both parathyroidectomy and treatment with alendronate reduce bone resorption, and increase OPG/RANKL ratio (Szymczak & Bohdanowicz-Pawlak, 2013). In a clinical trial, it was reported that no changes in serum OPG was found in patients with hyperparathyroidism when compared pre- and postoperatively (Stilgren et al., 2003).

The fact that PTH has different effects on RANKL and OPG at different stages of osteoblast development leads to a new paradigm of osteoclast regulation. The osteoclastogenic activity of PTH occurs primarily by suppression of OPG gene expression in early osteoblasts and elevation of RANKL gene expression in mature osteoblasts (Huang et al., 2004).

The genetic polymorphisms of the OPG gene (TNFRSF11B) and RANK gene (TNFRSF11A) have been associated with Paget's disease of bone. They contribute to an increase risk for developing the Paget's disease which is characterized by increased bone resorption by osteoclasts and uncontrolled bone remodeling (Chung & Van Hul, 2012).

Juvenile Paget's disease is a rare, autosomal recessive bone disease characterized by a greatly accelerated bone turnover that presents in infancy or childhood. Juvenile

Paget's disease can result from OPG deficiency caused by homozygous deletion the gene that encodes OPG (Whyte et al., 2002; Cundy et al., 2005).

Chronic inflammatory diseases

The T cells seem to be the link between inflammation and bone loss. RANKL expression occurs at the surface of activated, but not quiescent, murine T cells. RANKL derived from T cell has as a signal involved in optimal T cell activation. Also, T cell derived RANKL can regulate the osteoclast development and activation resulting in bone resorption so it plays an important role in the bone remodeling (Kong et al., 1999a).

RANKL expression is upregulated by many soluble factors affecting bone resorption, including the proinflammatory cytokines, interleukin-1, and TNF-α. T cells express a cell-surface membrane-bound RANKL that is cleaved by metalloproteinases into a soluble form. There may be some functional differences between membrane-bound and soluble RANKL, with cell-bound OPGL being more effective mediators of osteoclastogenesis when measured by *in vitro* assays (Kong, et al., 1999a; Sakata et al., 1999). Proinflammatory cytokines such as IL1 and IL6 and TNF- α can increase the production of the RANKL and decrease the OPG production. These mediators and change of OPG production are associated with the chronic local inflammation and viral infections (Nakashima & Penninger, 2003; Tunyogi-Csapo et al., 2008). OPG functions as a decoy receptor for RANKL, competing with RANK for binding with RANKL, effectively inhibiting osteoclastogenesis both in vitro and in vivo. Thus evaluation of RANKL levels must go hand in hand with OPG levels, as the balance of the two will determine whether osteoclastic or osteoblastic activity dominates (Simonet, et al., 1997; Kong, et al., 1999a; Yeung, 2004).

Autoimmune diseases

The RANKL/RANK/OPG system plays as an important link between the immune system and bone metabolism. The function of the OPG/RANKL system is similar to that of the interleukin–cytokine system (Kohli & Kohli, 2011).

Rheumatoid arthritis is a chronic disease which is characterized by progressive synovial inflammation and joint destruction. The RANK/RANKL/OPG system plays a significant part in the pathogenesis of local and generalized bone loss in rheumatoid arthritis (Vega et al., 2007). The osteoblastic stromal cells, synovial fibroblasts and activated T-cells express the RANKL result in an increase in RANKL/OPG ratio, leading to enhanced osteoclastogensis in erosive arthritis (Lubberts et al., 2003; Fili, et al., 2009). Otherwise, some studies have shown that serum levels of OPG and RANKL in patients with rheumatoid arthritis are higher than that in healthy people. These can be explained by anti-TNF therapy, where by regulates the OPG/RANKL balance by stimulating the bone erosion in arthritis (Oyajobi, 2007; Fili, et al., 2009).

Osteopetrosis

Osteopetrosis is a rare inherited disorder of generalized whereby bone mass increase as a result of decreasing the osteoclastogenesis and bone resorption (Felix et al., 1996). RANKL, OPG, and their signaling pathway may play a potential role in the pathogenesis of osteopetrosis. It has been reported that transgenic overexpression of OPG has resulted in osteopetrosis in mice (Simonet, et al., 1997). OPG may regulate bone metabolism via overexpression of OPG in the bone, thus results in a dramatic increase in bone density and inhibition of osteoclast maturation. Secondly, OPG specifically inhibits osteoclastogenesis *in vitro*. Thirdly, systemic delivery of OPG produces an increase in bone density in the tibial metaphysis and blocks the loss of bone induced by ovariectomy. Fourthly, in situ hybridization data indicates the mouse gene is

expressed at high levels in the cartilaginous primordia of bones throughout the fetus. Lastly, the human gene is localized in chromosome in region closely linked to the gene involve in the skeletal disorder resulting in bone deformation (Simonet, et al., 1997).

Bone tumors and bone metastases

In bone metastases, the RANK / RANKL pathway is essential in the pathology of bone destruction. Bone tumor cells can activate the osteoclasts by causing increased RANKL levels and/or decreasing OPG levels locally, resulting in excessive osteoclast activity (Mundy, 2002; Canon et al., 2012). In severe osteolysis, RANKL/OPG ratio is increased and involved in the development of benign and malignant bone tumors and the progress of osteolytic lesions by tumor metastases (Grimaud et al., 2003; Milone et al., 2013).

RANKL expression is increased in bone metastases associated with different types of solid tumors including breast cancer while the expression of OPG is inhibited because of the tumor cells present in the bone marrow secrete factors such as IL-1, IL-11, and PGE2 (Clezardin & Teti, 2007; Clézardin, 2011).

Treatment with OPG-Fc successfully inhibits tumor-induced bone destruction by complete inhibition of osteoclastogenesis. Subsequently, the inhibition of bone resorption results in reduction of released growth factors and calcium from the bone matrix and increased in tumor cell apoptosis (Canon et al., 2008; Canon, et al., 2012).

Cushing syndrome

Cushing syndrome is defined as signs and symptoms associated with prolonged exposure to improper high levels of cortisol hormone. This condition results from diseases is associated with excess cortisol and adrenocorticotropic hormone levels, and glucocorticoid drugs intake (Abbas et al., 2005).

Serum OPG levels also positively correlated with morning serum cortisol. In patients with Cushing syndrome, serum OPG levels has been shown higher than healthy control subjects, but it remained unchanged after the recovery, even when the bone is restored. The elevation of OPG level could be due to persistent damage to the cardiovascular system by glucocorticoid (Ueland et al., 2001; Hofbauer, et al., 2004).

Chronic periodontitis

In healthy periodontium, Sakata and co-workers (1999) have demonstrated that OPG is expressed by cultured human gingival fibroblasts, periodontal ligament cells, and dental pulp cells, but not by epithelial cells. OPG production is continuous by resident periodontal fibroblasts and potentially endothelial cells (Kobayashi-Sakamoto et al., 2004).

Lymphocytes, macrophages, and neutrophils infiltrate the gingival connective tissue in periodontitis and interact with osteoblasts, periodontal ligament fibroblasts, and gingival fibroblasts. Macrophages and T lymphocytes release inflammatory mediators, for example, IL-1, IL-6, TNF-α, and prostaglandin E2, which stimulate osteoblasts to produce RANKL and induce bone resorption indirectly and also T lymphocytes can also promote alveolar bone resorption by direct production of RANKL (Taubman & Kawai, 2001).

RANKL expression is increased with T, B-lymphocytes and macrophage infiltration, respectively in chronic periapical lesions. RANKL seems to be closely related to periapical inflammatory cells (Fan et al., 2011).

Gingival fibroblasts stimulated with lipopolysaccharide produce OPG and inhibit the ability of RANKL to stimulate monocyte differentiation into osteoclasts and thus inhibit osteoclastogenesis (Nagasawa et al., 2002). Also, lipopolysaccharide induces RANKL

expression in osteoblasts (Zou et al., 2003). The RANKL expression on the periodontal ligament was upregulated *Actinobacillus actinomycetemcomitans lipopolysaccharide* (Tiranathanagul et al., 2004). The osteoclastogenesis induced by *Porphyromonas gingivalis*, *Treponema denticola*, and *Treponema socranskii* mediated by enhancing RANKL expression and depression of OPG by PGE2 (Choi et al., 2005).

Enterococcus faecalis lipoteichoic acid could upregulate the expression of RANKL and OPG at different rates, suggesting a potential role of lipoteichoic acid in the bone resorption process of refractory apical periodontitis through the regulation of RANKL and OPG (Zhao et al., 2013).

The various forms of periodontitis are differentially regulated by the expression of RANKL and OPG and the relative RANKL/OPG ratio acts as indicative of disease occurrence (Bostanci et al., 2007).

Crotti and co-workers (2003) compared the RANKL and OPG expression in the granulomatous tissue adjacent to areas of alveolar bone loss from periodontitis patients to the tissue without periodontitis using immunohistochemistry. Their results revealed that significantly higher levels of RANKL protein in the periodontitis tissue were expressed compared with OPG protein in the healthy tissue.

Mogi et al. (2004) studied the alteration of RANKL and OPG levels in gingival crevice fluid (GCF) of patients with periodontitis. They found that an increased concentration of RANKL and a decreased concentration of OPG in GCF from periodontitis patients. They suggested that RANKL and OPG contribute to osteoclastic bone destruction in periodontal disease.

In the same line Bostanci et al. (2007) compared the levels of OPG, RANKL, and their relative ratio in GCF of healthy and periodontal disease subjects. They found that

the OPG concentrations in GCF were significantly decreased in all periodontal disease patients compared to healthy subjects. Also, they found OPG level in GCF was negatively correlated with all clinical parameters (probing pocket depth, clinical attachment level, papillary bleeding index and plaque index) but RANKL was positively correlated.

Koide and co-workers (2013) examined alveolar bone loss in OPG-deficient mice and RANKL-overexpressing transgenic mice. Alveolar bone loss in OPG deficient mice at 12 weeks was significantly higher than that in RANKL- overexpressing transgenic mice. OPG deficient mice but not RANKL- overexpressing transgenic mice exhibited severe bone resorption especially in cortical areas of the alveolar bone. An increased number of osteoclasts was observed in the cortical areas in OPG deficient mice but not in RANKL- overexpressing transgenic mice. They suggested the resorption in cortical bone areas to be prevented by OPG produced locally.

Periapical disease

OPG and RANKL have been identified in odontoblasts, ameloblasts, pulp cell lines, and periodontal ligament cells, and their expression is considered to play a role in osteoclastogenesis and bone resorption (Tobón-Arroyave et al., 2005; Qian & Huang, 2010). In periapical disease, abnormal expression of RANKL and OPG has been detected. An increased in RANKL level and a significant decreased in OPG level has been associated with bone absorption. In periapical cyst, more active bone absorption was observed compared to periapical granuloma (Meihua et al., 2012).

Potential therapeutic role of OPG in bone diseases

Animal studies

As OPG has an important role in the bone diseases, there are various experimental and clinical trials on the use of OPG in the treatment of different bone diseases.

Simonet et al. (1997) and Yasuda et al.(1998) reported that an increase in bone mass in mice after treatment with OPG at 10 mg kg^{-1} per day for 7 days and 24 mg kg^{-1} per day for 14 days. Furthermore, OPG treatment at a dose of 5 mg kg^{-1} per day for 14 days has been completely prevented ovariectomy-induced bone loss in rats (Simonet, et al., 1997). A study has confirmed the hypocalcemia effects of OPG after injection in normal rats. The result showed that increased in bone mineral density and bone volume accompanied by a decrease in osteoclast number. These facts suggested that the reduction of calcium concentration in normal rats' serum by administration of OPG is due to suppression of bone resorption by inhibition of osteoclastogenesis, especially maturation of osteoclasts (Tomoyasu, et al., 1998).

Bolon and co-workers (2001) observed that transferred OPG gene mediated vehicle by a single injection of a recombinant adenovirus carrying the OPG-Fc gene, prevents bone density loss induced by ovariectomy period. In addition, a single intravenous injection of OPG in young growing rats leads to significant increase in bone volume and density, which are associated with suppression of osteoclastic bone resorption (Capparelli et al., 2003).

Other preclinical studies demonstrated a potential therapeutic role of OPG in the prevention and reduction of lytic bone lesion associated with the skeletal tumor. Lamoureux et al. (2007) suggested the targeting of RANKL may be possible to modify the osteosarcoma itself and inhibit its development.

In an experimental periodontitis, the human OPG has been shown to have strong preventive effects on alveolar bone loss in rats. Yao et al. (2011) revealed that OPG with BMP-2 improves osteoblastogenesis and new bone formation by recruitment of mesenchymal stem cells. OPG treatment is still being used in preclinical bone metastasis models. The result revealed that the proliferation of tumor cell and apoptosis

of tumor cell-osteoclast activity have been decreased. Whereby the bone turnover and the pro-tumor growth factors releasing from the bone matrix have been prevented (Canon, et al., 2012).

Human studies

Additionally, there are a few clinical trials on the use of OPG systemically. One of these studies is done by using a single subcutaneous dose of human recombinant OPG (3 mg kg^{-1}) in post-menopausal women (Bekker PJ, 1999) (Hofbauer & Heufelder, 2000). It was observed that biochemical markers of bone resorption have been reduced and thus OPG has been shown to reduce the bone turnover.

Another study performed by Body et al. (2003), who investigated the use recombinant OPG in patients with bone disease related to breast carcinoma or multiple myeloma. The results indicated that recombinant OPG is effective in reducing bone resorption marker levels as an acceptable treatment for these diseases.

Drug Delivery

Local drug delivery system

The term local drug delivery system refers to the technology utilized to present the drug to the desired body site of drug release and absorption. The advantages of controlled drug delivery systems are mainly to achieve an optimum concentration, usually for prolonged times, to enhance activity of labile drugs, due to their protection against hostile environments, to diminish side effects due to the reduction of high initial blood concentrations and to eliminate patient discomfort compared to parenteral administration.

There are two probable methods to increase the drug action: sustained and controlled drug release to decrease or remove side effects of the drug and site-specific drug

delivery to diminish unwanted systemic effects. These two approaches have been investigated with different natures or synthetic vehicles (Schwach-Abdellaoui et al., 2000).

Matrix materials for drug delivery comprised ceramics, polymers, and composites of the two. A ceramic material is prepared from an inorganic, non-metallic material which can have a crystalline structure. Ceramics usually have a high compressive strength and low ductility so they provide high resistance to deformation but they are brittle materials. Matrices for bone regeneration are calcium phosphates, bioactive glass, and calcium sulfates. The calcium phosphates are the best material because the inorganic constituent of bone is composed of the calcium hydroxyapatite. Bioactive glass and calcium phosphate enhance bone-matrix interface strength by stimulating the formation and deposition of calcium phosphate from solution. There is also the biomaterial metallic scaffolds such as porous titanium or tantalum. The titanium is bioinert material but relatively high stiffness as compared to the adjacent bone can lead to stress shielding problems and the subsequent loosening of the implant (Matassi et al., 2011).

Polymers can be of natural or synthetic origin. A natural biodegradable polymer such as type-I collagen, fibrin, hyaluronic acid and chitosan, exhibits good biocompatibility and osteoconductive properties. However, the use of these materials is limited due to their very low mechanical stability. The composites consist of a combination of materials of different properties. Thus, they may complement advantages of the individual materials to optimize the composite material. The combination of bioactive ceramics such as calcium phosphates with polymers improves the mechanical properties of scaffolds (Matassi, et al., 2011).

Chitosan (Carrier)

Chitosan is a cationic natural carbohydrate polymer derived from chitin by the partial deacetylation. Chitin is a natural biopolymer originated from crustacean shells such as crabs, lobsters, and shrimps. Chitosan is also naturally found in some microorganisms such as yeast and fungi. It comprises of β-(1-4)-glucosamine and N-acetyl-d-glucosamine monomeric units (Ilium, 1998).

Chitin is insoluble in most solvents but chitosan is soluble in most organic acidic solutions at pH less than 6.5 including formic, acetic, tartaric, and citric acid (LeHoux & Grondin, 1993).

Commercially available chitosan are in the forms of dry flakes, solution, and fine powder forms. The average molecular weight of chitosan is ranging between 3800 and 2,000 Daltons. The quality and properties of chitosan products, such as particle size, density, purity, viscosity, deacetylation, molecular weight, and polymorphous structure may differ widely because the characteristics of the final products are influenced by many factors involved the manufacturing process. These factors are important characteristics of pharmaceutical formulations based on chitosan (Nair et al., 2009).

Lysozyme that is found in the fluid of body and egg white of chicken could degrade chitin/chitosan polymers. It recognizes and digests n-acetyl glucosamine sequences in the chitin/chitosan molecules, thus lysozyme degradability rises with increasing degree of n-acetylation in the polymer chain. High deacetylation of chitosan matrix is degraded after a few days of lysozyme treatment and the matrix with low deacetylation continued comparatively constant for a long time (Nwe et al., 2009).

Physical forms of chitosan

Chitosan is available in different physical forms including resins, microspheres, nanoparticle, hydrogels, membranes, fibers and chips. According to the particular application of the chitosan, the particular physical form is selected.

(a) *Chitosan bead/resin*

The drug loaded in chitosan may be important in the drug delivery through the different routes as sustained and controlled release dosage forms. It has various therapeutic uses depending upon the drug loaded into them for example antibiotics (Anal & Stevens, 2005; Srinatha et al., 2008), non-steroidal anti-inflammatory drugs (Arica et al., 2005) and corticosteroid drugs (Mennini et al., 2008).

(b) *Hydrogel*

Hydrogels of the biopolymer is a significant class of polymeric materials due to their interesting properties for potential application in various fields such as biomedical, pharmaceutical and environmental industries. It has been used as the vehicle of antibiotics against periodontal pathogens (Ji et al., 2009) and for the treatment of *Helicobacter pylori* infection in peptic ulcer disease (Chang et al., 2009) and anti-inflammatory drug (Wang et al., 2009) and other medications.

(c) *Film/ membrane*

Chitosan film or membrane has been used in different biomedical applications. Antibiotic loaded in chitosan film was evaluated by Noel (2008), who supported effective release of amikacin and daptomycin that inhibited the growth of *Staphylococcus aureus*. Incorporating antibiotics into chitosan could provide alternative methods of treating musculoskeletal infections. A study on CaSO4-chitosan composite membrane explored a promising application in guided tissue regeneration. It has been observed that it could effectively isolate bone defect from the entrance of connective

tissue cells and provide a space where bony tissue cells could grow into later (Kuo et al., 2009).

(d) *Microparticles/ Nanoparticles*

Chitosan microspheres/nanoparticles are used to provide controlled release of many drugs and to improve the bioavailability of degradable substances such as proteins, as well as to improve the uptake of hydrophilic substances across the epithelial layers. Nanoparticles are solid colloidal particles with diameters ranging from 1-1000 nm. They consist of macromolecular materials and can be used therapeutically as an adjuvant in vaccines or drug carrier in which the active ingredient is dissolved, entrapped, encapsulated, adsorbed or chemically attached. Polymers used to form nanoparticles can be both synthetic and natural polymers (Tiyaboonchai, 2003; El-Sherbiny et al., 2015)

(e) *Chips*

PerioChip is a pioneer in the field of biodegradable delivery frameworks for reducing pocket depth in chronic periodontitis. Chitosan is prepared in the biodegradable chip and used for local drug delivery. Periodontal chips that forms from chitosan and contain drug have clinical benefits that are achieved when using these chips as an adjunct to conventional scaling and root planning (Junbo & Cunxian, 2009; Al-Bayaty, et al., 2013).

(f) *Porous scaffolds*

Chitosan scaffolds for tissue engineering applications are developed and used for skin tissue engineering (Ma et al., 2003), articular cartilage tissue engineering (Yan et al., 2010), bone tissue engineering (Levengood & Zhang, 2014; Cama et al., 2015).

Uses of chitosan

Chitosan has numerous features e.g. (natural source, biodegradable and unique cationic nature) that make it attractive for numerous applications. It can be used in cosmetics (moisturizer in personal-care products) (Jimtaisong & Saewan, 2014), agriculture (seed coating, fungus control agents) (El Hadrami et al., 2010; Ziani et al., 2010; Zeng et al., 2012), water treatment (Hu et al., 2013) and food industry (Moreira et al., 2011).

Chitosan is the preferred material in biomedical, biotechnological and pharmaceutical applications as wound dressings, antimicrobial and antifungal agents (Dai et al., 2011; Jayakumar et al., 2011; Chien et al., 2013; Karunanithy et al., 2013).

It is has been used in gene and drug delivery vehicles (Duceppe & Tabrizian, 2010; Tiyaboonchai, 2013). This is based on its capability of binding a high amount of fats. Moreover, it has no caloric value, thus chitosan can be used perfectly for promoting weight loss (Mhurchu et al., 2005).

Chitosan can be used for preventing heart disease, controlling high blood pressure, renal failure treatment and producing contact lenses (Bachtell, Goodell, Grunkemeier, Jin, & Gregory, 2006; Jing, Li, Ji, Takiguchi, & Yamaguchi, 1997; S.-H. Park et al., 2009; Shigemasa & Minami, 1996; Vasudev, Chandy, & Sharma, 1997; Yoon et al., 2008).

Chitosan-based biomaterials have been tested for the treatment of bone defect (Florczyk, et al., 2013; Jung, et al., 2013). Clinically, chitosan also has dental applications as it was used to repair socket after dental extraction (Ezoddini-Ardakani, et al., 2011b). It was also applied as a biodegradable dental chip containing

chlorhexidine or thymoquinone for the management of chronic periodontitis in patients (Jothi, et al., 2009; Al-Bayaty, et al., 2013).

Animal model

Animal models for bone defect repair

The need for an animal model

Animal models facilitate the evaluation of materials in different applications, for example in different tissue qualities (normal or unhealthy bone), long time durations and ages (Pearce et al., 2007). This is mainly because standardized defects can be created in animals unlike humans, for ethical reasons. The harvesting of biopsy in human for histology and testing new treatments is not acceptable. The animal models are efficiently complementary to *in vitro* studies (Struillou et al., 2010). In general, animal models represent the simplified replicas of the actual system of study. Since they have a similar functions and structures as the systems under study, the information derived from such model may be applied with caution to the system of interest. More important, animal models are often simpler to control and manipulate, and ethical concerns may be easier address (Liesbechner, 2004).

Animal model selection

The animal selection depends on many factors including cost, availability, ease of housing, ease of handling, tolerance to captivity and acceptability to society. Other factors include resistance to infection, low maintenance care, biological characteristics analogous to humans, adequate facilities, tolerance to surgery to extrapolate the results to the human, understanding of the species-specific bone characteristics – such as bone microstructure and composition, as well as bone modelling and remodeling properties, are important (Schimandle & Boden, 1994).

Variety of different animal models could be used for biomaterials testing to repair a bone defect. Rodents and rabbits have high bone metabolism so healing will be fast, shorter study duration and relatively cost effective. On the other hand, the disadvantage is these animals are close to the human. The choice for large animal models is based on their reproducibility, surgical accessibility of experimental sites and similar pathologies under study. Large domestic animal models such as sheep, goats and pigs have similar size and bone characteristics to humans. Dogs are better animal model compared to sheep but regarded as human companion, thus pose more ethical issues (Hillier & Bell, 2007; Pearce, et al., 2007).

Defect Characteristics

In order to be able to evaluate the effects of bone healing in an experimental model, the control defect must heal slowly than the experimental model. By definition, the critical-sized defect that is the smallest size tissue defect that will not completely heal over the natural lifetime of animal (Spicer et al., 2012). Also another definition, a critical-sized defect is a defect that undergoes less than 10% of spontaneous healing during the entire life of the animal. The size of the defect depends on the anatomy and physiology of the species considered (Di Bella et al., 2008). Non- critical sized defect was healed by forming bone islands and there is a new bone formed. The critical sized defect was healed by formation of fibrous connective tissues. Various studies into critical sized defect have been undertaken on clavarial defects for evaluations of bone graft (Spicer et al., 2012; Cooper et al., 2010). The information obtained from research is done on the animals approximates what may be expected in humans as the greater the anatomical, physiological and organic are similar. Some similarities have already been stated concerning bone composition, density, and remodeling between human beings and animal models. Bone density and resistance to fractures in rabbits are very similar

to humans. (Harcourt-Brown & Harcourt-Brown, 2002; Pearce, et al., 2007; Calasans-Maia et al., 2009).

Type of defect

There are four types of bone defects including calvarial, long bone (mandible) segmental, partial cortical (cortical window, wedge defect, or transcortical drill hole), and cancellous bone defect (drill holes). The calvarial and long bone segmentals are more used than others. The commonly used animals are rabbits, rats, dogs and sheep. For calvarial models, rabbit and rats are first choices and for segmental defects, rabbits and dogs are used. Dogs and sheep are often used for experimental conditions (An & Freidman, 1998).

The rabbit and rat defect model are very common and suitable as the calvarial bone has a good size for the easier surgical procedure and specimen handling and it has a plate which permits creations of a uniform circular defect that allows appropriate radiographic and histological analysis. Also the defect does not need any fixation as it is supported by dura and the overlying skin (An & Freidman, 1998).

The rabbit as animal model

Rabbits are viable and suitable models for experimental researches in different branches of dental and medical sciences. White New Zealand rabbits are frequently used in a variety of experiments, including orthopedics (Mendes et al., 2001; Castaneda et al., 2006) and craniomaxillofacial surgery (Calasans-Maia et al., 2008). The advantages of rabbits as experimental models are easy to handle and observe, can work with a large number of individuals, have short vital cycles (gestation, lactation and puberty), easy to standardize the environment, allow genetic standardization, permit transplantation or transmission of tumors and there is a large amount of basic data available. The disadvantages of rabbits are they need to live in a totally artificial

environment require standardized diets and diseases under study need to be are artificially induced. Rabbits are medium-sized models of choice because they are easy to handle and readily available to be observed (Harcourt-Brown & Harcourt-Brown, 2002).

In rabbits, the skeletal growth is expected to coincide with the epiphyseal plate's closure and usually happens at puberty i.e. around 6 months of age. The defect size, anatomical site and its stability are factors that regulate the quality and quantity of bone healing in experiments. This is because muscular and load stresses and the degree of mobility can affect the results. Animal species, cortical bone, bone structure and vascularisation, involvement and the presence of periosteum are to be considered as well (Cacchioli et al., 2007).

CHAPTER 3: MATERIALS AND METHODS

Optimization of osteoprotegerin-chitosan gels Formulation

The combination effect of OPG with different molecular weights of chitosan on osteoblast and NHPL fibroblast was evaluated to optimize the most effective concentration of chitosan and OPG before the formulation of gels.

Materials

Cell viability assay is an appropriate method for screening new substances within a short time in order to determine the effective dose of materials to enhance the cell number. The materials used in this experiment are low molecular weight (LMW), medium molecular weight (MMW) and high molecular weight (HMW) chitosan that were purchased from Sigma. Human OPG protein (Peprotech Recombinant Human OPG, 1mg, USA) was applied. Tris buffer (5 mmol L^{-1}, pH 7.5), phosphate buffered saline (PBS) and dimethyl sulfoxide (DMSO) were used throughout the experiment. Normal human periodontal ligament (NHPL) fibroblast and NH osteoblast cells were purchased from Lonza (Lonza Inc., Walkersville, MD, USA). Penicillin-streptomycin was obtained from Bioscience Ltd., MTT, propidium iodide and acridine orange from Macalai, Japan. The alamar Blue (AB) fluorescent assay (Sigma) was used to measure cell viability

Instruments

All the experiments were performed by using inverted microscope (BX60 Olmpus), centrifuge (Universal 32R Hettich), microplate reader (Infinite M1000 PRO (TECAN), humidified CO_2 incubator and scanning electron microscope (SEM) (low vacuum operating mode; Quanta FEG 250; FEI, Eindhoven, the Netherlands).

Cell culture

The NHPL fibroblast and NH osteoblast cells were cultured in Dulbecco's modified eagle medium (DMEM). The medium was supplemented with 10% fetal bovine serum (FBS) and 1% antibiotics (penicillin-streptomycin) and incubated at 37 °C in humidified CO_2 incubator with 5% CO_2. The medium was changed twice a week until confluent cell monolayer was formed and observed under an inverted microscope.

Biocompatibility study (chitosan, osteoprotegerin, and osteoprotegerin-chitosan combination)

Cell viability assay of raw materials

The effect of different molecular weights of chitosan (LMW, MMW, and HMW) and OPG on NHPL fibroblast cells viability was evaluated after treatment. The cultured cells were trypsinized, seeded in a 96-well microplate (8×10^3 cells per well) and incubated at 37 °C in 5 % CO_2 for 24, 48 and 72 hours to allow cell attachment as described earlier (Souza et al., 2010). The medium was freshened and treated with serial dilutions of chitosan (100, 50, 25, 12.5, 6, 3, 1.5, 0 μg mL^{-1} and OPG (30, 15, 7.5, 3, 1.5, 0.75, 0.35, 0.19, 0.09, 0.045, 0.024 μg mL^{-1} then incubated for 24, 48 and 72 hours. Following incubation, 20 μL of MTT solution (5 mg mL^{-1}) solution was added to each well, followed by incubation for 4 hours. All media was removed and 100 μL of DMSO was added to dissolve the crystal formation. The optical density was measured at a wavelength of 570 nm, using a microplate reader (Tecan Infinite M 200 PRO, Männedorf, Switzerland). The percentage of the cell viability was determined using the following formula:

$$cell\ vaibility\ \% = \left(\frac{X}{X_c}\right) \times 100\%$$

Where X the absorbance of treated cell, and X_c is the absorbance of the control group (untreated cells). The tests were repeated at least three times to ensure reproducibility.

Cell proliferation assay of osteoprotegerin combined with chitosan

In this assay, NHPL fibroblast cell proliferation assay was carried out by MTT on various concentrations of the OPG-chitosan combination. The different molecular weights of chitosan (fixed concentration) and different concentrations of OPG (high, moderate and low concentrations) were selected based on the cell viability assay results. Cells (8×10^3 cells per well) treated with OPG-chitosan combinations together with control samples include cells without treatment incubate for 24, 48, 72 hours. Each sample was assayed in triplicate. At the end of incubation periods, 20 µl of MTT solution (5 mg ml^{-1} MTT dissolved in PBS) was added per well followed by 4 hours incubation at 37°C. The optical density was measured at a wavelength of 570 nm using a microplate reader (Tecan Infinite M 200 PRO, Männedorf, Switzerland).

Morphological observation osteoprotegerin combined with chitosan

NHPL cells were seeded into a 24-well microtiter plate (with a density of 3×10^4 cells per well) and were incubated for 24 hours at 37°C and 5% CO_2. Then the cells were treated with different MWs of chitosan, combined with 0.024 µg mL^{-1} OPG which exhibited the higher ability to induce the cell proliferation, and incubated for 24, 48 and 72 hours. The cellular morphological changes of the treated and untreated cells were observed under a Leica DM IRB (Leica Microsystems, Wetzlar, Germany) inverted microscope and compared with untreated, viable cells.

Acridine orange and propidium iodide (AOPI) double-staining assay of osteoprotegerin combined with chitosan

Acridine orange (AO) and propidium iodide (PI) are nuclear DNA staining (nucleic acid binding) dyes. AO is permeable to both live and dead cells and stains all nucleated

cells, generating green fluorescence. This assay was conducted to assess the morphology and quantify the viable and nonviable (apoptotic) cells. Viable cells are indicated by green nuclei with round intact structure and nonviable cells will display orange-to-red areas.

NHPL fibroblast cells were quantified using AOPI staining, according to standard procedures and examined under a fluorescence microscope (Lieca attached with Q-Floro Software, Solms, Germany). The treatment was carried out in a 25 mL culture flask (Nunc, Roskilde, Denmark). NHPL fibroblast cells were cultured at a concentration of 2×10^5 cell mL^{-1} and treated with different MWs of chitosan (LMW, MMW, and HMW) combined with a 0.024 µg mL^{-1} concentration of OPG. Flasks were incubated in an atmosphere of 5 % CO_2 at 37 °C for 24, 48 and 72 hours. The cells were then spun down at 220 x g for 5 min. The supernatant was discarded and the cells were washed twice, using cold PBS after being centrifuged at 220 x g for 5 min to remove the remaining media. Five microliters of fluorescent dye containing AO (10 µg mL^{-1}) and PI (10 µg mL^{-1}) were added into the cellular pellet at equal volumes. The freshly stained cell suspension was dropped onto a glass slide and covered with a cover slip. The slides were then observed under the fluorescence microscope within 30 minutes before the fluorescent colour begin to fade. The percentages of viable and nonviable cells were determined based on the morphological criteria assessed under the UV-fluorescence microscope.

In vitro biocompatibility evaluation of osteoprotegerin-chitosan gels

NHPL fibroblast and NH osteoblast (Lonza, Walkersville, USA) were used to evaluate the biocompatibility of gels by means of AB assay. MTT assay wasn't used in this assay because MTT solution interacted with gel and giving false results.

In vitro viability assay of osteoprotegerin-chitosan gel

NHPL fibroblast and NH osteoblast cells were cultured in DMEM and osteogenic media supplemented with 10% fetal calf serum and 1 % penicillin-streptomycin. Aliquots (20 µL) containing 40×10^3 cells were then seeded on top of the gels, which had been previously placed in 24 well culture trays. Two hours after cell seeding, 1 mL of culture medium was added to each well and incubated at 37°C in a 5 % CO_2 humidified atmosphere. Blank was wells with no cells and control was wells with cells without adding gels. Cell viability will be assessed by AB fluorescent assay. The AB fluorescent assay (Sigma) was used to measure cell viability. To measure the viability of gel-adherent cells, the medium was gently aspirated from the vacated culture wells and replaced with 10 % AB reagent to measure the viability of cells cultured in tissue culture on the gels. Cells were incubated with a reagent for 5 hours in culture conditions and then media samples were collected in a 96-well plate for absorbance detection (excitation 570 nm, emission 600 nm) using a microplate reader (Biotek ELx808 Absorbance Microplate Reader, Winooski, VT, USA). The absorbance of AB assay is theoretically proportional to the growth rate and viability of cells. Thus, the mean of the cell viability was determined by the measurement of the absorbance of AB assay, and the percentage of the cell viability was determined using the following formula:

$$cell\ vaibility = \left(\frac{X}{X_c}\right) \times 100\%$$

Where X the absorbance of treated cell, and X_c is the absorbance of the control group (untreated cells). The tests were repeated at least three times to ensure reproducibility. Based on the reference, the cytotoxicity responses were qualitatively rated as severe, moderate, slight and non-cytotoxic when the percentage of the cell viability is < 30 %, 30-59 %, 60-90 % and > 90 %, respectively (Rodrigues et al., 2012; Jahromi et al., 2014).

Cells adhesions to osteoprotegerin-chitosan gel by scanning electron microscope (SEM)

The adhesion of NHPL fibroblast and NH osteoblast cells to gels were assessed after 72 hours of seeding of cells on gels by SEM. This assay can also determine whether cells were growing on the gel.   For that, cell- seeded gels were washed in PBS and fixed in 4% glutaraldehyde then incubated at 4 $^{\circ}$C overnight. Afterward, the cell-seeded gels were washed again in PBS, subjected twice to a 30, 70, 95 ethanol series (10 minutes each), and finally air dried. Samples were analyzed with a Quanta FEG 250 scanning electron microscope.

Formulation of osteoprotegerin-chitosan gel

Two sets of different molecular weights (MWs) of water-soluble chitosan (10, 25, 50 kDa gels were prepared by dissolving 50 mg of water-soluble chitosan in Tris buffer (5 mmol L^{-1}, pH 7.5). The mixtures were then left overnight to allow chitosan to completely dissolve. For 1 set of the gels, 1 mg mL^{-1} recombinant human OPG protein (Recombinant Human OPG, PeproTech, Rocky Hill, New Jersey, USA) was added. The other set was left without any addition of recombinant human OPG protein. Chitosan binder (85 kDa), was added to all the gel formulations. They were then mixed and allowed it to stand overnight under vacuum at room temperature (25°C). The gels were later sterilized by gamma radiation (4 kGy) and kept in desiccators. In order to ensure the OPG protein in the gel was not affected by the gamma radiation, the amounts of protein release from gels before and after radiation were measured by using human osteoprotegerin ELISA kit (Cusabio Biotech, China). The flow of the process for the preparation is shown in Figure 3.1.
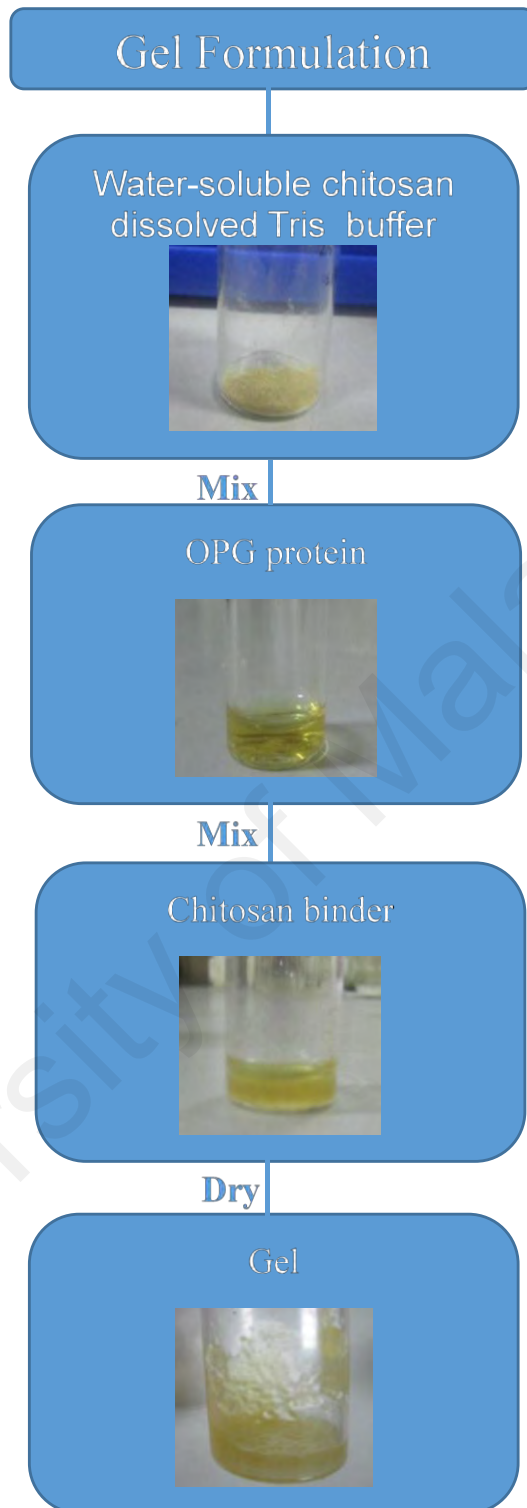
Figure 3.1: The process of the gel formulation from raw chitosan, osteoprotegerin, and chitosan binder.

Gamma sterilization

In order to achieve sterilization of gel with minimum loss of components or alteration of their functional activities, gamma irradiation, which has been increasingly employed for preservation of foodstuffs, medical products, pharmaceuticals, cosmetics, and sterile packaging materials (Ruhl et al., 2011). The gels (500 mg per vial) was sealed in a glass vial and was irradiated at Malaysian Nuclear Agency, Malaysia. Using a Gamma radiation (dose rate of 4 kGy) and irradiated gel samples were sealed tightly in small glass bottles with paraffinic wax. In order to ensure the radiation did not damage the OPG protein, the OPG release from gel after 24 hours is measured before and after radiation by using of Human OPG ELISA kit, Cusabio Biotech.

Physicochemical properties of osteoprotegerin-chitosan gel

Fourier Transform Infrared Spectroscopy (FTIR Measurements)

The FTIR spectrum was recorded on a spectrometer (Thermoscientific Nicolet 6700). The spectra were obtained at a frequency range of 400 - 4000 cm^{-1} with a resolution of 4 cm^{-1}. The information was collected in the FTIR analysis using FTIR system. The FTIR analysis was based on the identification of absorption bands associated with the vibrations of functional groups presented in macromolecules (Tangsadthakun et al., 2017). The experiment was run in triplicate and the means were averaged.

Thermogravimetric (TGA) Measurements

In this study, TGA was performed under a nitrogen atmosphere in a TA Instruments. TGA was used to evaluate the thermal stability and determine the decomposition temperature of gels. TGA was done on a Perkin-Elmer Pyris Diamond TG/DTA thermal instrument TGA 4000. TGA analysis was carried out in a temperature range of 50-900°C under a nitrogen atmosphere with a heating rate of 20 °C minute^{-1}.

Approximately 3-10 mg of sample was weighed, then sealed into the pan and analyzed by the TGA. A thermograph curve of weight loss against temperature was constructed from the data obtained by the instrument. The conversion rate curve was produced to indicate the mass loss conversion (%) during the heating time. The experiment was run in triplicate and the means were averaged.

Differential Scanning Calorimetry (DSC) Measurements

By using DSC, the thermal properties were being investigated. DSC studies used a DSC Mettler-Toledo (model. DSCC822e) instrument in the range started from 25 °C to 250 °C and cooling to 250 °C to 25 °C, under nitrogen at a flow rate of 20 cm^3 min^{-1} and a scan rate of 10 °C min^{-1}. The experiment was run in triplicate and the means were averaged.

Study of the water uptake ability (swelling test) of osteoprotegerin-chitosan gel

Pre-weighed dry gels (W_0) were immersed in 5 mL of PBS solution, pH 7.4 at 37 °C, and incubated for 24 hours. Following that, the gels were blotted with a filter paper, blew dry with a stream of air and the wet weight ($W_{24\ h}$) was determined. The percentage of water absorption (S%) of the gel was calculated from the given equation (Banerjee et al., 2009).

$$S\% = \left(\frac{W_{24h} - W_0}{W_0} \right) \times 100\%$$

Where W_{24} represents the wet weight of gels after 24 hours of incubation and W_0 is the initial weight of the gels. The values were expressed as mean ± standard deviation (n = 3). The experiment was run in triplicate and the means were averaged.

Equilibrium water content of osteoprotegerin-chitosan gel

Another parameter for gel swelling is percentage equilibrium water content (EWC %), which can be calculated from the following equation

$$EWC\% = \left(\frac{M_s - M_0}{M_s} \right) \times 100\%$$

Where M_s is the mass of the gel in equilibrium swelling mass (the weight of mass did not change), and M_0 is the mass of the dry gel at time 0. The values of EWC% by obtaining gels were calculated. The values were expressed as mean ± SD (n = 3).

In vitro degradation and solubility of osteoprotegerin-chitosan gels

The dry gels (5 mg) are placed in a tube containing 5 mL of PBS (pH 7.4) mixed with 1.5 mg mL^{-1} lysozyme. The concentration of lysozyme was chosen to correspond to the concentration in human serum (Freier et al., 2005). Gels of known dry weights were incubated in the lysozyme solution with gentle mechanical agitation (40 horizontal stokes per minute) in a constant temperature incubator shaker for the period of study. The lysozyme solution was replaced daily to ensure continuous enzyme activity (Masuda, Ueno, & Kitabatake, 2001). After 7, 14, 21 and 28 days, samples were removed from the medium, dried and weighed. The extent of *in vitro* degradation was expressed as a percentage of weight, loss of the dried film (n= 3 samples of each gel) after lysozyme treatment. To separate between enzymatic degradation and dissolution, control samples was stored for 28 days under the same conditions as described above but without the addition of lysozyme. The experiment was run in triplicate and the means were averaged.

Evaluation the osteoprotegerin release from osteoprotegerin-chitosan gels

Known dry weight of the OPG-chitosan gel (5 mg) is placed in a glass flask and 5 ml of phosphate buffer (pH 7.4) was added. Then the flask was kept in an incubator shaker

and shaker was adjusted to 40-50 horizontal stokes per minute at 37°C, the supernatant was collected and replaced with fresh PBS solution at various time intervals of 1, 2, 3, 4, 5, 6, 7, 14, 21 days and while replacing it with fresh 1ml of phosphate buffer. The samples were centrifuged and filtered. The protein release from the gel was analyzed by using NanoOrange Protein Quantitation Kit (Invitrogen). The experiment was run in triplicate and the means were averaged.

In vivo study

This section described the materials and methods used in the study to describe the bone formation during healing in surgically created parietal bone defects in the rabbit model and its toxicity effects of the OPG-chitosan gel by means H & E stain, IHC and biochemical assays (liver and kidney function tests).

The animal experiment was carried out according to the Institutional Animal Care and Use Committee (FOM IACUC) and registered as number 20150115/ DENT/ R/ NAB at the University of Malaya (Appendix B).

Based on previous assays and the results of biodegradation, solubility, OPG release, cell and metabolic viability, it was found that the OPG-25 kDa chitosan gel has better properties than the OPG-10 kDa and OPG-50 kDa chitosan gel combinations. Thus, the OPG-25 kDa chitosan gel (best formula) was used to evaluate the osteogenic potential effect in the *in vivo* study.

Experimental Animal

Eighteen New Zealand white female rabbits were used. The animals were obtained from the Animal Experimental Unit (AEU), University of Malaya and housed in the same place under standard laboratory conditions. All animals were examined by a

veterinarian and their suitability for inclusion in the study was determined. The inclusion criteria were:

1. The rabbits were 6 months old.

2. The rabbits were weighted between 3.5- 4 kg.

3. The rabbits' skulls have no congenital defect that may interfere with surgical procedure.

They were allowed free access to food supply throughout the experimental period. Each rabbit was given a number coding for identification. The surgery was performed in an operating theater at Animal Experimental Unit (Figure 3.2).

Figure 3.2: The image shows the prepared surgical area

Surgical Protocol

General anesthesia was used in all surgeries which were performed under the sterile conditions in an operating room. The 18 rabbits were randomly divided into 3 groups; with 6 rabbits in each group. In Group I (control group) the surgical sites were left untreated (surgery only). In Groups II (test group), the surgical sites were filled up with chitosan gel and in Group III (test group) the surgical sites were filled up with OPG-chitosan gel. All the 3 groups underwent a similar surgical procedure which involved surgical defects created on the parietal bone. Three rabbits were sacrificed at each time interval, these being 6 weeks and 12 weeks post-surgically (Figure 3.3).
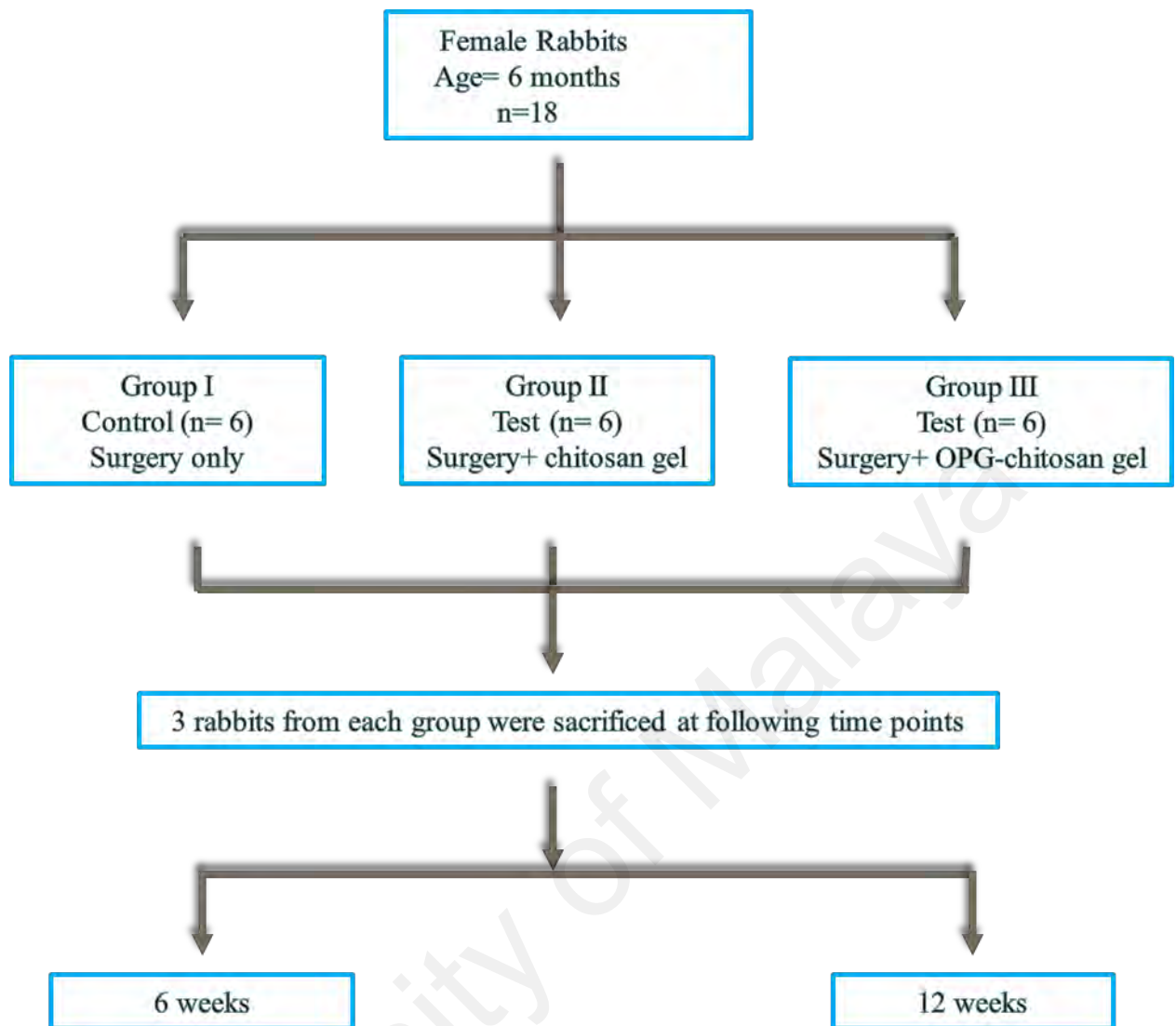
Figure 3.3: Distribution of animals in test and control groups.

Anesthetic Management

General anesthesia was induced by an intramuscular injection of 30 mg/kg of ketamine 100 mg mL^{-1} (Troy laboratories PTY. Limited, Smithfield, Australia) and 3 mg kg^{-1} of xylazine 20 mg mL^{-1} which was analgesic, sedative and relaxant injection (Troy laboratories PTY. Limited, Smithfield, Australia) (Bondarenko et al., 2014). Local anesthetic solution (2 % lidocaine with adrenaline) was used for local hemostasis. The drape was placed over the animal leaving only the surgical site was exposed. Physiosuite monitor was used during surgery for temperature monitoring and

homeothermic warming. Sodium chloride (0.9 %) in the range 30 mL kg^{-1} per hour was provided to prevent a drop in blood pressure (Figure 3.4).

Figure 3.4: Images of (A) operating table and (B) physiosuite monitor that regulate the body temperature of rabbits.

Surgical Sites

A total of 18 surgical defects were surgically created in the parietal bone in 18 rabbits. The parietal bone was selected as a suitable experimental site, as this bone has a good size for the easy surgical procedure and specimen handling. It has a plate which permits the creation of a uniform circular defect for appropriate radiographic and histological analysis. Also, the cranial defect does not require any fixation as it is supported by dura and the overlying skin (An & Freidman, 1998).

Flap Design

A sagittal incision was made in the skull along the midline from the frontal to the occipital bone. Following that, a full thickness skin-periosteal flap was raised to expose the parietal bone using a periosteal elevator (Figure 3.5).
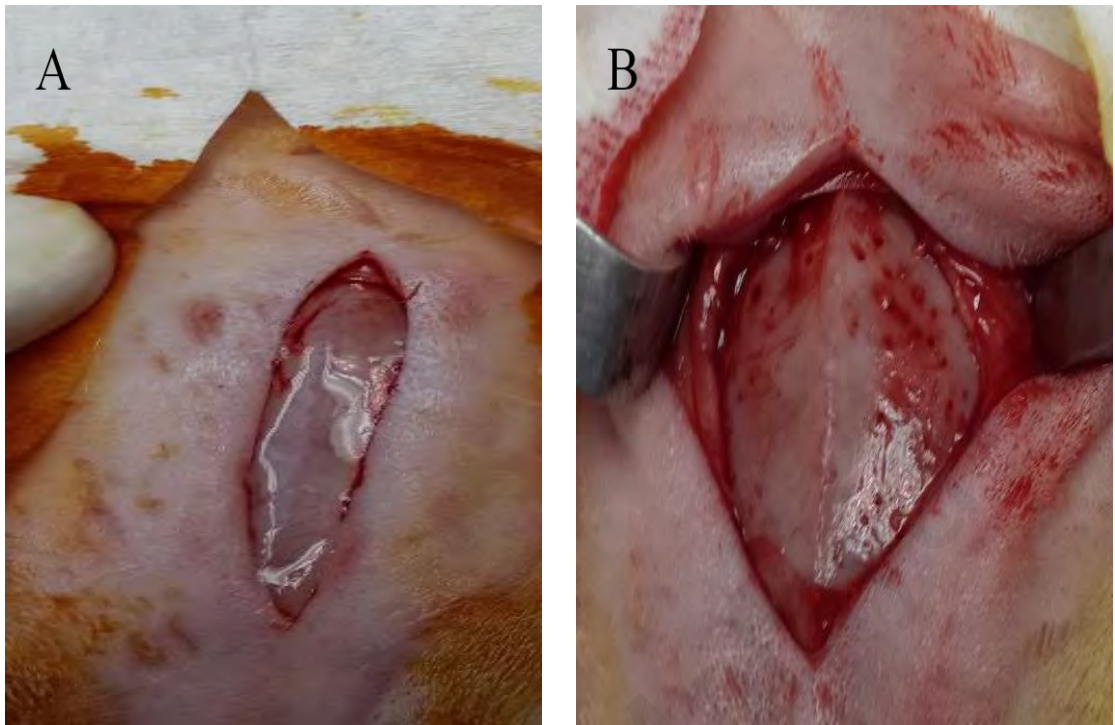
Figure 3.5: Images of (A) Full thickness skin-periosteal flap and (B) exposed parietal bone

Surgical Defects

A circular defect with 15 mm diameter was created in the parietal bone using trephines of the corresponding sizes. A surgical headpiece with a portable surgical motor under cool saline irrigation was used to prevent heat that may cause bone dead. The bone was removed, then the defects were treated accordingly prior to suturing. The soft tissues (periosteum, connective tissue, and skin) were repositioned and then sutured layer by layer. The periosteum was repositioned and secured using 4.0 vicryl on a half round needle. The skin flap over the defect was approximated and sutured using 3.0 vicryl on a half round needle (Figures 3.6).
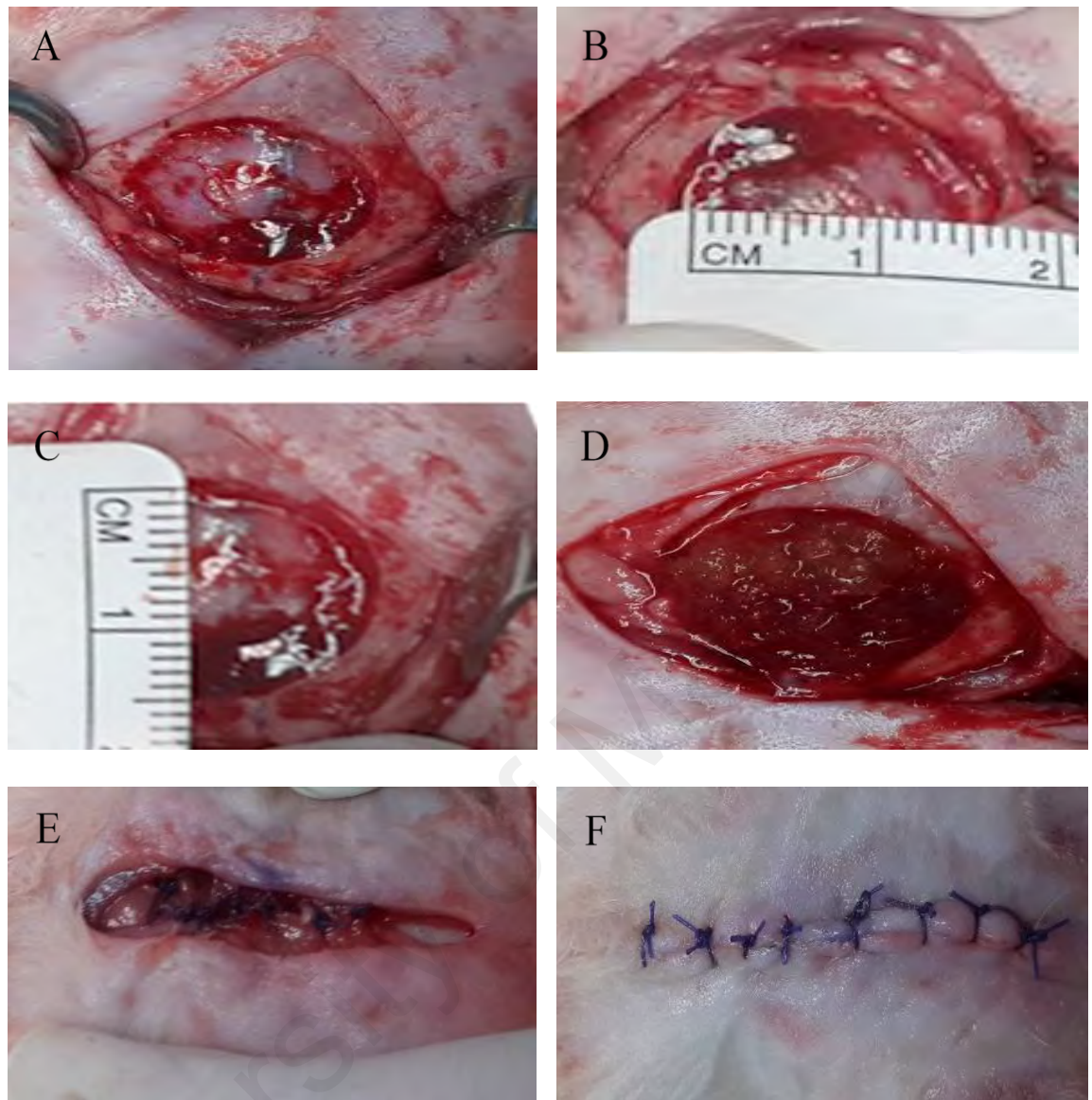
Figure 3.6: Images of surgical procedures. (A) Round surgical defect, (B) and (C) Extension of a surgical defect in 15 mm width and 15 mm length, (D) Defect filled with OPG-chitosan gel (E) Periosteal suturing and (F) Skin Suturing.

Post-operative Management

Tincture iodine and dressing were applied over the suture incision. Each animal was given post-operative medications i.e. meloxicam (according to weight i.e. between 0.3 - 1.5 mg kg^{-1}) (Turner et al., 2006) was given for three days. In addition, an intramuscular injection Kombitrim® 1ml/10 kg (sulfamethoxazole and trimethoprim) (Kela Labratoria n.v, Hoogstraten, Belgium) was given for three days to prevent the post-operation

infection. Once the rabbits regained conscious, it was placed in a cage and allowed for water and food supply.

Blood Collections

From each animal, blood samples were collected before the surgery and before the sacrifice. Three millimeters of blood was collected from marginal ear veins from each rabbit. All blood samples were centrifuged and the collected sera were stored in – 20 $^\circ$C until assay. Kidney and liver functions tests were performed (Figure 3.7).

Figure 3.7: The vacutainer containing blood sample.

Euthanasia and block harvesting

After anesthesia was induced by usual means, the rabbit was euthanized by using cardiac puncture with an overdose of barbiturates (Dolethal, Pentobarbitone sodium 200 mg ml^{-1} solution, 0.7ml kg^{-1} IV) according to the assigned time points either 6 and 12 weeks. A skin incision was made on cranium bone close to earlier surgical sites. The previously grafted sites were excised with a bone cutting round bur. An *en bloc* (20 mm × 20 mm) around the surgical site was be harvested (Figure 3.8). The *en bloc* was then placed into a container containing 50 ml 10% normal buffered formalin (NBF)

Figure 3.8: Image of the harvested *en bloc* specimen.

Methods of Evaluation

Clinical Evaluation

The bone formation during healing was evaluated clinically by visual means to determine the closure of surgical defects. The soft tissue appeared thin and transparent. On the other hand, the bone tissue appeared dense and opaque.

Radiographic Evaluation

The surgical area (parietal region located between occipital region and anterior frontal region) was imaged by XtremeCT (Scanco Medical AG, Switzerland) (Figure 3.9).
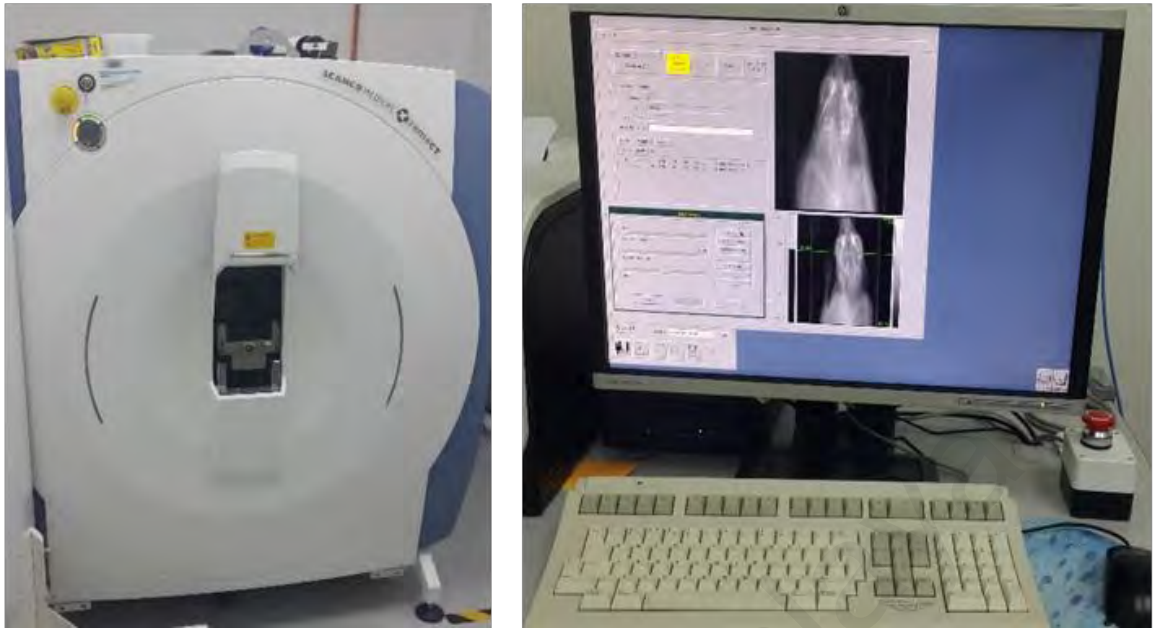
Figure 3.9: The images shows Scanco XtremeCT device used in the experiment.

A normal parietal bone (round, 15 x 15 mm dimension) which was removed during the surgery was scanned and used as a reference. All the surgical sites for all groups (be it 6 and 12 weeks after surgeries) were scanned. The scan length was set to 25 mm and with an isotropic voxel size of 82 μm, each measurement result in 154 parallel CT slices.

The Scanco XtremeCT device allowed the following evaluations of the healing surgical defects:

(i)   A 3D model colour map comparison

(ii)   Bone volume and bone volume density comparison

(iii)   Comparison of tissue density at the periphery and centre of healing surgical defects

The 3D model colour map was constructed by superimposing the reference (normal bone) with the standardized scanned area healing surgical defects of different groups

and different time points. The differences between the reference and the surgical defects were shown with the following colour coding:

(i)   Green indicates no changes between the reference (normal bone) and healing surgical defect

(ii)   Yellow indicates some change between the reference (normal bone) and healing surgical defect.

(iii)   Red indicates big change between the reference (normal bone) and healing surgical defect

The Scanco XtremeCT also calculated the mean bone volume and the percentages of bone volume by density. It also allowed comparison of tissue densities at periphery and center of the surgical defects. The measurements were analyzed using the Materialise Mimics Innovation Suite 17.0, Materialise 3-matic® Medical 9.0 and SkyScan "CT-analyser" software.

Histological Evaluation

(a) *Tissue Preparation*

➢ **Fixation**

The block specimen was fixed in 10 % natural buffer formalin (NBF). The block was placed in a pot containing 50 mL NBF and the fixation process was undertaken 48 hours. The ratio of tissue to fixative volume was 1:50.

➢ **Decalcification**

The block specimen was decalcified with 100 ml 10 % Ethylenediamine tetra acetic acid (EDTA). The decalcification solution was changed every day. The ratio of tissue

from implant site to decalcification solutions was 1:50. Decalcification was considered complete when there were no radiopacities in radiographic films that were taken for specimens after decalcification. After 3 weeks, decalcification was completed, specimens were washed in PBS for 30 minutes. The bone formation was evaluated by H and E stain and IHC.

➢ **Processing for blocking**

The block processing was carried out using a Leica TP 1020 tissue processor. This is an automatic machine where the specimen underwent a long cycle schedule. The specimens were treated through twelve stations with series of graded concentrations of ethanol (70 %, 95 %, 100 %, 100 % and 100 %) and xylene, and then Paraplast wax (56°C melting point). Finally, the specimens were embedded in molten (56°C) paraffin wax. The specimen was positioned with outside surface (periosteal side) facing outward. The blocks were stored in airtight container for future use.

➢ **Sectioning**

A microtome (Leica, Germany), with disposable microtome blade (Leica 818 high profile disposable microtome blade) was used for sectioning. Four μm thick sections were collected and stained with H and E as a histology guide. The sections were floated on a water bath (45°C) before being mounted on silanized glass slide, MUTO. Specimens were identified according to a specific antibody treatment (osteopontin and osteocalcin) and negative control for antibodies, H and E staining. All dried up for 15 to 20 minutes and heat treated in an incubator at 60°C overnight. The slides were stored at 4°C. Figure 3.10 summarised the flow of the bone preparation until histological work.
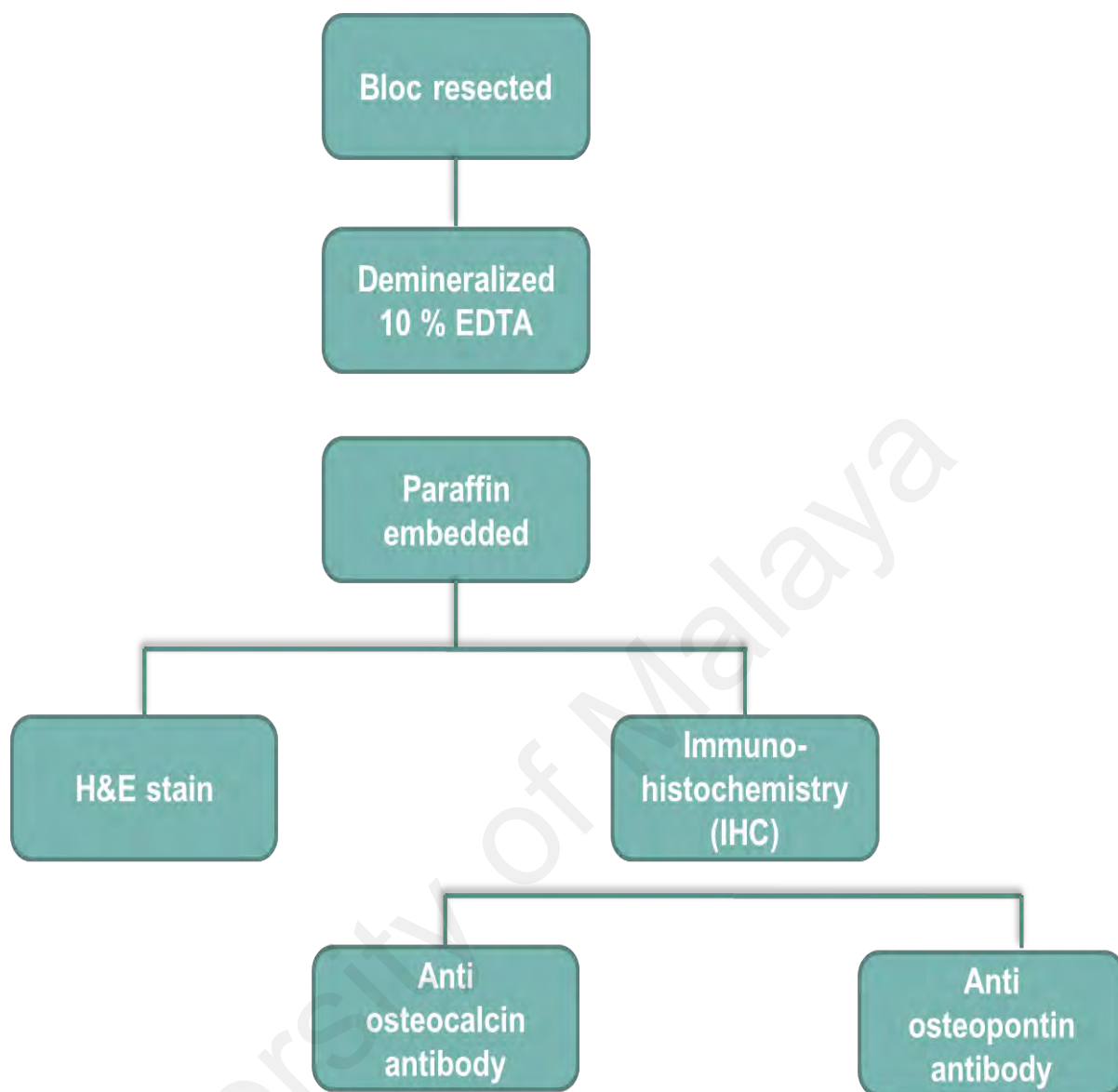
Figure 3.10: Image of bone preparation including fixation, decalcification, and histological investigations.

(b) *Immunohistochemistry (IHC)*

(i) Selection of Antibody

For this study, antibodies were selected based on a review of the literature in relation to previous use in rabbit and availability. The selected antibodies: Osteopontin (clone 1B20; Novus Biologicals, Cambridge, UK), Osteocalcin monoclonal antibodies (OCG3, Abcam, Cambridge, UK) and Cathepsin K polyclonal antibody (Biovision, USA) have

been cited satisfactory for results in rabbit bone tissue (Arrigoni et al., 2013; Bondarenko, et al., 2014).

(ii) IHC Protocol

All slides were labeled accordingly prior to any IHC work.

➤ Removal of paraffin and rehydration of tissues

Fixed sections were placed in fresh xylene bath and incubated at room temperature for 5 minutes. The previous step was repeated twice with fresh xylene. Excess liquid was drained and the slides were placed in a fresh absolute ethyl alcohol bath, 95 %, 85 %, 75 % alcohol bath and distal water bath for 5 minutes at room temperature respectively.

➤ Antigen retrieval

Target retrieval solution, concentrated x10 (Dako, USA) was used in this experiment. Slides were placed in an unsealed container filled with sufficient preheated antigen retrieval solution. This followed by microwaving the slides in a microwave oven (LabPulse™ Microwave Tissue Processor) for 10 minutes. After that, slides were washed in PBS.

➤ Proteinase K treatment

One drop of proteinase K (Dako, USA) (40 µl) was mixed with 2 mL 0.05 mol L^{-1} Tris-HCL (pH 7.5 to 7.7). The tissues were covered with the proteinase K solution for 5 minutes. Then, slides were washed in PBS.

➤ Blocking endogenous peroxidase

This was done by adding two to three drops of peroxide blocking reagent on each slide so that the sections were covered completely for 15 minutes. Then they were washed with PBS bath and dried.

➤ Exposure to the primary antibody

Osteopontin, osteocalcin and kathepsin K monoclonal antibodies were placed on the sections. Slides were then incubated horizontally in a humid chamber at room temperature for 30 minutes. Excess reagent was thrown off and the slides were rinsed for 5 minutes in two consecutive jars of PBS and dry. After that, the sections were covered by chromogen for 5 minutes then washed with distal water and dried. Slides were placed in an unsealed container filled with sufficient hematoxylin solution for 5 minutes. The slides were washed in running water for 5 minutes then in water distal water to clean. The slides were placed in 75 %, 85 %, 95 %, 100 % alcohol bath and xylene twice for 3 minutes respectively. Finally, the slides were mounted and immunohistochemical reaction verifying was done by light microscope and scanned by using digital slides scanner (3DHISTECH Ltd, Hungary). The results were assessed by using computer assisted image analysis (Java-based, image-processing software, ImageJ, National Institute of Mental Health, Bethesda, MD, USA). Verification of the immunohistochemical reaction was performed using a light microscope and scanned using a digital slide scanner (3DHISTECH Ltd., Budapest, Hungary). The results were assessed using computer-assisted image analysis (ImageJ; National Institutes of Health, Bethesda, MD, USA). The image was opened and the image threshold was adjusted until all stained areas were selected. A histogram was displayed to provide assistance. Staining was assessed by setting a threshold using the threshold tool. The threshold tool settings that successfully quantified the staining in a positive-stained specimen were

repeated in every image for comparison. The analysed–set measurement was selected, and the parameters to be measured were chosen (Jensen 2013). The mean and standard deviation were calculated for each sample.

> **Quality Control**

A negative control reagent was used with each specimen to identify any non-specific staining. If a non-specific staining could not be clearly differentiated from the specific staining, the labeling of the test specimen should be considered invalid. In this experiment rabbit immunoglobulin fraction (Normal) (Dako, USA) was used as negative control.

Serum biochemical parameters

The blood samples were collected from all rabbits before surgery and before sacrificing. The blood samples were then permitted to clot at room temperature before centrifuging at 1000 g for 10 min. The serum was separated and analyzed for kidney function tests such as creatinine, urea nitrogen, and liver function tests such as alkaline phosphatase (ALP) and alanine aminotransferase (ALT) using a chemistry analyzer (HITACHI, 902, Japan) with standard diagnostic kits (Roche).

Statistical Analysis

For each microplate of cell culture, the reading values calculated from the exposed cells were converted into percentages with the negative control values considered to be 100%. Statistical analysis was performed using parametric One-Way ANOVA test was used for comparison between the mean values of different groups. The percentage of the bone formation markers was subjected to statistical analysis to analyze the difference in bone regeneration at 6 and 12 weeks post-surgery using independent-samples t-test. In the *in vivo* study as the data are normally distribution but sample size was small, the

non- parametric tests (Kruskal–Wallis test and Mann-whitney test) also run. The significance value was set at ($p < 0.05$). Values were presented as a mean (arithmetic mean) and standard deviation.

In vitro biocompatibility study of different concentrations of osteoprotegerin and chitosan

The cell viability after treated with different molecular weights of chitosan and osteoprotegerin

The cytotoxic effects of LMW, MMW, and HMW chitosan on the NHPL fibroblasts cells were ascertained by means of MTT assay. Table 4.1 summarizes and compares the percentage of viable NHPL fibroblasts following treatment with different MWs of chitosan (LMW, MMW, and HMW) over different time exposures and under control conditions using the MTT assay. Regardless of chitosan MW, the viability of the NHPL cells was $\geq$ 90%, following 24, 48 and 72 hours of exposure as compared to the untreated cells.

Table 4.1: The percentage of NHPL fibroblast cells viability treated with different MWs of chitosan

Time exposure	Percentage of cell viability		
	Low molecular weight of chitosan 0.1 mg/mL	Moderate molecular weight of chitosan 0.1 mg/mL	High molecular weight of chitosan 0.1 mg/mL
24 hours	$\geq 100 \pm 10\ \%$	$\geq 92 \pm 7\ \%$	$\geq 90 \pm 5\ \%$
48 hours	$\geq 100 \pm 14\ \%$	$\geq 100 \pm 12\ \%$	$\geq 96 \pm 8\ \%$
72 hours	$\geq 100 \pm 16\ \%$	$\geq 100 \pm 9\ \%$	$\geq 100 \pm 17\ \%$

The table shows effects of different MWs of chitosan on NHPL cell line viability *in vitro* at 24, 48 and 72-hour treatments. The viability percentage values were obtained from the MTT assay. Data are reported as means ± SD for measurements in triplicate.

The cytocytotoxic effects of OPG on the NHPL fibroblasts cells were ascertained by means of MTT assay. The viability assay result of OPG was shown in Figure 4.1 that summarizes the percentages of viability of NHPL fibroblast cells according to different OPG concentrations at different exposure times. In general, the viability of cells decreased gradually as exposure time increased. At 24 hours, the cell viability was not effected at all concentrations of OPG but at 48 hours, the cell viability was decreased at

higher concentration of OPG. At 72 hours, the viability of cells decreased gradually as OPG concentration increased. At 30 µg mL^{-1}, the viability was reduced to less than 80 % after 48 hours and to less than 60 % after 72 hours. Results also showed that the viability of cells treated with 0.024 to 1.5 µg mL^{-1} OPG was reported as $\geq$ 90 % over exposure time.
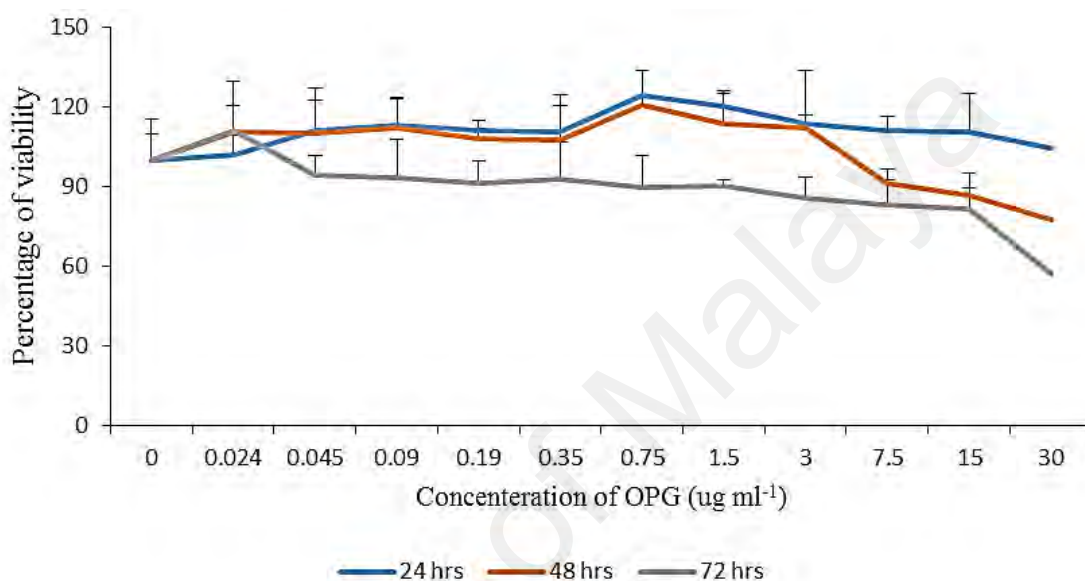
Figure 4.1: Percentage of NHPL fibroblast cells viability after treated with different osteoprotegerin concentrations (0-30µg/mL) at 24, 48 & 72 hours.

Proliferation assay of osteoprotegerin, low molecular weight, Medium molecular weight or high molecular weight chitosan combined with different concentrations of osteoprotegerin

The effect of OPG on cell proliferation was studied in vitro. The cells treated with OPG showed optical densities at two concentration levels (0.024 µg mL^{-1} and 0.18 µg mL^{-1}) that were higher than cells treated with 1.5 µg mL^{-1} OPG and the controls (zero concentration OPG). The growth rates of the treated cells compared to the untreated cells and the highest cell proliferation rate was displayed at the concentration of 0.024 µg mL^{-1} after 72 hours of incubation (Figure 4.2).

When combined with 0.024 μg mL^{-1} OPG, the LMW chitosan showed a higher cell proliferation rate than LMW chitosan combined with 1.5 and 0.18 μg mL^{-1} concentrations of OPG (Figure 4.2).

The cells were treated with MMW chitosan (100 μg mL^{-1} combined with different concentration of OPG (1.5, 0.18, 0.024 μg mL^{-1}), the proliferation of cells was evaluated at 24, 48, 72 hours. Chitosan combined with 0.024 μg mL^{-1} OPG showed a higher cell proliferation rate than chitosan combined with 1.5, 0.18 μg mL^{-1} OPG over three exposure time (Figure 4.2).

The HMW chitosan combined with the same concentrations of OPG (0.024, 0.18 and 1.5 μg mL^{-1}) were used to evaluate the growth of the cells. The 1.5 μg mL^{-1} OPG-chitosan combination induced a greater proliferation of cells than the other two combinations after 24 hours. However, there was no marked difference in the proliferation of cells at 0.024 μg mL^{-1} and 1.5 μg mL^{-1} concentration levels after 72 hours of incubation, and they had increased more than the controls (Figure 4.2).
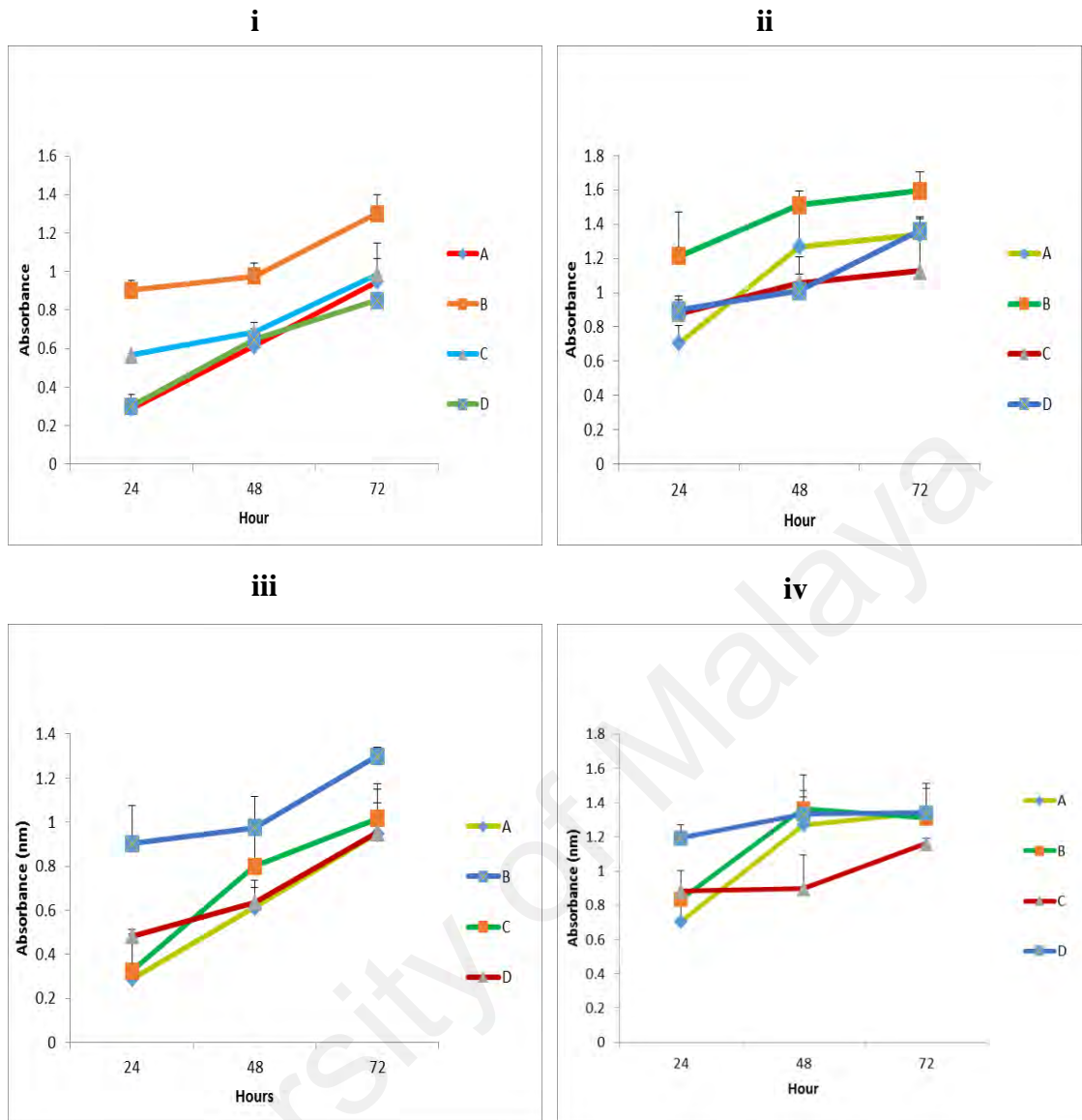
Figure 4.2: (i) Comparison of absorbance rates at low, moderate and high concentrations of osteoprotegerin. (A) Control (untreated cells), (B) 0.024 µg mL⁻¹ osteoprotegerin, (C) 0.15 µg mL⁻¹ osteoprotegerin and (D) 1.5 µg mL⁻¹ osteoprotegerin. (ii,iii,iv) Comparison between LMW ,MMW and HMW chitosan samples respectively in different concentrations of osteoprotegerin. (A) Control (untreated cells), (B) 0.024 µg mL-1 osteoprotegerin-chitosan combination, (C) 0.15 µg mL-1 osteoprotegerin-chitosan combination and (D) 1.5 µg mL⁻¹ osteoprotegerin-chitosan combination.

Morphological changes of cells after treatment with osteoprotegerin-chitosan combinations

In general, regardless of the MW of chitosan, the treated cells appeared to have normal morphology, such as flattened surfaces, and they adhered to the surface of well with very minimal rounded cells (not attached cells) at the various time exposures. Figure 4.3 is a phase contrast image showing morphological appearance of NHPL fibroblast cells, following treatment with LMW, MMW and HMW chitosan in combination with 0.024 µg mL^{-1} concentration of OPG. We noticed that there was no difference between the morphology of cells treated with gels compared to the control group of untreated cells.
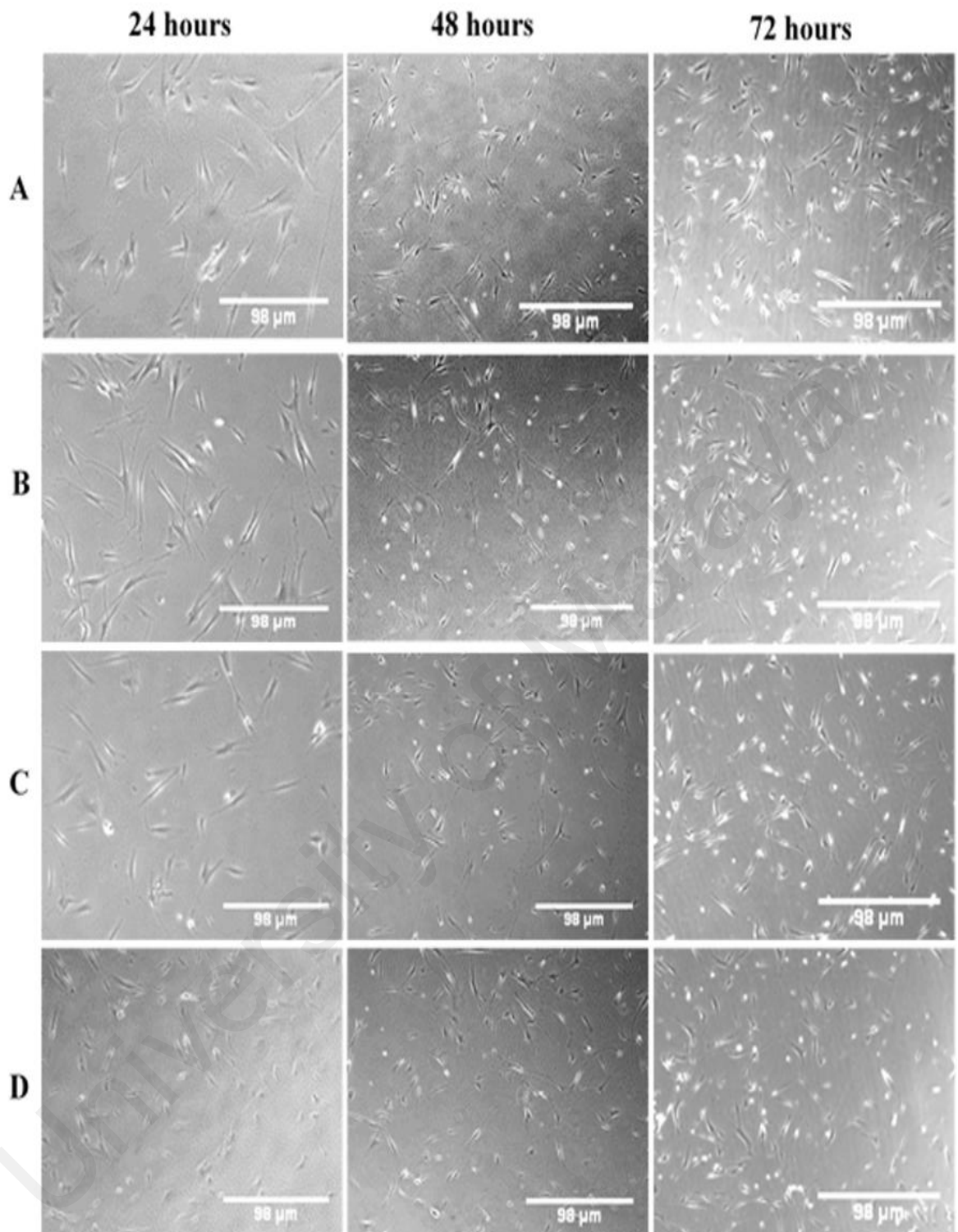
Figure 4.3: The morphological changes of NHPL fibroblast cells observed under an inverted microscope after 24, 48 and 72 hours (at 4x magnification). (A) Control (untreated cells), (B) Osteoprotegerin –low molecular weight chitosan combination, (C) osteoprotegerin -MMW chitosan combination and (D) OPG-HMW chitosan combination.

Quantification of the cell viability after treatment with osteoprotegerin-chitosan combinations using AOPI double-staining

In order to determine the viable NHPL fibroblast cells were counted using a fluorescence microscope. In general, following exposure to different OPG-chitosan combinations at different time exposures, most of the cells were viable and showed fluorescent green with intact cell walls and minimal amounts of dead cells. The cell viability percentages after treated with OPG in combination with different MWs of chitosan are summarized in Table 4.2. The fluorescent images of the NHPL fibroblast cells, following treatment with LMW, MMW and HMW chitosan in combination with 0.024 µg mL^{-1} OPG after 24, 48 and 72 hours is showing in Figure 4.4.

Table 4.2: The NHPL fibroblast cell viability percentages treated with OPG combined with different MW chitosan

Combinations	24 hours	48 hours	72 hours
Control (untreated cells)	87 % ± 10	89% ± 13	92 % ± 14
OPG in LMW chitosan	91% ± 16	85 % ± 15	89% ± 20
OPG in MMW chitosan	92% ± 19	92 % ±18	90% ± 11
OPG in HMW chitosan	88% ± 12	90 % ± 9	91% ± 7

The viability percentages of different MW chitosan were combined with OPG on NHPL cell lines in vitro at 24, 48 and 72-hour treatments. The viability percentage values were obtained from the AOPI double-staining assay. Data are reported as means ± SD for measurements in triplicate.
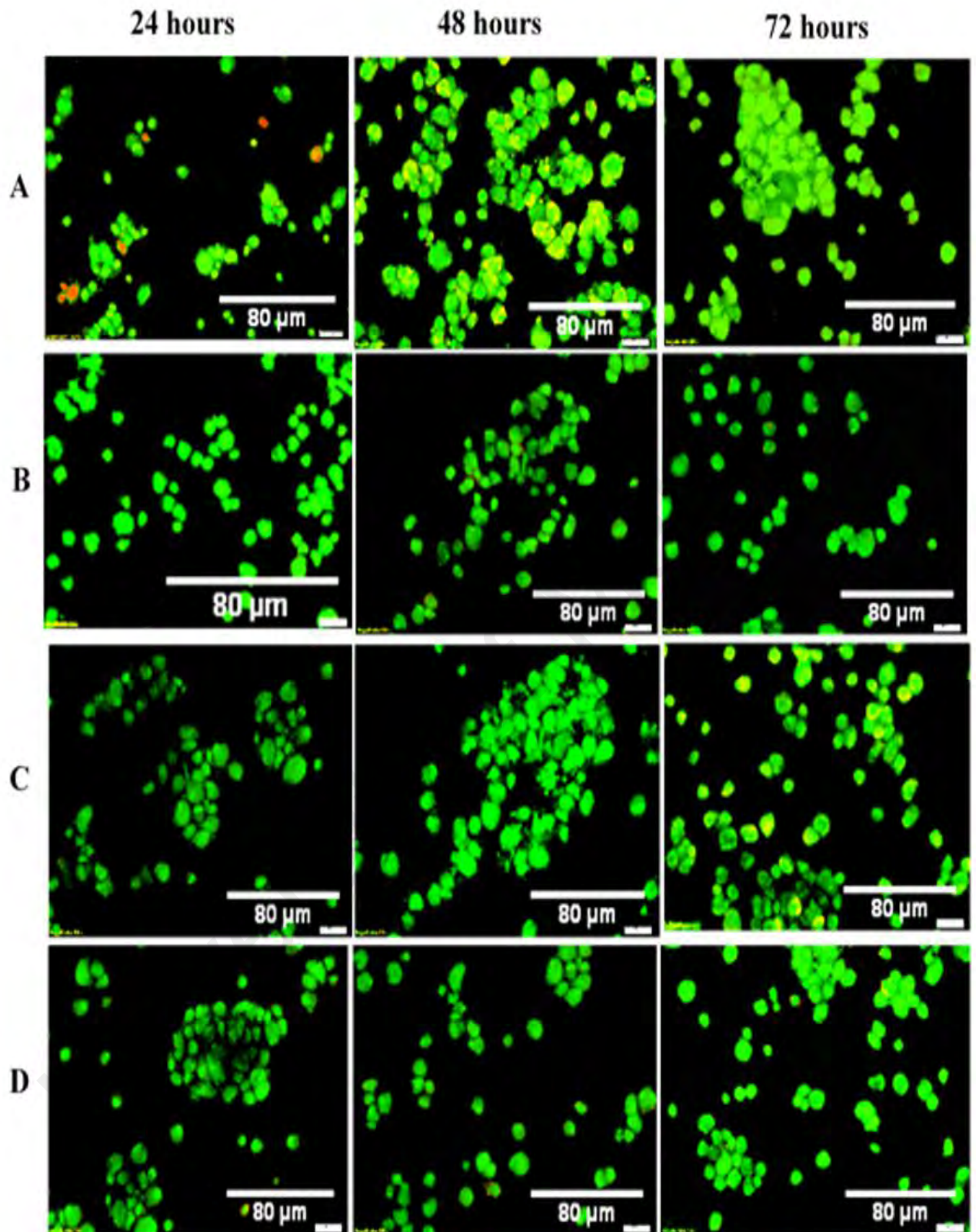
Figure 4.4: AOPI Viability: Dual fluorescence for viable and nonviable cells treated with osteoprotegerin-chitosan combinations and untreated cells. (A) Control (untreated cells), (B) Osteoprotegerin-LMW chitosan combination, (C) Osteoprotegerin-medium molecular weight chitosan combination and (D) Osteoprotegerin-high molecular weight chitosan combination.

In vitro biocompatibility results

Alamar Blue (AB) fluorescent assay results

The metabolic cell viability study showed the viability of NHPL fibroblast and NH osteoblast cells adhered on different types of gels. Results show that after 24 and 48 hours of incubation time, both OPG-chitosan gel and chitosan formulations displayed higher cell viability than the control samples (Figure 4.5 and 4.6). However, after 72 hours incubation time, the cell viability percentages of both cells for 10 kDa chitosan gel was less than the control, but others were almost equal or higher than controls. Thus, they can be considered that all gels are not- toxic as the viability are almost more than 90 % over an extended period. There was no significant difference between viability percentages of NHPL fibroblast cells measured at 24, 48 and 72 hours for control, chitosan or OPG-chitosan gels ($p > 0.05$). OPG-chitosan and chitosan gels (10 kDa) at 72 hours were significantly lower than OPG-chitosan gel (10, 25 or 50 kDa) at 24 and 48 hours ($p > 0.05$). The OPG-chitosan (10 kDa) at 24 hours was significantly higher compared to at 72 hours ($p > 0.05$).

Similarly, there was no significant difference between viability percentage of NH osteoblast cells at 24, 48 and 72 hours for control, chitosan or OPG-chitosan gels ($p > 0.05$). At 24 hours, viability percentages of control was significantly lower than chitosan gel and OPG-chitosan gel (25 and 50 kDa) ($p > 0.05$).
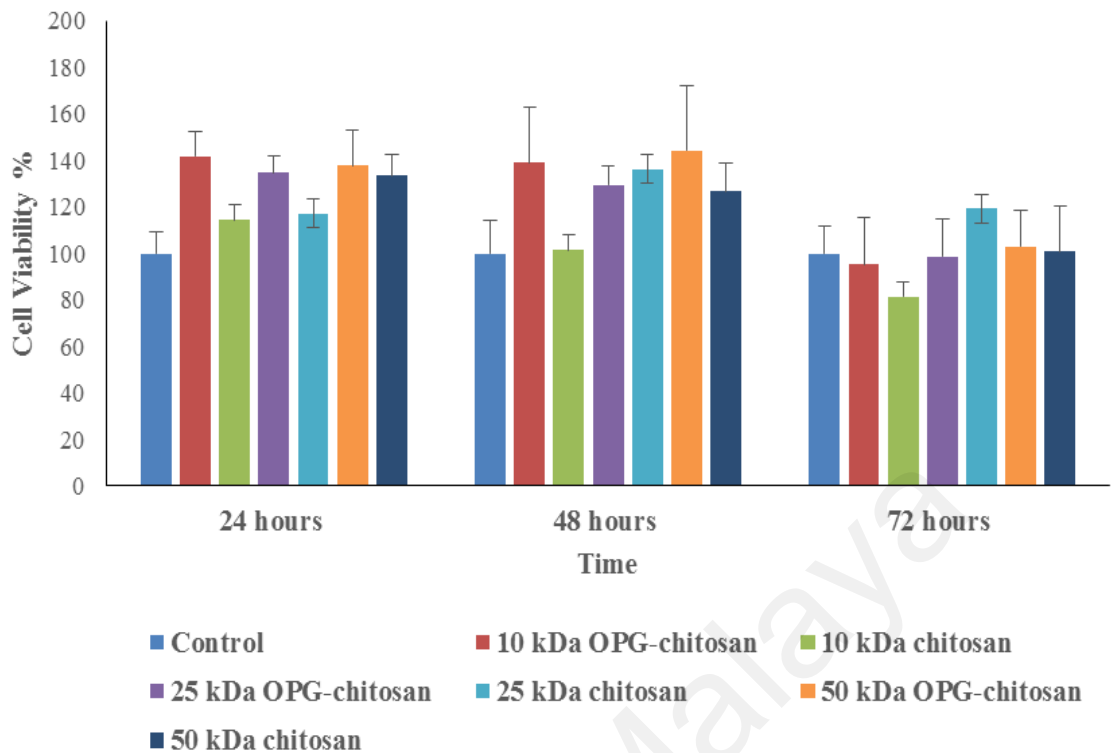
Figure 4.5: Effect of different osteoprotegerin-chitosan gels on metabolic viability (AlamarBlue assay) of NHPL fibroblast-seeded onto the gels after 24, 48 and 72 hours (Columns are the average data, bars are the standard deviation).
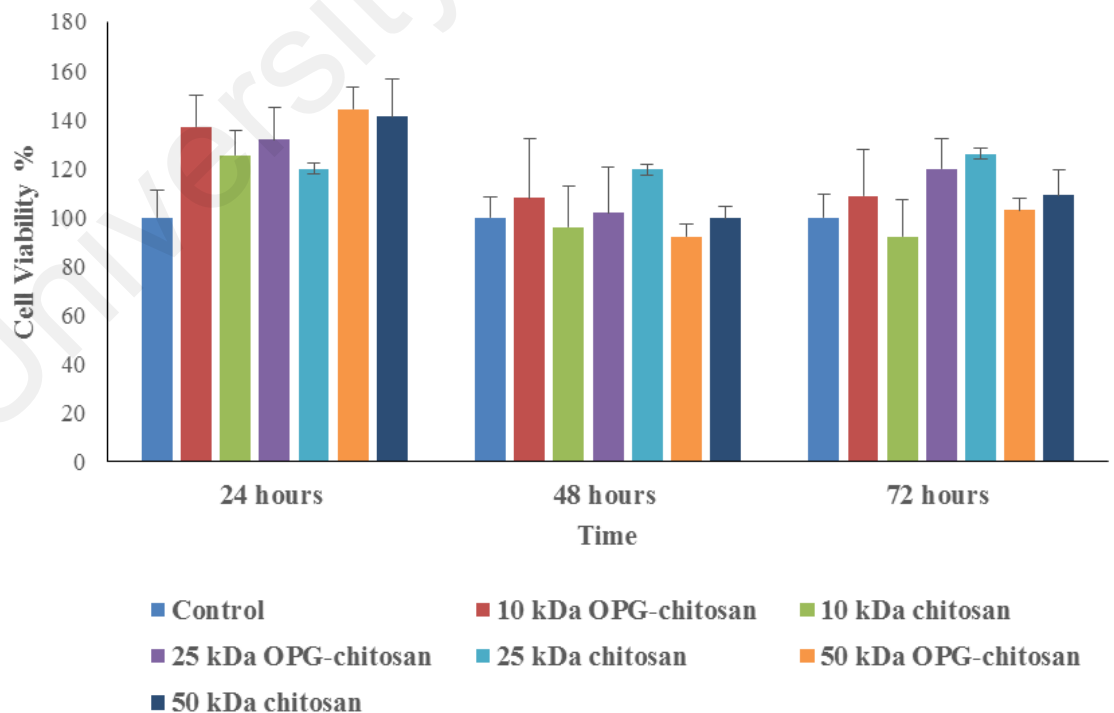
Figure 4-6: Effect of different osteoprotegerin-chitosan gels on metabolic viability (AB assay) of NH osteoblast cells seeded onto the gels after 24, 48 and 72 hours (Columns are the average data, bars are the standard deviation).

Scanning electron microscope (SEM)

The morphology of the gels was observed using SEM (Figure 4.7) exhibits the OPG-chitosan gels (50, 25, 10 kDa), the gel surfaces possess an irregular surface which can play an important role in the adsorption process. The roughness of the particle surface itself causes the increase in the surface area.

Figure 4.8 shows SEM micrographs of NHPL fibroblast and NH osteoblast cells cultured on the specimen surfaces for 72 hours. We noted that the cells were well attached and spread out, displaying a flat configuration and normal morphology on the surface of three different gels. Moreover, neighbor cells connected with each other through cytoplasmic extensions and they spread out on their surface of gels in 72 hours and deleterious or cytotoxic responses were observed. The cells were well spread and had many extended cytoplasmic processes.
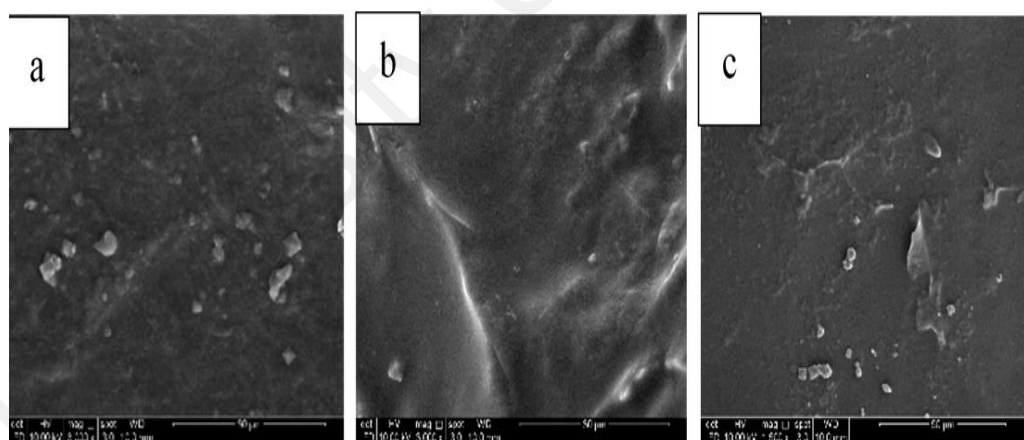
Figure 4.7: SEM micrographs of OPG-chitosan gels with different MWs of chitosan (3000x). (a) OPG-chitosan gel (50kDa), (b) OPG-chitosan gel (25 kDa) and (c) OPG-chitosan gel (10 kDa).
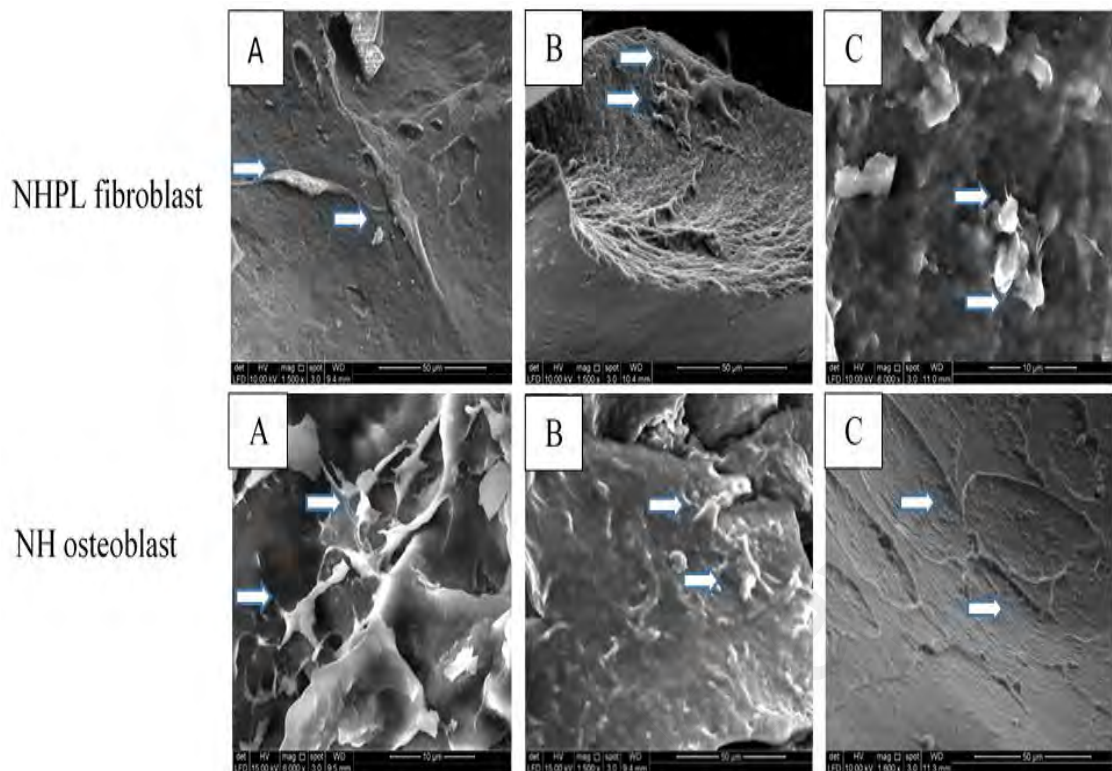
Figure 4.8: SEM micrographs of NHPL fibroblast and NH osteoblast cells cultured on gel surfaces for 72 hours. The arrows show the cells attached and growing on the gel surfaces. A) Osteoprotegerin-chitosan gel (10 kDa), (B) Osteoprotegerin-chitosan gel (25 kDa) and (C) Osteoprotegerin-chitosan gel (50 kDa).

Measurement of osteoprotegerin protein release from osteoprotegerin-chitosan gel before and after sterilization

In order to ensure the protein in the gel was not affected by gamma radiation, the concentration of the OPG protein was measured by OPG ELISA kit. It is 0.91 ± 0.09 before gamma radiation while after radiation is 0.85 ± 0.04. The result of ELISA assay showed that there is no significant difference between the concentration of OPG before and after gamma radiation ($P > 0.05$).

Physicochemical properties of osteoprotegerin-chitosan gel

Comparison of functional groups for different chitosan and osteoprotegerin-chitosan gels

Table 4.3 and Figure 4.9 summarized the wavelength for functional groups of 3 different MWs chitosan gels (10, 25 and 50 kDa) and 3 OPG-chitosan (10, 25 and 50 kDa) gels. For the chitosan gels, all the peaks are clearly recognizable and ranged as follows: OH group from 3353 –3355 cm^{-1}, CH group from 2907 and 2910 cm^{-1}, amide I group from 1635 - 1636 cm^{-1}, amide II group from 1574 - 1581 cm^{-1} and vibration of CO from 1072 - 1073 cm^{-1}. The interactions between chitosan and proteins are represented by amide II bands as in OPG-chitosan gels, there was a shift of these bands i.e. from 1590 to 1610 cm^{-1} in NH amid II protein.

Table 4.3: Wavenumbers of some type of bands occurring in IR spectra of (50, 25, 10 kDa) chitosan and OPG-chitosan gels.

Type of gels	Type of Band						
	C-O	C-O Stretch	CH$_3$	NH amide II	C=O amide I	CH	OH
	Wavenumbers (cm^{-1})						
50 kDa Chitosan	1032	1073	1378	1581	1636	2909	3355
25 kDa Chitosan	1031	1074	1370	1574	1635	2910	3355
10 kDa Chitosan	1033	1072	1370	1581	1635	2907	3353
50 kDa OPG-chitosan	1033	1077	1376	1590	1635	2906	3355
25 kDa OPG-chitosan	1031	1077	1378	1610	1636	2904	3351
10 kDa OPG-chitosan	1031	1075	1378	1610	1635	2906	3355
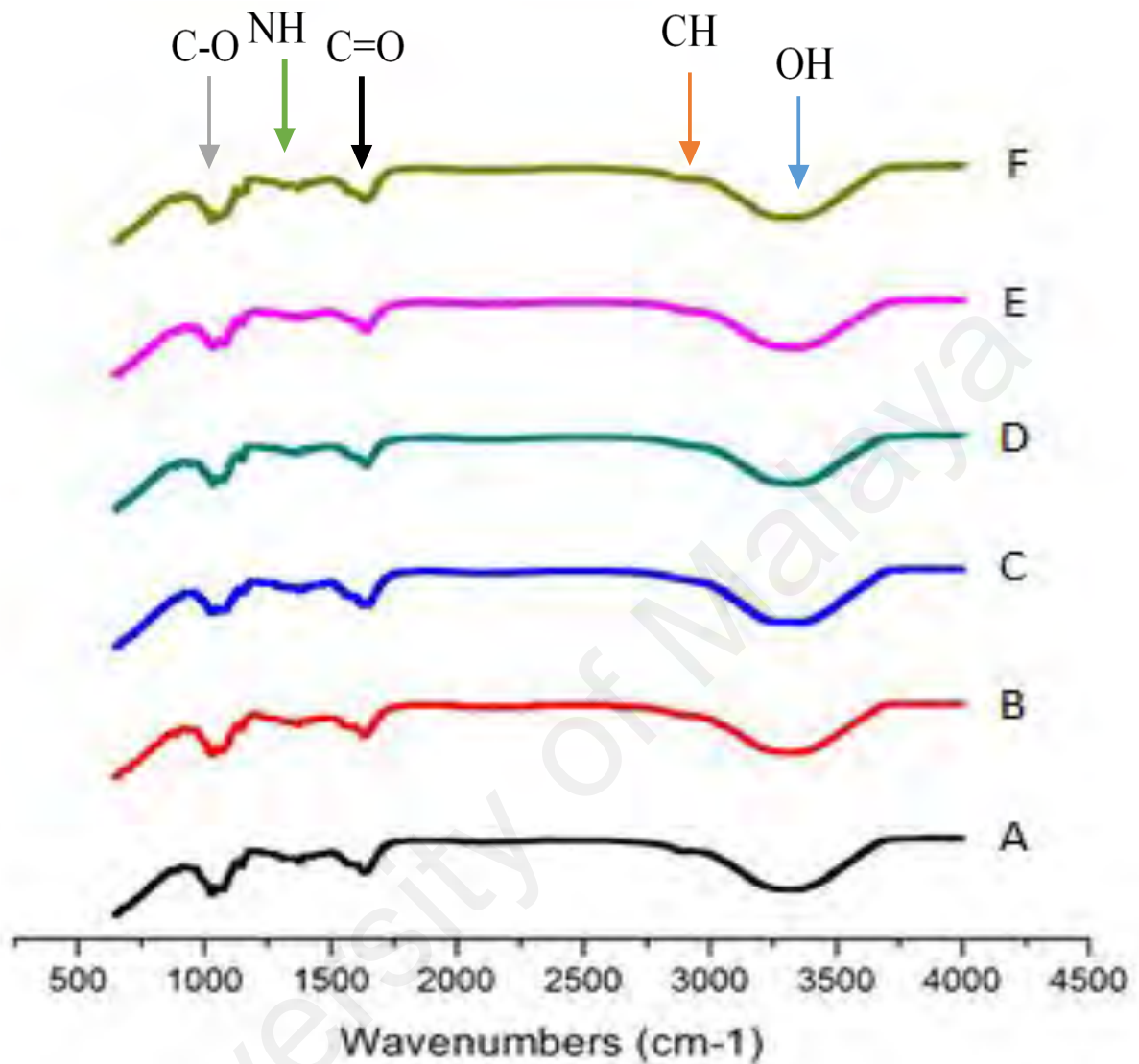
Figure 4.9: FTIR absorption spectra of different MWs chitosan and osteoprotegerin-chitosan gels by using attenuated total reflection technique. (A) Chitosan gel (50 KDa), (B) Chitosan gel (25 kDa), (C) Chitosan gel (10 kDa), (D) Osteoprotegerin-chitosan gel (50 kDa), (E) Osteoprotegerin-chitosan gel (25 kDa), (F) Osteoprotegerin-chitosan gel (10 kDa).

Thermogravimetric analysis

Figure 4.10 is showing the thermogravimetric analysis of the 3 different MW chitosan gels (10, 25 and 50 kDa) and 3 OPG-chitosan (10, 25 and 50 kDa) gels. There was no marked difference in the peaks of all six gels. The first transition was in the range of 50 - 180 °C with a weight loss range from 61 to 76 %. This is thought to be due

to the moisture vaporization. The second weight loss begins in the range 200–400 °C and the corresponding weight loss is range from 9 to 18 %, is attributed to the decomposition of chitosan polymer chains. The TGA spectrum demonstrated that around 80 % of the chitosan gets disintegrated within 800°C. The remaining residue (1 to 2 %) mostly contains inorganic complex (containing C, N, and O).
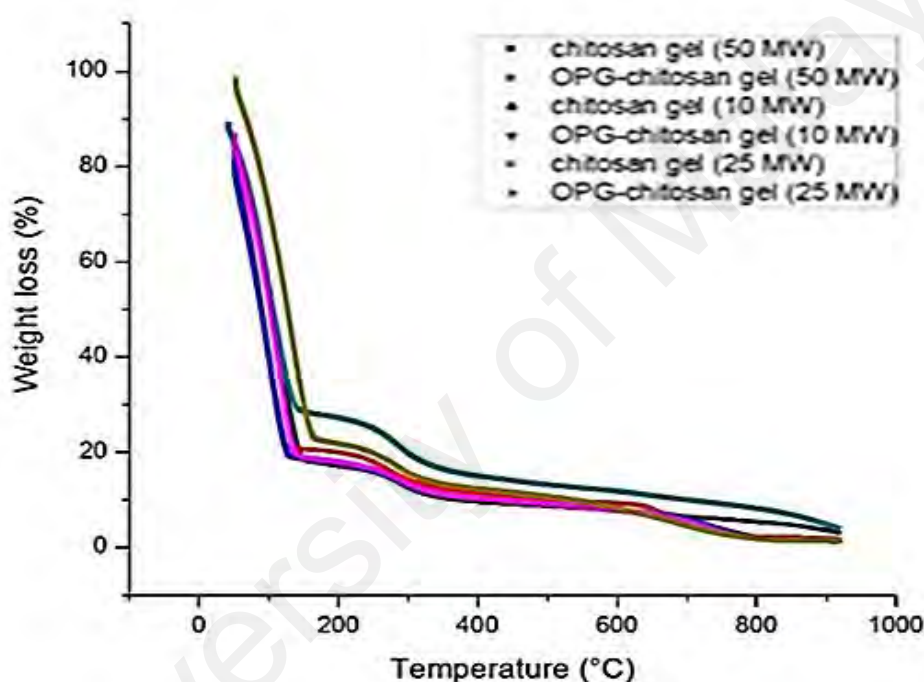
Figure 4.10: Thermogravimetric of the different MWs of chitosan and OPG-chitosan gels based on the sample weight loss transitions against temperature.

Differential Scanning Calorimetry Measurements (DSC)

The DSC curves of all gels show a broad endothermic peak between 100 to 160 °C. This peak is attributed to the loss of water associated with the hydrophilic groups of the polymer (Figure 4.11).
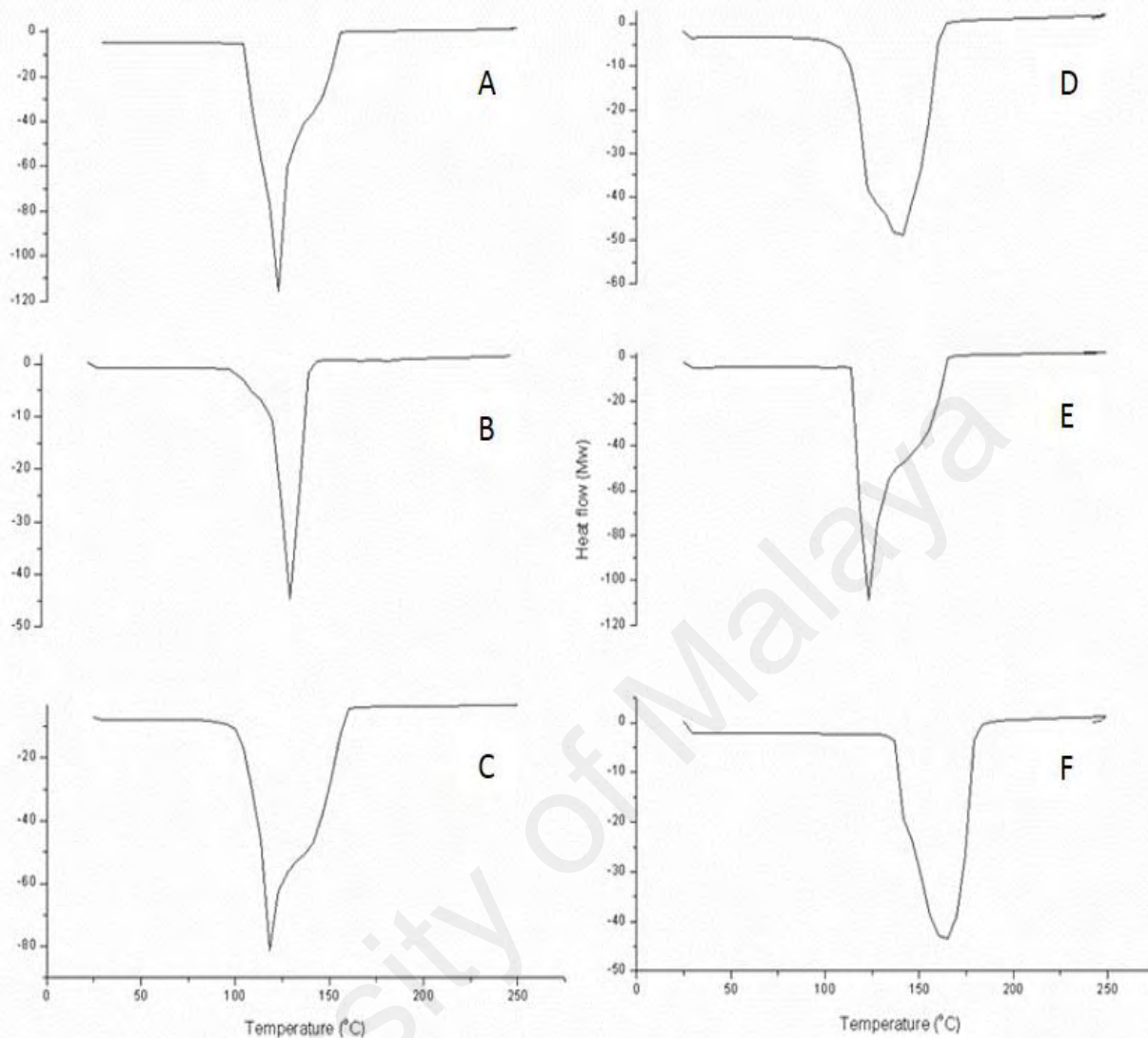
Figure 4.11: DSC thermograms curves of different gels show the endothermic peak between 90 to 150 °C. (A) OPG-chitosan gel (50 kDa), (B) OPG-chitosan gel (25 kDa), (C) OPG-chitosan gel (10 kDa), (D) Chitosan gel (50 kDa), (E) Chitosan gel (25 kDa) and (F) Chitosan gel (10 kDa).

Swelling test and equilibrium water content (EWC)

Figure 4.12 is showing the swelling behavior (water uptake) of gels (10, 25, 50 kDa). The 10 kDa of chitosan showed the highest water binding capacity, followed by 25 kDa chitosan and 50 kDa. It was concluded that an increase in MW results in a decrease in water uptake.

The mean percentages of swelling behavior (water uptake) for the OPG-chitosan gels (10, 25, 50 kDa) were 18.3± 0.7, 11.8± 0.5 and 7.7± 0.7 respectively. The OPG-chitosan gel (10 kDa) showed the significantly highest water binding capacity (p<0.05), followed by the OPG-chitosan gel (25 kDa) (p<0.05) while the OPG-chitosan gel (50 kDa) has the significantly lowest water binding capacity (p<0.05).

The mean percentages for equilibrium water content (EWC) for OPG-chitosan OPG-chitosan gels (10, 25, 50 kDa) (90.8%, 91.8%, 89% respectively) were greater than the percent water content values of the body i.e. about 60%.
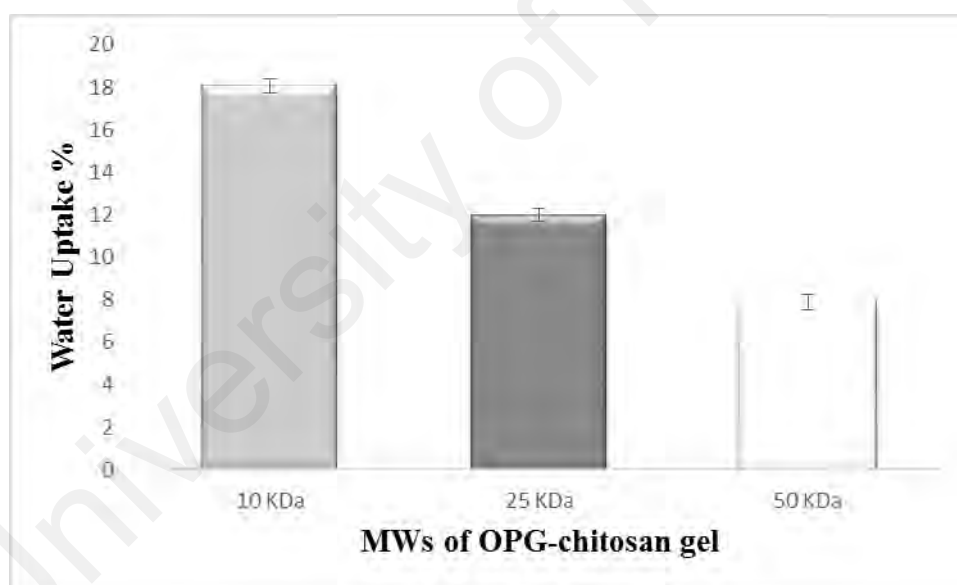
Figure 4.12: Percentages of water uptake of different MWs of OPG-chitosan gels.

In vitro biodegradability and solubility of OPG-chitosan gels

The *in vitro* enzymatic degradation properties of the gel are summarized in Figure 4.13 OPG-chitosan gels (10 and 25 kDa) showed almost complete degradation (≥ 89 % ± 2.1) in 28 days. However, the OPG-chitosan gel (50 kDa) could prolong the complete

degradation more than 28 days. The 50 kDa gel showed a slower mass loss, only up to 77 % ± 5 at 28 days of degradation.

At 7 and 21 days, no significant difference in biodegradation percentages between OPG-chitosan gel (10 kDa) and OPG-chitosan gel (25 kDa) ($p > 0.1$) was observed. However, a significant difference in biodegradation percentages was observed between the OPG-chitosan gel (10 kDa) and OPG-chitosan gel (50 kDa) ($p < 0.05$). At 14 days, the highest significantly biodegradation percentages present in the OPG-chitosan gel (10 kDa) ($p < 0.006$). OPG-chitosan gel (10 kDa) and OPG-chitosan gel (25 kDa) showed almost complete degradation (≥ 90 %) in 28 days. However, OPG-chitosan gel (50 kDa) could prolong the complete degradation more than 28 days. The OPG-chitosan gel (50 kDa) showed a slower mass loss, only up to 67 % at 28 days of degradation.

In order to separate between enzymatic degradation and dissolution, the samples were stored for 28 days under the same conditions without lysozyme. At all times, the significantly highest solubility percentage present in the OPG-chitosan gel (10 kDa) ($p < 0.05$) followed by OPG-chitosan gel (25 kDa) and OPG-chitosan gel (50 kDa). There is no significant difference between OPG-chitosan gel (25 kDa) and OPG-chitosan gel (50 kDa) ($p > 0.05$). The solubility of OPG-chitosan gel (10 kDa) was 58 % ± 9 but for OPG-chitosan gel (25 kDa) and OPG-chitosan gel (50 kDa) were < 35 % ± 4.5 up to 28 days (Figure 4.14).
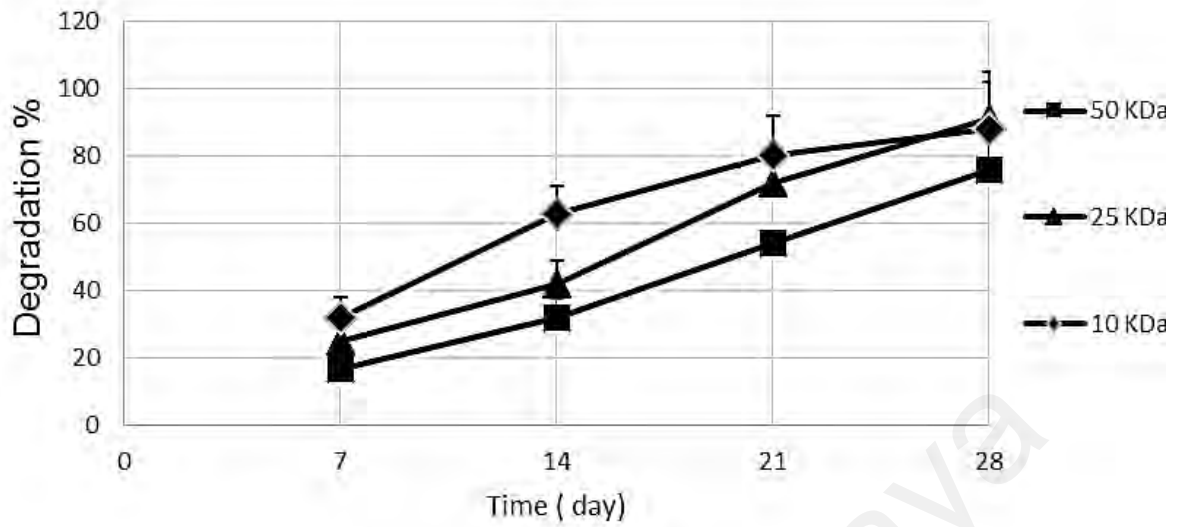
Figure 4.13: Percentage of biodegradation of different chitosan gels biodegradations after 7, 14, 21 and 28 days in PBS at 37°C with 1.5mg ml^{-1} lysozyme.
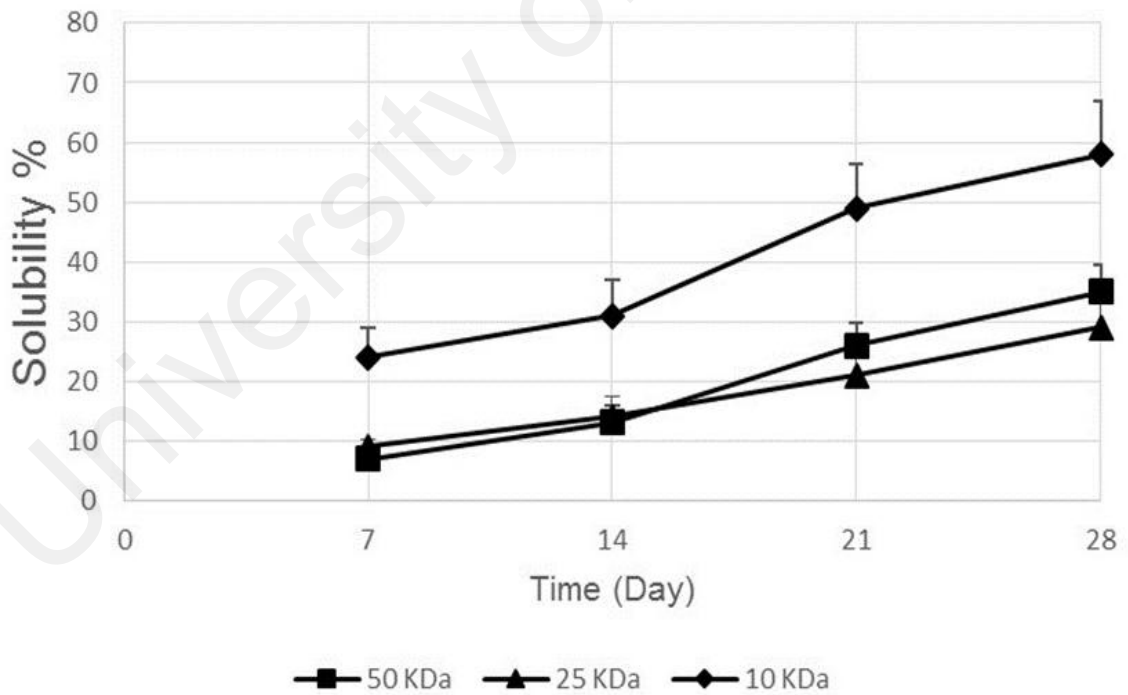
Figure 4.14: Percentage of solubility of different chitosan gels after 7, 14, 21 and 28 days in PBS at 37°C without lysozyme.

In vitro cumulative OPG release assay

The release profile of OPG from the OPG-chitosan gels is shown in (Figure 4.15). There was no significant difference in the release of protein in first two days. However, there was the significantly higher release of OPG from OPG-chitosan gel (25 and 10 kDa) than OPG-chitosan gel (50 kDa) in the following three days (P < 0.05). In period extend from 6th to 14th day, there was a significant difference between different gels. The highest release rate is displayed by the OPG- chitosan gel (25 kDa), followed by OPG- chitosan gels (10 and 50 kDa).). After 21 days, there was no significant difference between OPG- chitosan gel (10 kDa) and OPG-chitosan gel (25 kDa). At 28 days, there was a significant difference between OPG-chitosan gels (25 and 50 kDa) (p < 0.05) but no significant difference between OPG-chitosan gels (50 and 10 kDa).
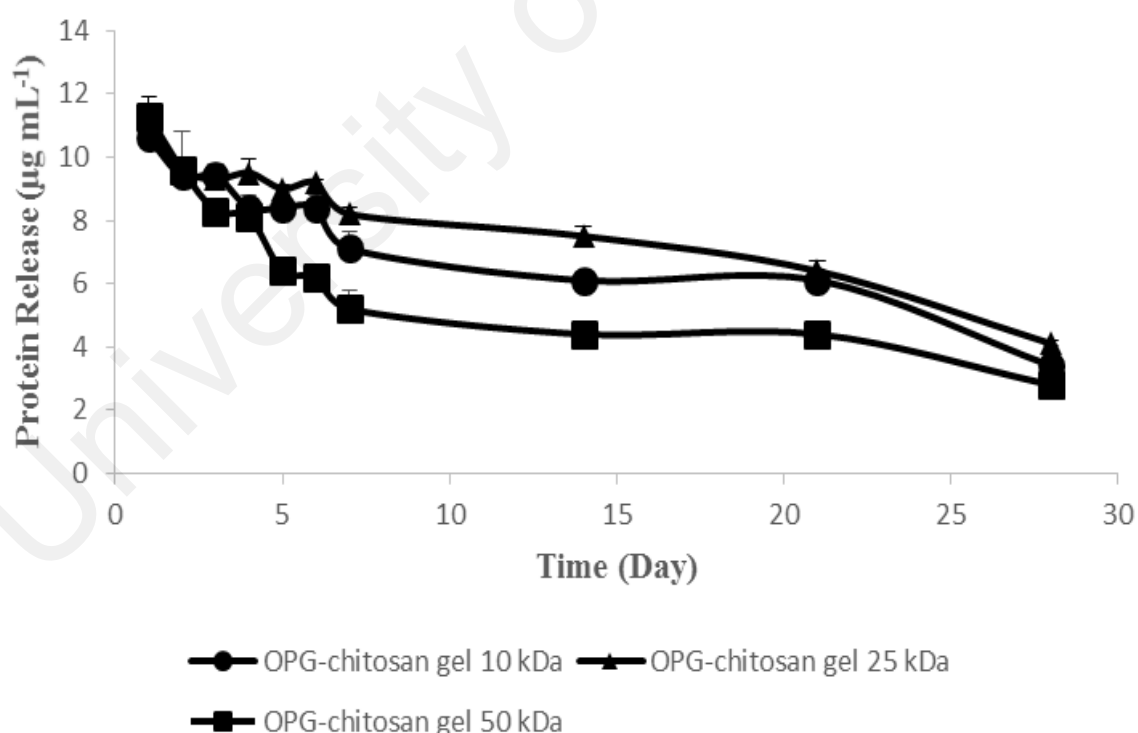
Figure 4.15: Cumulative OPG protein release from 10, 25 and 50 kDa OPG-chitosan gels for 28 days.

In vivo results

Clinical findings

At baseline, the critical size defect was created and its size was 15 mm × 15 mm (Figure 4.16).
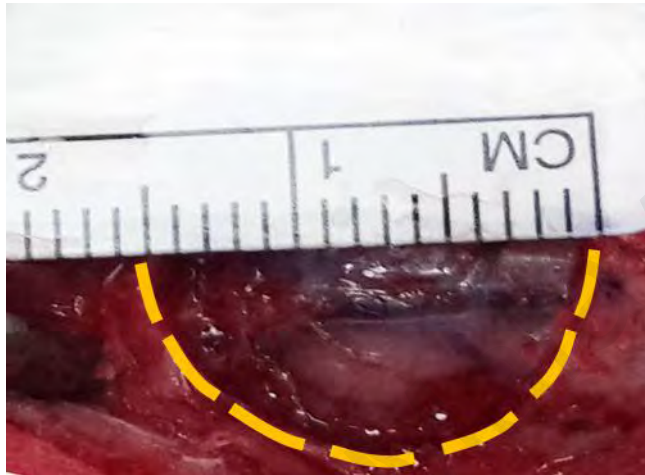
Figure 4.16: The critical size bone defect at baseline. The dotted line indicates the peripheral border of the bone defect. The width of the defect is 15 mm.

At 6 weeks, Group III (OPG-chitosan gel) showed partial healed surgical defects filled up with dense and opaque structure (bone). On the other hand, Groups I (surgery only) and II (chitosan gel) showed the defects filled were complete with thin and transparent tissue soft tissues. At 12 weeks, Groups II and III showed the surgical defects were filled up with hard tissue compared to Group I. For Group I, the defects were partially healed and there were soft tissue gaps (Figure 4.17).
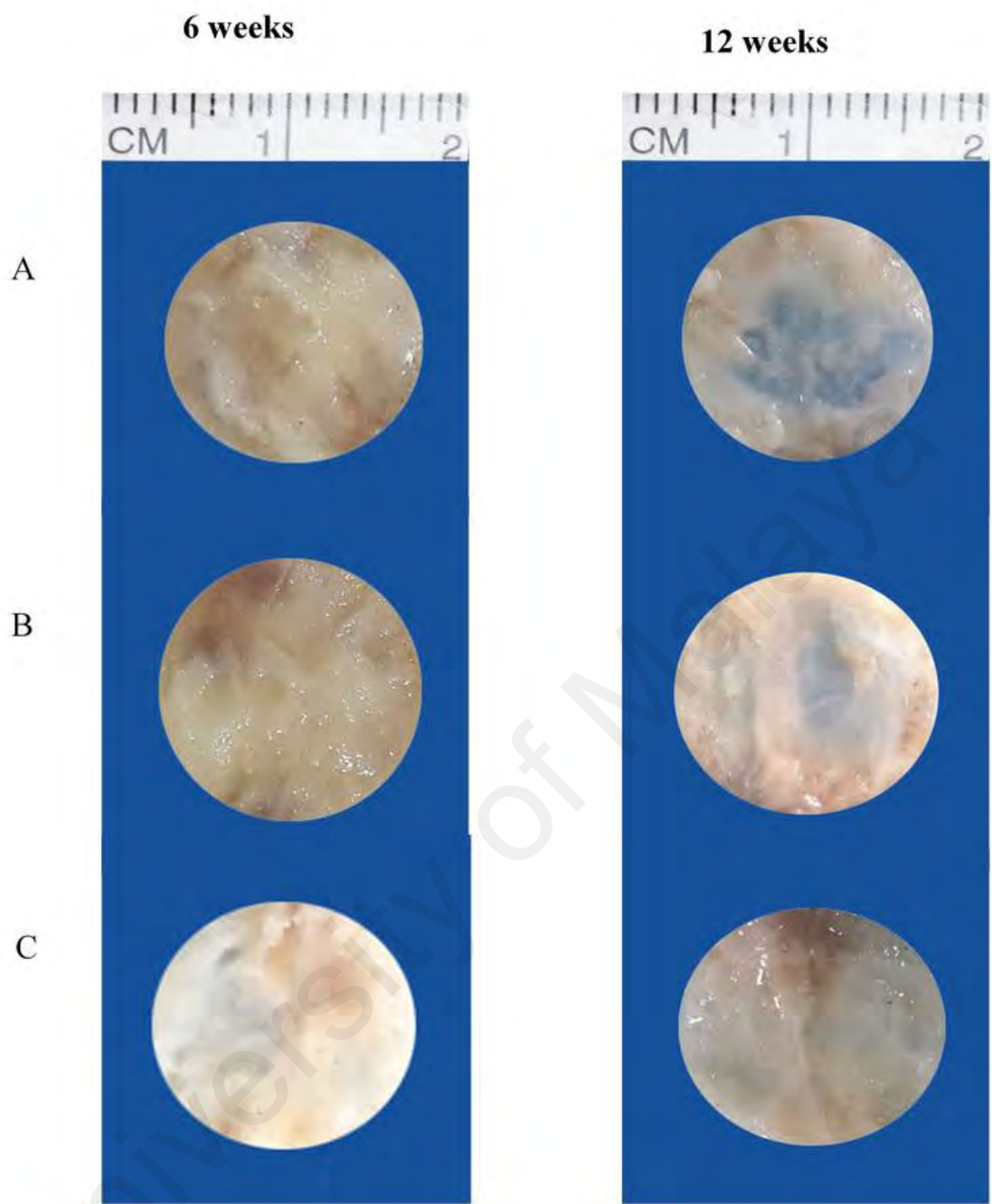
Figure 4.17: Gross appearance of specimens containing surgical defects at 6 and 12 weeks. (A) Group I, (B) Group II (C) Group III.

The results of extremeCT

3D model colour map comparison

Figure 4.18 showed the construction of a 3D model of the surgical areas of different groups at 6 and 12 weeks post-surgery. By using the Materialise Mimics, a standardized area of 15 mm × 15 mm dimension of the surgical sites was cropped for all the groups. It was observed that the bone was growing from the periphery of the defects towards the center. All groups showed evidence of surgical of closure at 6 and 12 weeks post-surgery. At 6 weeks post-surgery, the defect closure was more prominent in Group III compare to Groups II and I. At 12 weeks, Group III showed complete surgical defect closure. Meanwhile, Groups I and II showed partial defect closure, with more closure in Group II.

B

C
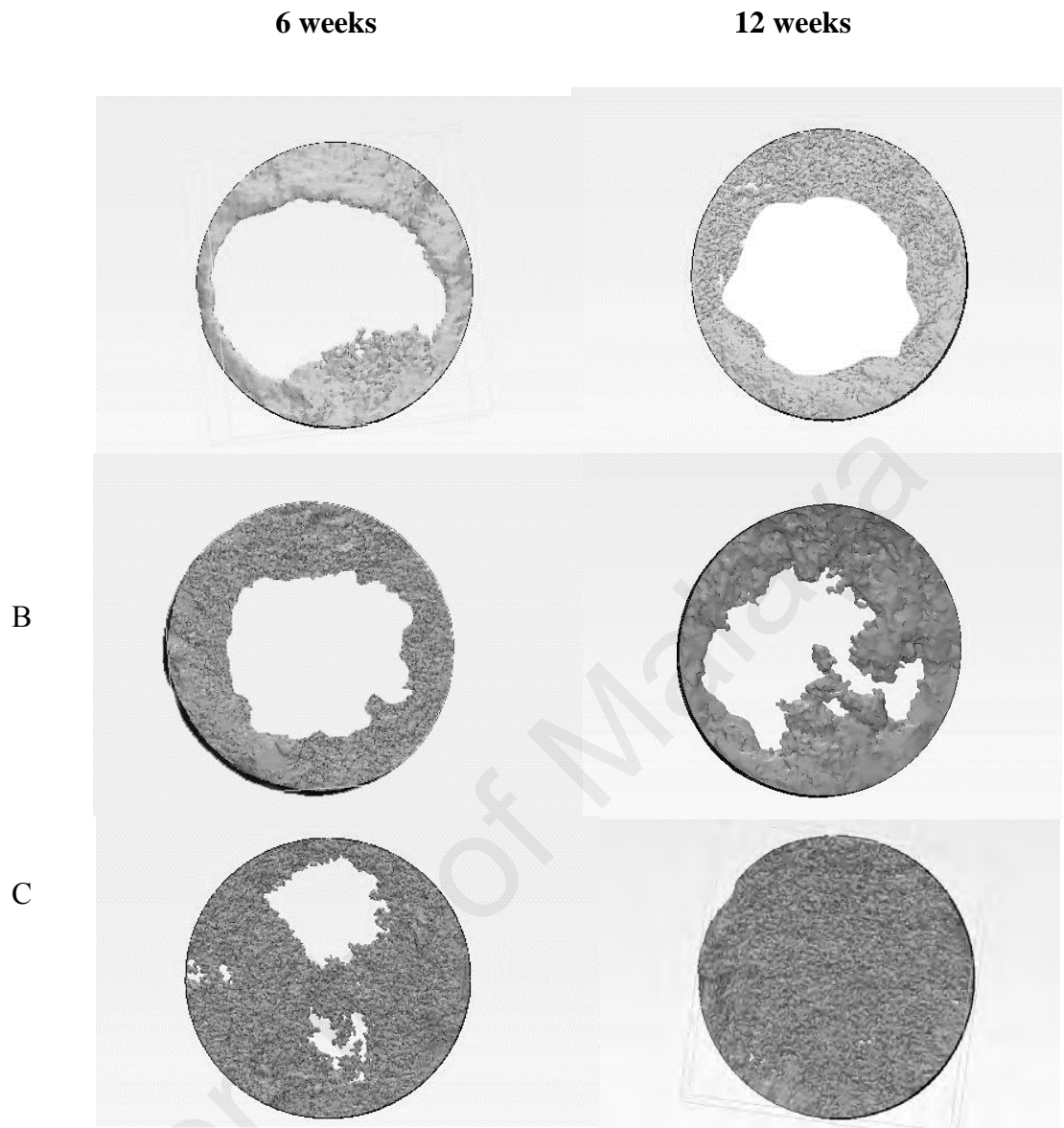
Figure 4.18: Construction of 3D model of defects. (A) group I, (B) group II (C) group III.

Figure 4.19 showed the 3D colour map for normal bone that was taken from the surgical site before surgery as a reference. The image exhibited the green color that means there is no difference between the both bone structures.

Figure 4.19: Image shows a 3D colour map for normal bone.

Figure 4.20 showed the comparison of the 3D models colour map for surgical sites at different time points. For intragroup comparison, Group I showed major differences in the healed tissues of surgical defects at 6 and 12 weeks when compared with the reference (normal bone). However, at 12 weeks, more bone formation was observed at the periphery of defect compared to at 6 weeks. Similar observation was seen in Group II, with more bone formation was observed at 12 weeks compared to at 6 weeks post-surgery. Group III showed almost complete bone formation at 6 weeks, and complete bone formation (no difference) when compared to the reference at 12 weeks.

For intergroup comparison, at 6 weeks, the tissues in Group III had the most similarity (almost complete bone formation) to the reference (normal bone) compared to Groups I and II. At 12 weeks, Group III was relatively unchanged (complete bone formation) compared to the normal bone, followed by Group II and the least bone formation was in Group I.

6 weeks **12 weeks**

A

B

C
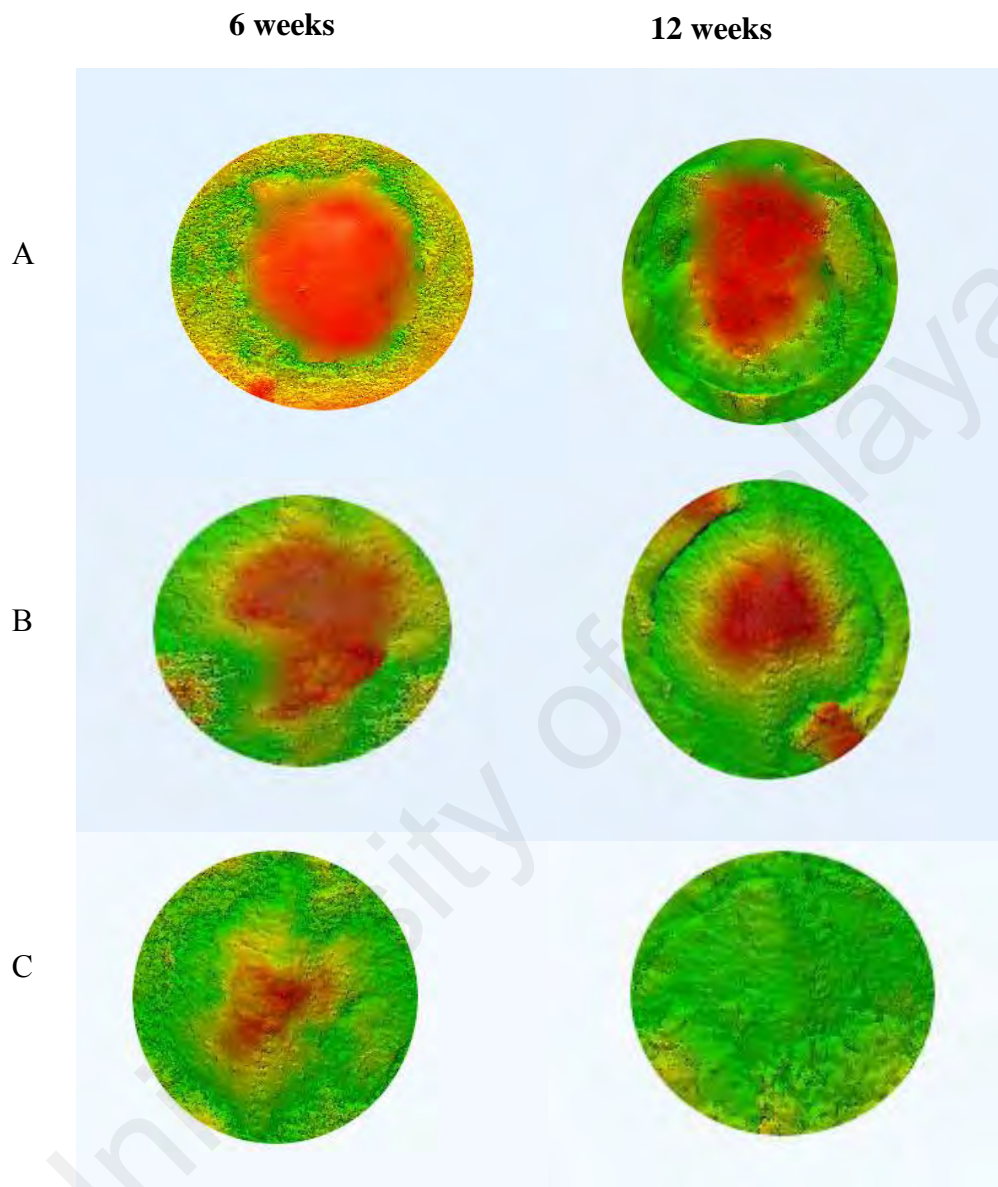
Figure 4.20: Comparison of 3D colour map of different groups at different time points (A) Group I (B) Group II (C) Group III.

Bone volume and bone volume density

Table 4.4 summarized the means and standard deviations of bone volume (mm3) and mean percentages of bone volume density for all groups over different time points.

Table 4.4: Comparison of means bone volume and bone volume density for Group I, II and III at 6 and 12 weeks.

	Bone volume (mm^3)			Bone volume density %		
	6 weeks	12 weeks	P value	6 weeks	12 weeks	[b] P value
Group I	189±36	267±55	p ≥ 0.05	21±3.2	[b]61±6	p ≤ 0.05
Group II	256±51	[ab]385±30	p ≤ 0.05	[a]45±5	[ab]77±7	p ≤ 0.05
Group III	[a]353±50	[ab]537±55	p ≤ 0.05	[a]71±1	[ab]88±2	p ≤ 0.05
[a]P value	p ≤ 0.05	p ≤ 0.05		p ≤ 0.05	p ≤ 0.05	

[a] indicates between groups significant difference over time based on One-Way ANOVA (p≤0.05). [b] indicates between groups significant difference over time based on independent-samples t-test (p < 0.05).

Intragroup comparison showed that Group III had the significantly higher bone volume at 12 weeks compared to at 6 weeks (p < 0.05). Similarly, Group II had a significantly higher bone volume of 12 weeks compared to at 6 weeks (p < 0.05). However, for Group I no significant difference in bone volume was observed when compared at 6 and 12 weeks (p > 0.05).

Intergroup comparison showed that Group III had significantly higher bone volume compared to Group I and II at both 6 and 12 weeks (p < 0.05). There was no significant difference between the bone volume of Group II and Group I at 6 weeks (p > 0.05). While there was a significant difference in the bone volume of Group II compared to group I at 12 weeks (p < 0.05).

Intragroup comparison of bone volume densities of different groups showed that there were significant differences in bone volume density at 12 weeks compared to 6 weeks in all groups.

Intergroup comparison of bone volume densities revealed that bone volume densities of group III at 6 and 12 weeks were significantly higher than group I and II ($P < 0.05$). Bone volume density in group II was significantly higher than group I at 6 and 12 weeks.

As the sample size is small, the non-parametric tests also run for comparisons and they give the same result.

Comparison of tissue density periphery and centre of healing surgical defects

Figure 4.23 showed the comparison of tissue density at the periphery and centre of defect between different groups at 6 weeks. White arrow represents soft tissue outside the defect, blue arrow represents normal bone and black arrow represents the tissue in the centre of the defect. Reference to standard the slice was an anatomical landmark.
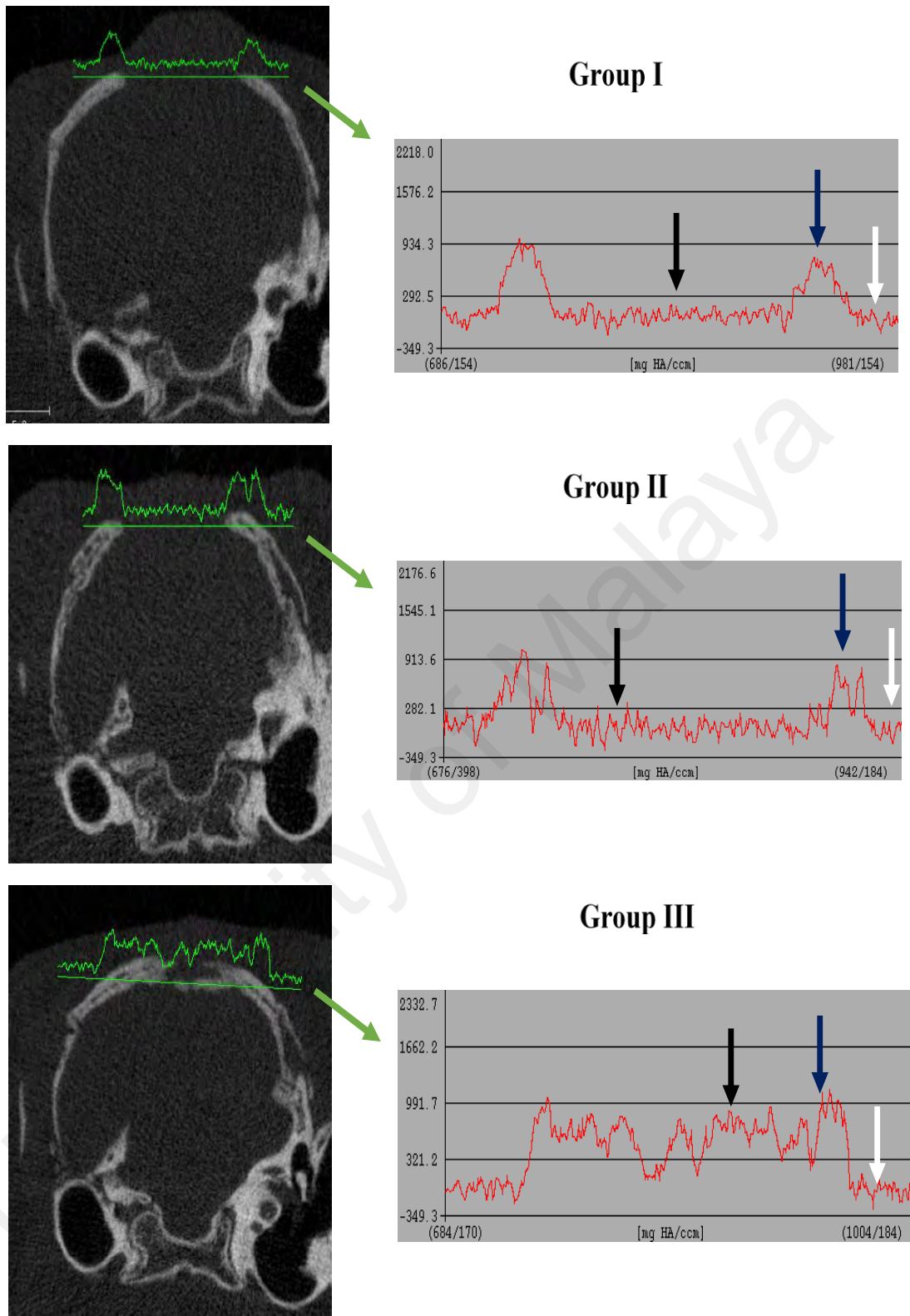
Figure 4.21: At 6 weeks: The graphs and images showed the density of tissues from outside the defect that represented the soft tissue extended to the whole defect starting from left to right in the Groups I, II and III.

At 6 week, in Group I, the density of tissue in the center of the defect (black arrow) was similar to the density of soft tissue at the periphery of defect (white arrow). Thus, the defect was filled with soft tissue. In Group II, the density of tissue in the center of the defect in was slightly higher than the density of soft tissue outside. In Group III, the density of tissue in the center of the defect was markedly higher than the density of soft tissue but less than the density of normal bone at the border of defect (blue arrow).

Figure 4.24 showed the comparison of tissue density at the periphery and center of the defect between different groups at 12 weeks. At 12 weeks, the centre of the defect was filled with soft tissue in Group I as the density of tissue in the defect is equal to the density of soft tissue outside the defect. In Group II, the density of tissue in the center of the defect was higher than the density of soft tissue but less than the density of bone. This tissue could be osteoid. While the density of tissue in the center defect of the Group III had almost the same density of bone on the border of the defect.
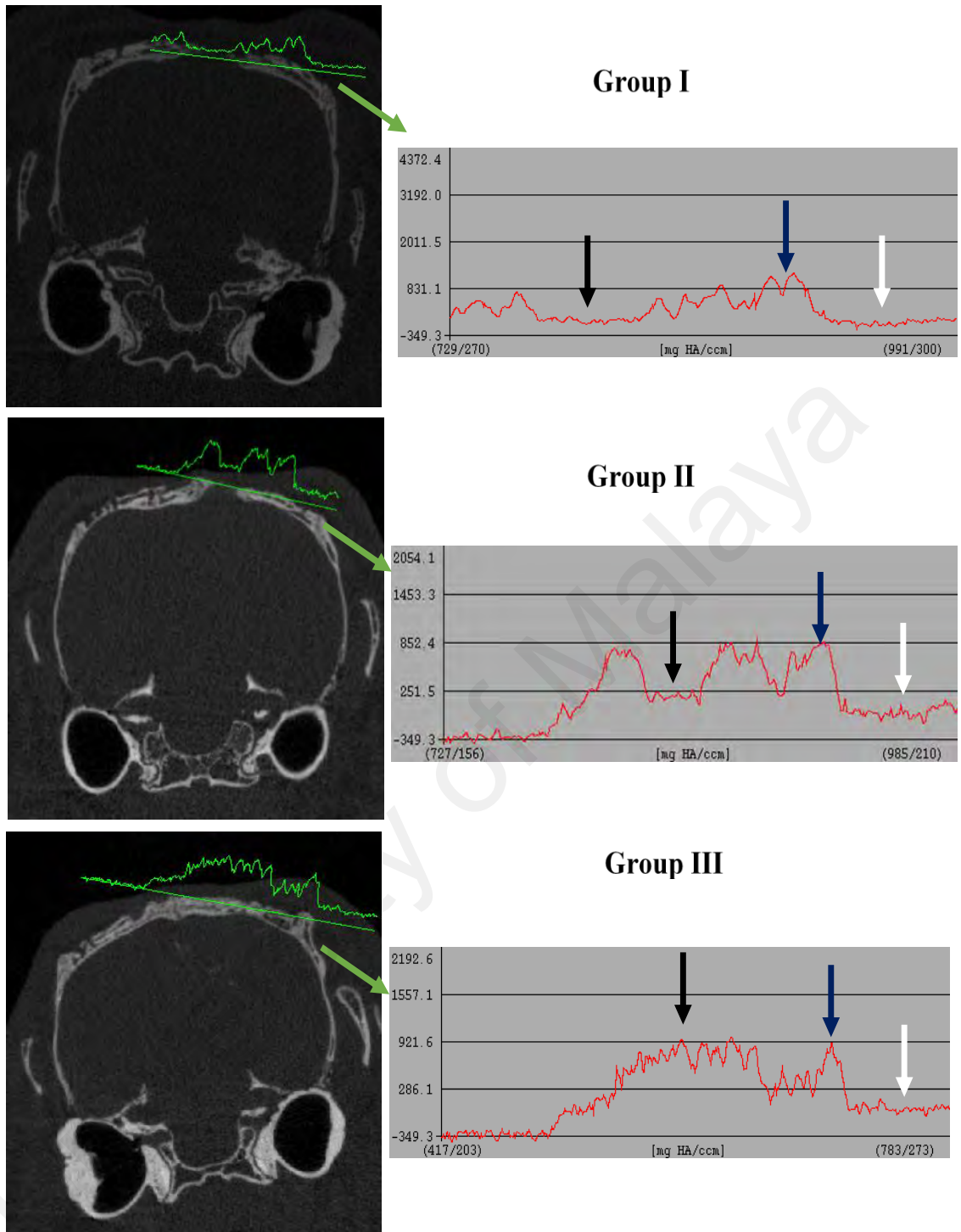
Figure 4.22: At 12 weeks**:** The graphs and images show the density of tissues from outside the defect that represented the soft tissue extended to the whole defect starting from left to right in the Groups I, II and III.

Hematoxylin and eosin stain results

The histological features of untreated and treated groups were observed, as shown by H and E staining. The normal bone was taken from a parietal bone on the same site of surgery to use as a reference. Figure 4.25 showed histological examination of the normal bone sections was showed normal architecture. The bone is lamellar and mature. The connective tissue within the normal bone was less prominent than that of the experimental defects.
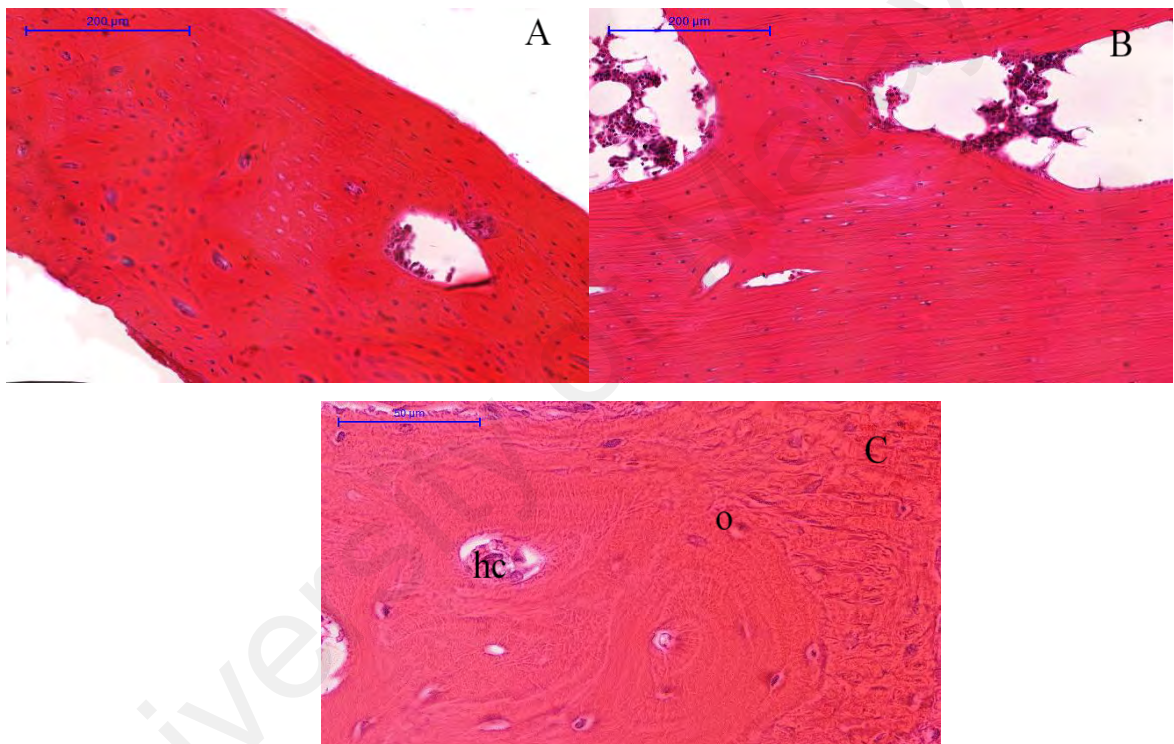
Figure 4.23: Photomicrograph of normal bone showing (A) the bone at the periphery and (B) center of bone H and E staining (Scale bar=200µm). (C) The bone section at high magnification (Scale bar=50µm), Osteocyte (o), Haversian canal (hc).

Figure 4.26 showed that at 6 weeks, the defects were filled with new bone and osteoid tissues in Group III, new bone and fatty marrow in Group II, less new bone formed in Group I.
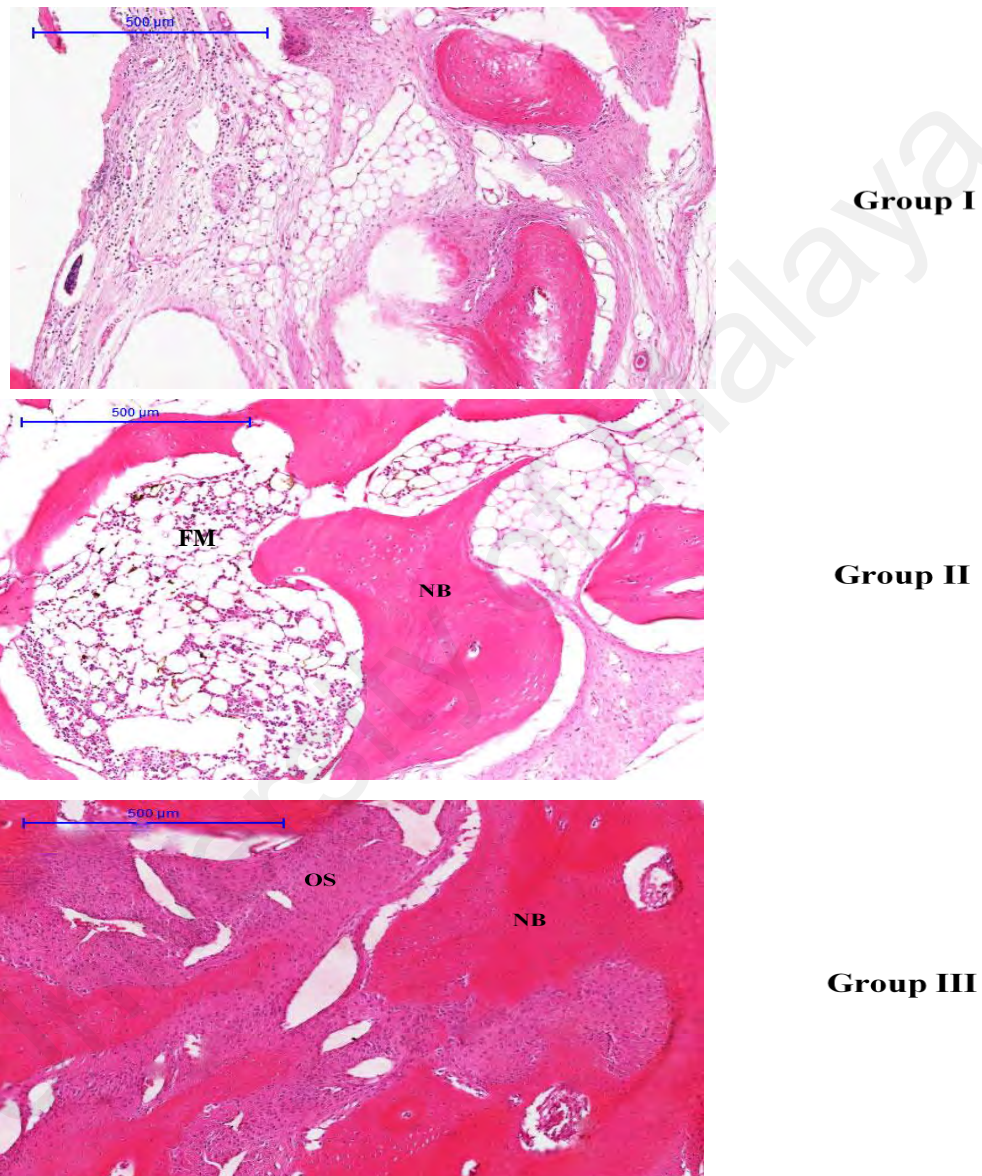
Figure 4.24: At 6 weeks: Photomicrographs of Groups I, II and III sites showed H and E staining of the bone sections. New bone (NB), Osteoid (OS), Fatty marrow (FM). (Scale bar: 50 µm).

At 6 weeks, the newly formed bone in the defects of experimental groups (Groups II and III) was higher compared to that formed in the defects of the control group (Group I). The connective tissue within the bone bridge in the Groups II and III was less prominent than that in Group I. No grafts particles were seen in 6 weeks and they were completely resorbed. New bone fill in each of the defects was expressed as osteoid bone within the region of interest. The trabecular bone in the Group II appeared thick and dense while the trabecular bone in the Group III had become lamellar bone.

Figure 4.27 showed the histological section in Group III that showed the newly formed bone had filled the defect completely. The newly formed bone resembled a bridge, which was arranged in a lamellar form in some areas with large osteons and Haversian canals containing highly cellular connective tissues within it especially at the central part.
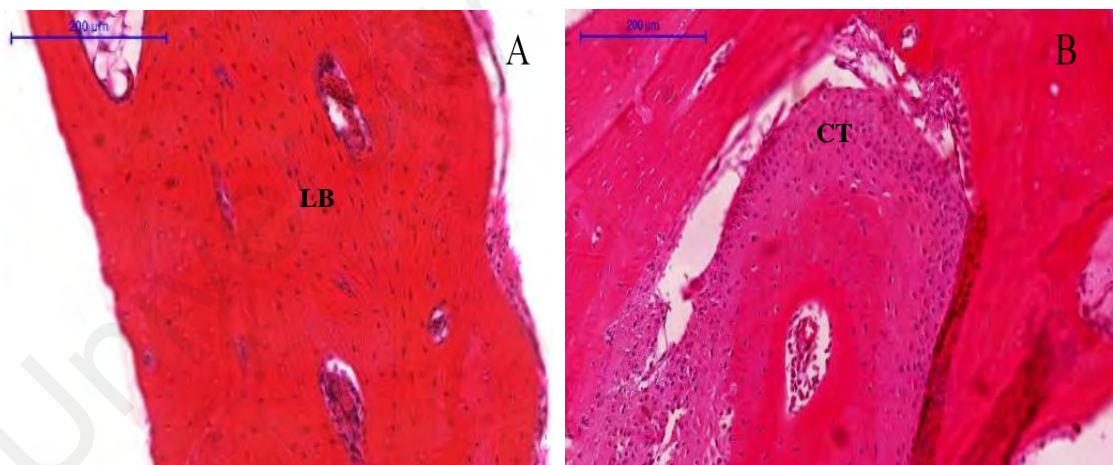
Figure 4.25: At 12 weeks: Photomicrograph of group III site showed the bone defect region closed by (A) mature bone (LB) that was fused to the host bone defect margin with (B) little connective tissue (CT) in the middle of defect. H and E staining (Scale bar=200µm).

Figure 4.28 showed the histological section in Group II that revealed a discontinuous bone tissue layers centrally whereas it was continuous at the margins.
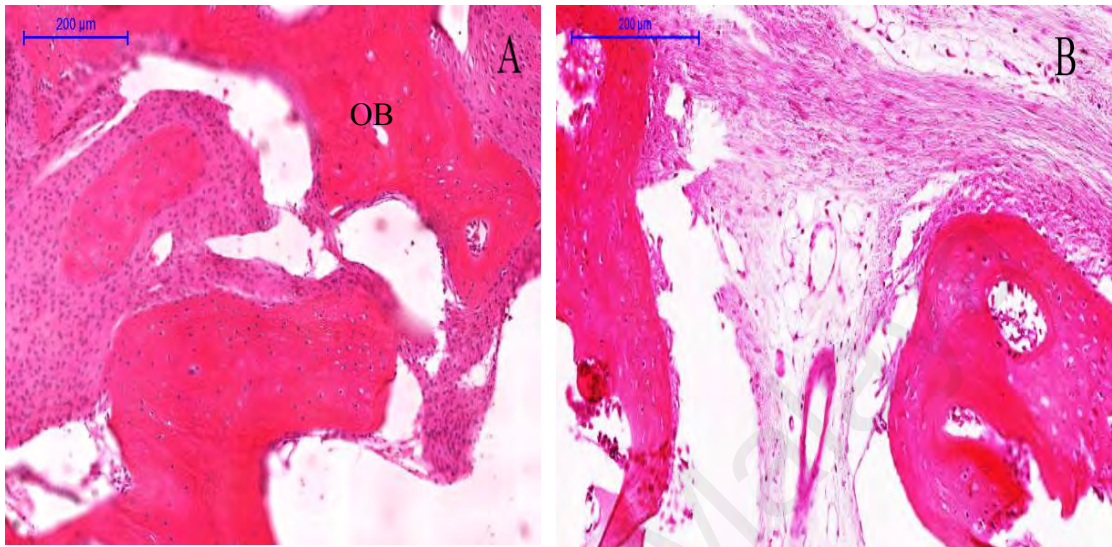
Figure 4.26: At 12 weeks: Photomicrograph of Group II show (A) the bone defect region filled with the continuous osseous bridge (OB) at the peripheral area of the defect and (B) discontinuous bone layers in the central part of the defect. H and E staining (Scale bar=200μm).

Figure 4.29 showed in Group I, the defect was not completely filled with bone trabeculae. Numerous osteoclasts were observed and osteogenic connective tissue filled the central gap of the defect.
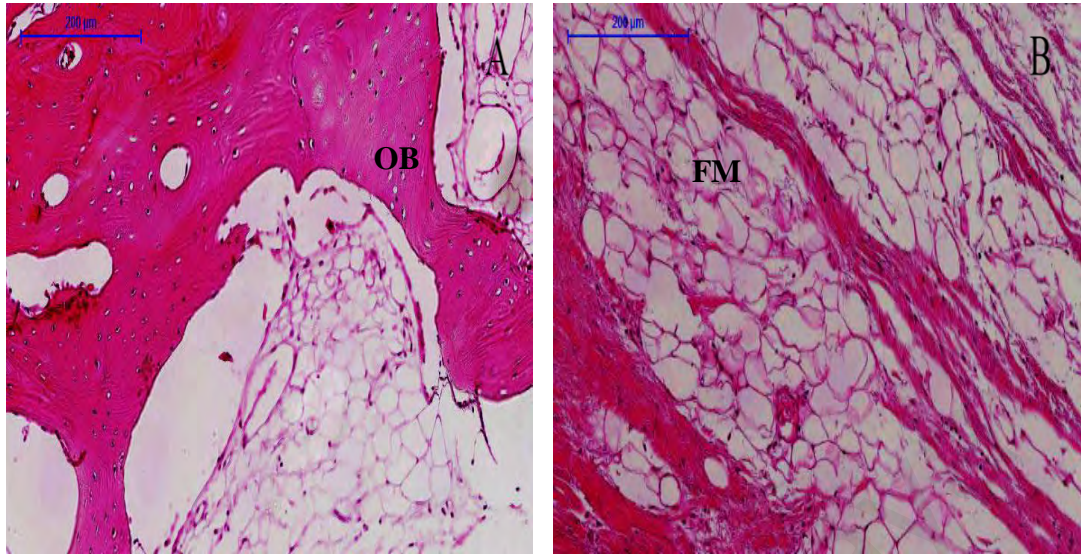
Figure 4.27: At 12 weeks: Photomicrograph of Group I show (A) the bone defect region filled with thin and continuous osseous bridge (OB) at the peripheral area of the defect and (B) Fatty marrow (FM) in the central part of the defect. H and E staining (Scale bar=200µm).

Figure 4.30 showed at high magnification, H and E staining of Group III showed more organized mature bone with osteon that has been formed with large harversian canals and lamellar bone. While in Group II showed discontinuous bone layers. However, Group I showed fatty marrow.
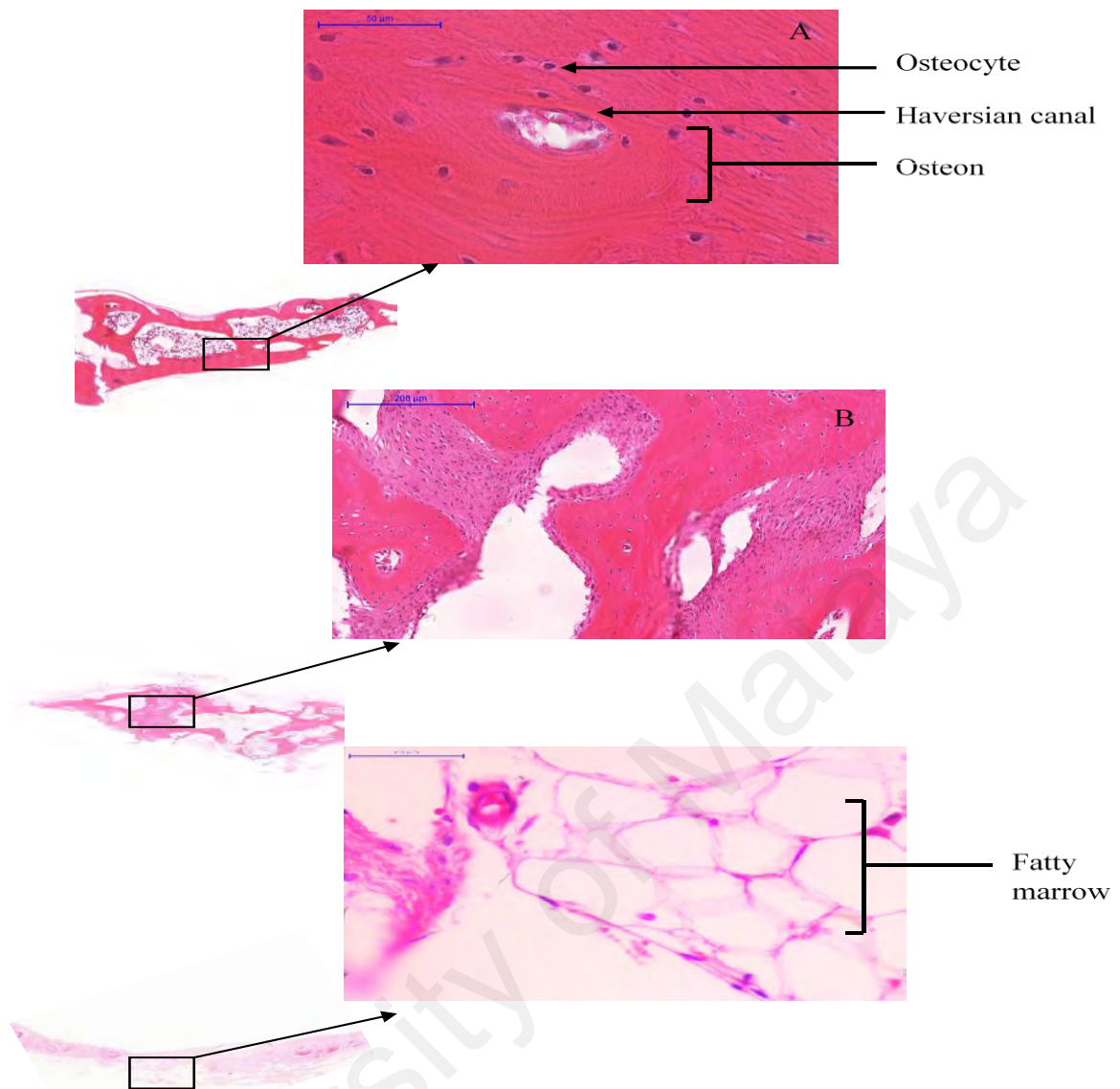
Figure 4.28: At 12 weeks: Photomicrograph of H and E staining. (A) Group III show osteon, large harversian canals and osteocyte (Scale bar=50µm). (B) Group II show discontinuous bone layers (Scale bar=200µm). (C) Group I show fatty marrow (Scale bar=50 µm).

Immunohistochemistry results

Osteoblast markers

At 6 weeks, osteopontin (OPN) immunolabeling was observed in the osteoclasts, osteoblast, and fibroblasts. In nearly all specimens OPN immunoreactivity appeared in the matrix of compact bone, cancellous bone, and osteoid. Osteocalcin (OC)

immunoreactivity appeared in the matrix of compact bone, less often in cancellous bone, and osteoid (Figure 4.31).
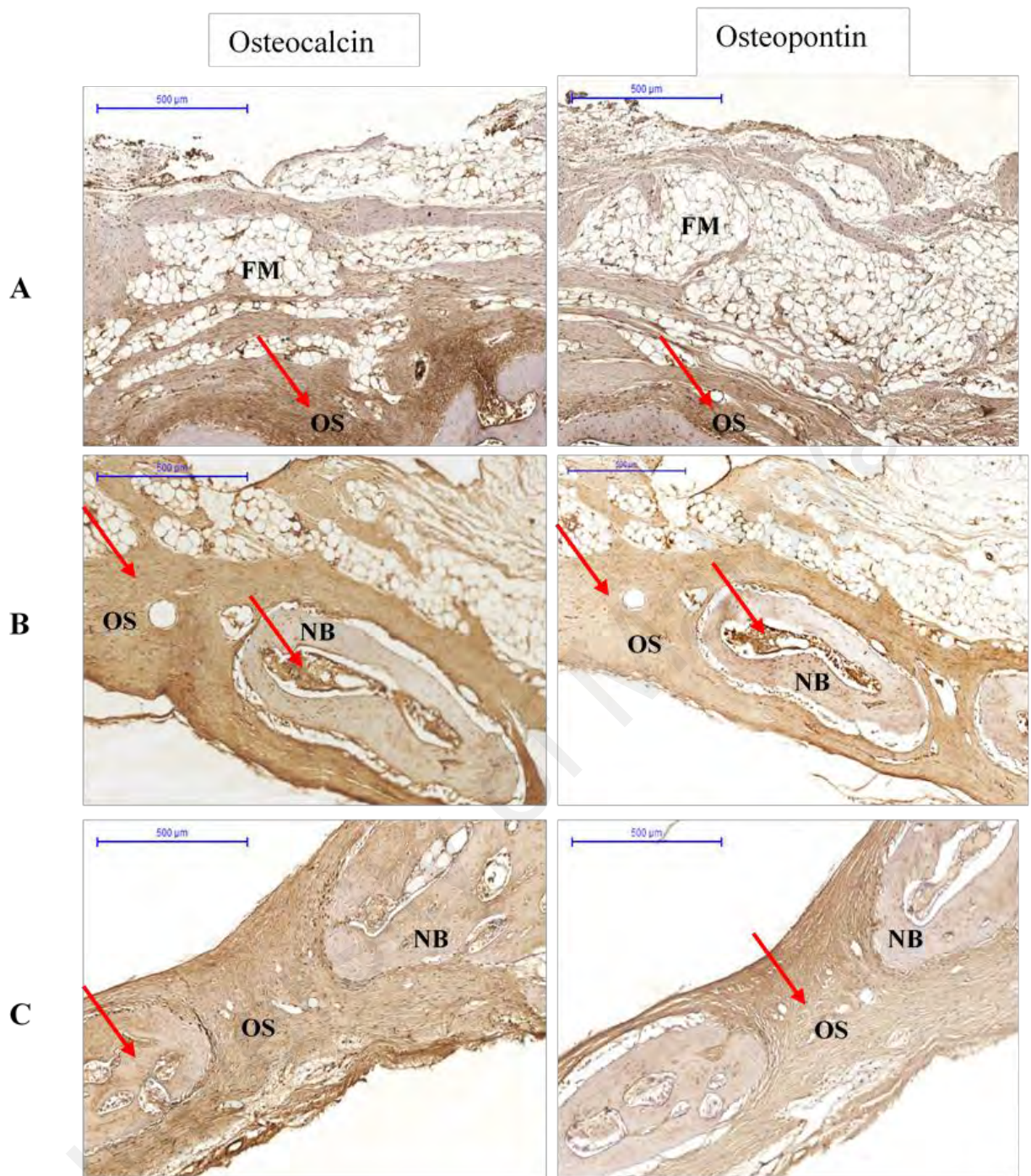
Figure 4.29: Photomicrographs of immunostaining for osteocalcin and osteopontin in (A) Group I, (B) Group II (C) Group III at 6 weeks. The pictures are arranged by staining technique (columns) and the investigated treatment (rows). Areas that stained positive for osteocalcin and osteopontin are indicated by red arrowheads. NB, new bone; OS, osteoid; FM, fatty marrow.

Table 4.5 shows the means of OPN and OC expressions percentages in groups I, II and III at 6 weeks.

Table 4.5: Comparison of means OPN and OC expressions % for Group I, II and III at 6 weeks

	Group I	Group II	Group III
OPN expression%	41 ± 3	57 ± 5	73 ± 3
OC expression%	45 ± 2	64 ± 4	78 ± 4

Based on the parametric test, One-Way ANOVA test, there was a significant difference in the mean percentage of OPN expression between Group III and Group I ($p < 0.05$). The highest expression of OPN was observed in the group III followed by Group II when compared to Group I (Figure 4.32).
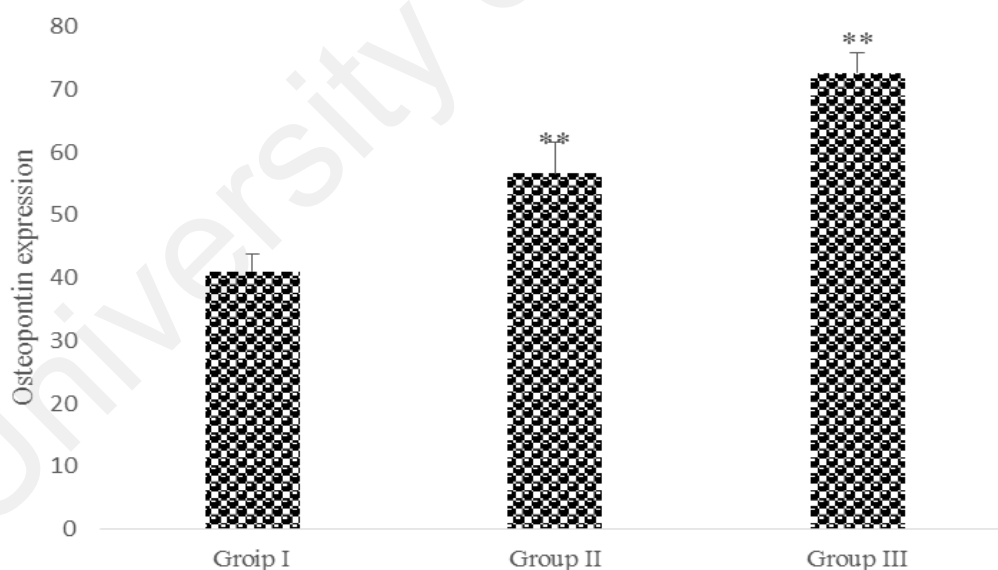
Figure 4.30: At 6 weeks: Statistical analysis of expression percentage of osteopontin as bone formation marker between Groups I, II and III. Data are presented from three independent experiments (n=3). Statistical differences between control and experimental groups were set at **$p < 0.05$.

Statistical analysis of expression percentage of osteocalcin shows that there was a significant difference in the mean percentage of OC expression between Groups III, II,

and I (p < 0.05). The highest OC expression was found in group III followed by Group II (Figure 4.33).
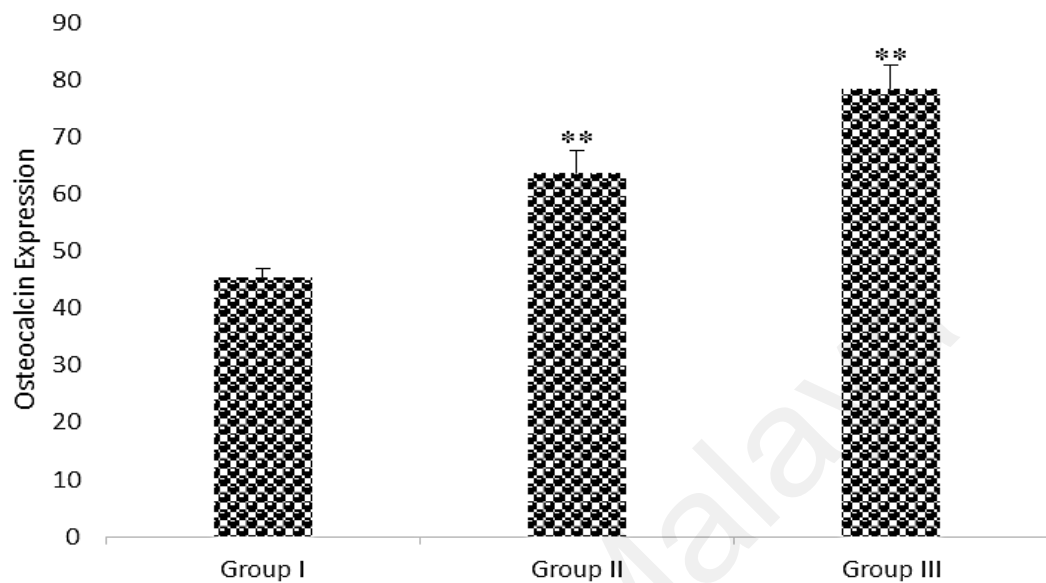
Figure 4.31: At 6 weeks: Statistical analysis of expression percentage of osteocalcin as bone formation marker between Groups I, II and III. Data are presented from three independent experiments (n=3). Statistical differences between control and experimental groups were set at **p < 0.05.

At 12 weeks, OPN expression was characterized by osteoid staining in all investigated groups. OPN immunolabeling was observed in osteoblasts. Stained areas in the bone matrix also occurred. OC was detected in a matrix of compact bone, but less expressed in osteoid and bone cells (Figure 4.34).
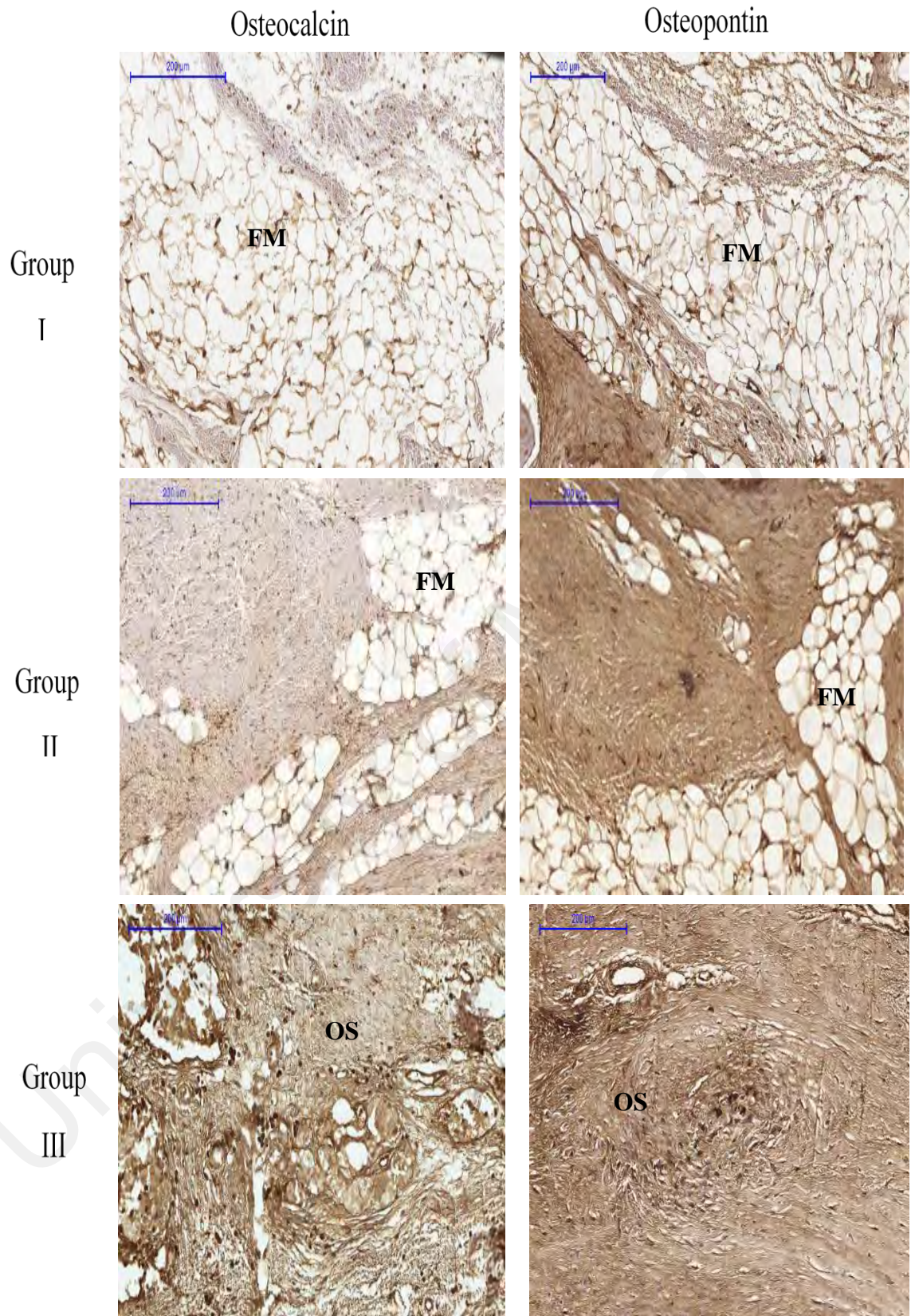
Figure 4.32: Photomicrographs of immunostaining for osteocalcin and osteopontin in (A) Group I, (B) Group II (C) Group III at 12 weeks. The pictures are arranged by staining technique (columns) and the investigated treatment (rows). Areas that stained positive for osteocalcin and osteopontin are indicated by red arrowheads. OS, osteoid; FM, fatty marrow.

Table 4.6 shows the percentage of OPN and OC expressions percentages in groups I, II and III at 12 weeks.

Table 4.6: Comparison of means OPN and OC expressions % for Group I, II and III at 12 weeks.

	Group I	Group II	Group III
OPN expression%	38 ± 5	41 ± 8	50 ± 6
OC expression%	24 ± 5	32 ± 2	60 ± 12

Based on the parametric test, One-Way ANOVA test, there was no significant difference in the mean percentage of OPN expression between group II and I ($p > 0.05$). While there was a significant difference in the mean percentage of OPN expression between the group III compared to group I ($p < 0.05$) (Figure 4.35).
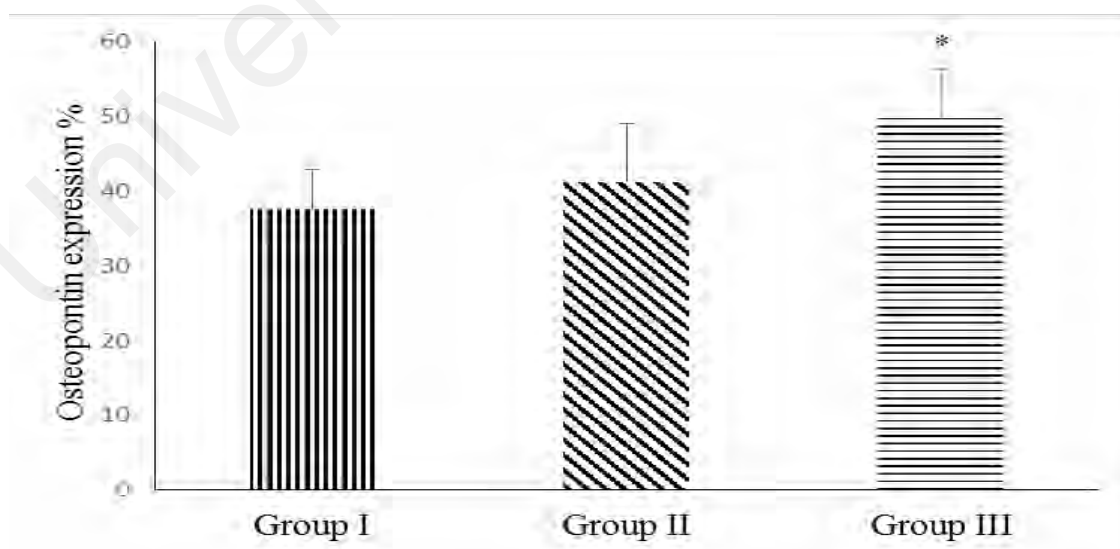
Figure 4.33: At 12 weeks: Statistical analysis of OPN expression percentages between Group I, II and III. * Significant difference in Group III compared to the Group I.

Regarding OC expression, there was a significant difference in the mean percentage of OC expression when compared between Groups II and Group I (P < 0.05). There was also a significant difference in the mean percentage of OC expression between the Group III and Group I (P < 0.05). The highest OC expression was found in group III followed by Group II (Figure 4.36).
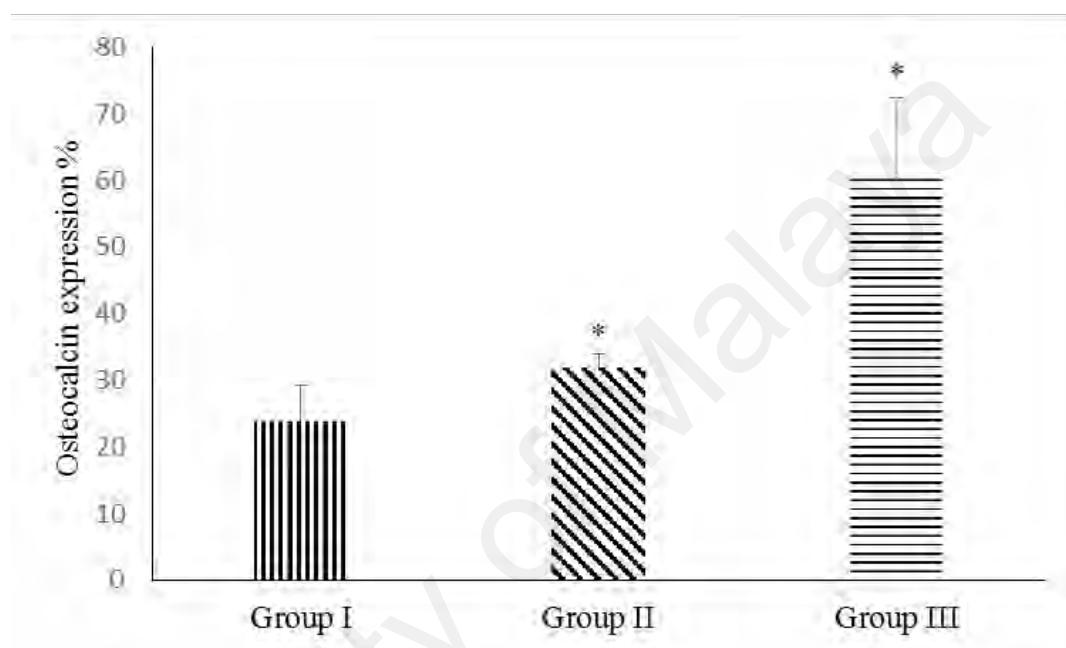
Figure 4.34: Statistical analysis of OC expression percentage as bone formation marker between Groups I, II and III. * Significant difference of Groups III and II compared to Group I.

In intragroup comparison, there is a significant difference in OPN expressions between 6 weeks and 12 weeks in all groups (p < 0.05). The higher expression of OPN was at 6 weeks in all groups. Similarly, there is a significant difference in OC expressions between 6 weeks and 12 weeks in all groups and the higher expression was at 6 weeks.

Comparing between the expression of both OPN and OC at 6 weeks and 12 weeks in all groups, there was no significant difference between the expression of OPN and OC in group III (p > 0.05). While in group II, there was a significant difference between the expression of OPG and OC at 6 weeks (p < 0.05).The osteocalcin had higher

expression. But in group I, there was a significant difference between the expression of OPN and OC at 12 weeks. The higher expression was in OPN marker.

As the sample size is small, non-parametric tests were also carried out and similar results were obtained.

Osteoclast marker

Cathepsin K is expressed and secreted by osteoclasts during active bone resorption. Cathepsin K may be a useful and specific biochemical marker of osteoclastic activity. More cathepsin K-positive areas were observed in the medullary region of the defect site than the cortical bone region at both 6 and 12 weeks. Cathepsin K-positive multinuclear cells were also detected within the newly-formed bone. In addition, fewer osteoclasts were detected at 12 weeks compared to the 6-week samples in all groups (Figure 4.37).
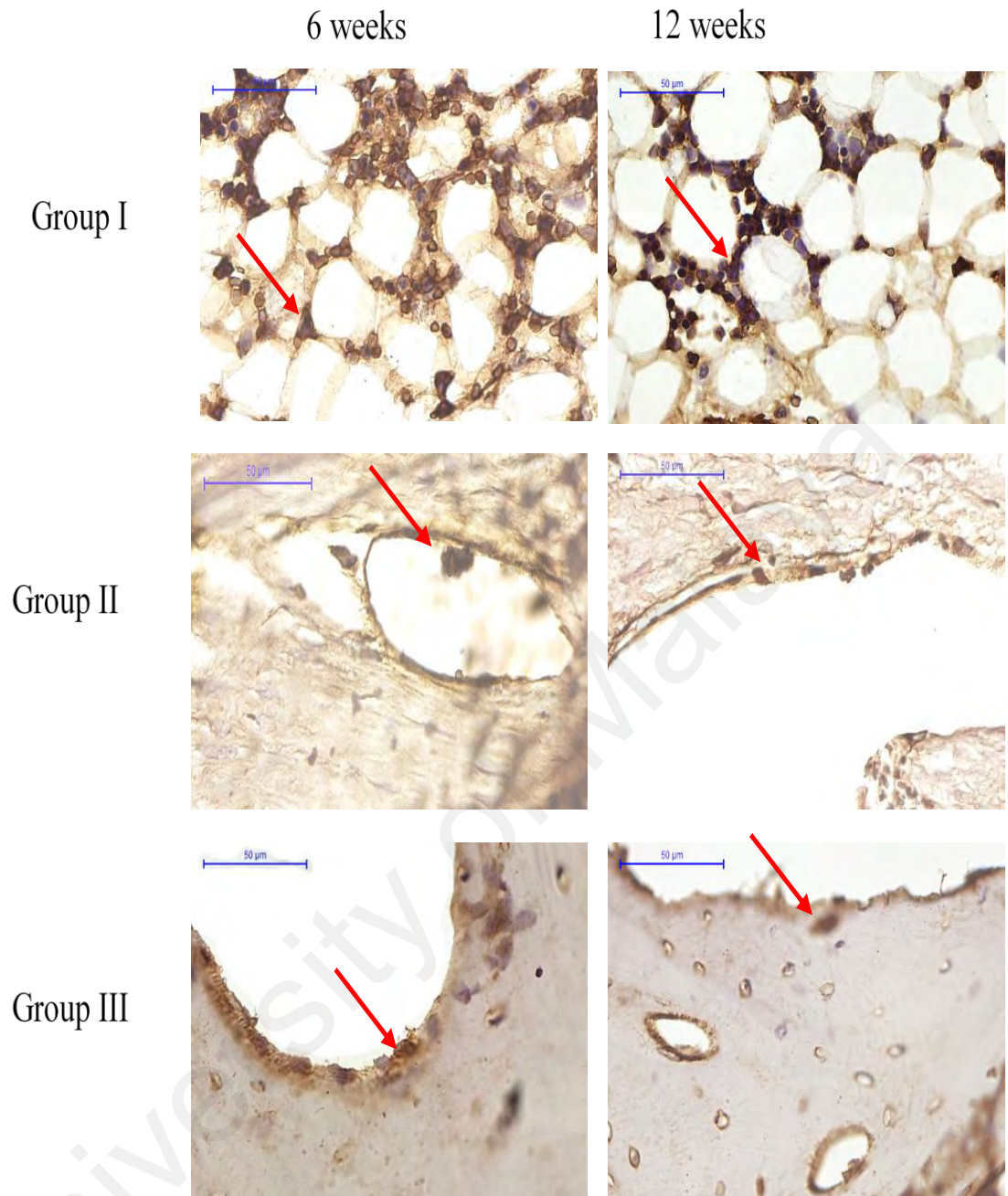
Figure 4.35: Cathepsin K immunostaining of osteoclast was performed at 6 and 12 weeks after surgery in Groups I, II and III. Cathepsin K-positive multinuclear cells (red arrowhead).

Serum biochemical parameters

Serum biochemistry data of rabbits treated in Groups II and III and group I (untreated rabbits) at the baseline and after 6 and 12 weeks of treatment are summarized in Tables 4.6 and 4.7. There were no significant changes in the levels of creatinine and urea nitrogen. In addition, no significant differences in serum electrolytes such as calcium, potassium, chloride were noted. The effects of OPG and/or chitosan on liver function parameters such as albumin, alanine aminotransferase, G-glutamyl transferase, alkaline phosphate and total bilirubin in serum were also examined. Animals treated in Group II and III and Group I (untreated animal) did not exhibit differences in these hepatic markers. Their effects on triglyceride, high-density lipoprotein cholesterol HDL, and total cholesterol levels are shown Table 4.8 and 4.9. Similarly, the treated rabbits showed no significant changes in triglyceride, HDL cholesterol and total cholesterol levels in different groups after treatments.

Table 4.7: Serum biochemical data for rabbits treated with OPG-chitosan and chitosan gels and untreated rabbits (control) at the base time and after 6 weeks of treatment.

Parameter	Pretreatment			Posttreatment			Normal range
	Group III	Group II	Group I	Group III	Group II	Group I	
Sodium mmol/L	142± 0	142±1	141±1	143 ± 0	141±1	141±0.7	139-146
Potassium mmol/L	4 ±0.1	5±0.4	5±0.7	3.8 ±0.1	3.95±0.1	5±0.6	3-5
Chloride mmol/L	103 ±0.7	102±0	101.5±0.2	100±4.2	101±1	99.5±4	104-116
Urea nitrogen mmol/L	8±0.42	7±1.5	8±0.2	6±1.5	7±0.07	9±0.07	6.35-16
Creatinine μmol/L	77 ± 6	78±2	77±5	102±15	77±7	85±4	60-140
Albumin (g/L)	41±0.0	38±1	41±1	39±4	40±4	40±1	20- 40
Total Bilirubin (μmol/L)	< 2	< 2	< 2	< 2	< 2	< 2	2-5
Alkaline Phosphate (U/L)	102 ±6	111±8	110±4.9	50 ± 10	81±3	69 ± 3	17-192

Table 4.8: Continued: Serum biochemical data for rabbits treated with OPG-chitosan and chitosan gels and untreated rabbits (control) at the base time and after 6 weeks of treatment.

Parameter	Pre-treatment			Posttreatment			Normal range
	Group III	Group II	Group I	Group III	Group II	Group I	
Alanine Aminotransferase (U/L)	30.5±3	94.5±2	36±15	35±0	53±12.7	52.5±3.1	38-86
G-Glutamyl Transferase (U/L)	5.5±0.7	5.5±0.9	2.5±0.7	6±1.5	6.5±1.4	5±1.4	6-22
Triglyceride (mmol/L)	0.5±0.1	0.7±0.1	0.65±0.2	0.5±0.1	0.7±0.15	0.75±0	-
Total Cholesterol (mmol/L)	1±0.2	0.9±0.1	1.1±0	1.3±0.3	0.85±0.2	1.2±0.1	-
HDL Cholesterol (mmol/L)	0.8±0.2	0.61±0.1	0.8±0.2	0.2±0.1	0.62±0.1	0.8±0.1	-
LDL Cholesterol (mmol/L)	0.9±0.2		0.2 ±0.1	0.1 ±0.3	0.2±0.5	0.1 ±0.4	-

Data are expressed as means ± SD of 3 rabbits for each group.

Table 4.9: Serum biochemical data for rabbits treated with OPG-chitosan and chitosan gels and untreated rabbits (control) at the base time and after 12 weeks of treatment.

Parameter	Pre-treatment			Posttreatment			Normal range
	Group III	Group II	Group I	Group III	Group II	Group I	
Sodium mmol/L	142± 2	142± 1	143±2	142± 2.6	143±1	143± 2	139.3-145.7
Potassium mmol/L	4±1	4±0.3	4±0.4	4±0.6	4±0.4	4±0.5	3-5
Chloride mmol/L	100±0.5	101±0.6	98±3.5	102±0.2	101±2	104±4	105-116
Urea nitrogen mmol/L	8±1	8±1	9±0.4	8±1	7±1	8±1	6-16
Creatinine µmol/L	85.7±10	87±1	89±2	89±10	83±2	87± 1	60-140
Albumin (g/L)	43.3±3	40.7±1	42±1	41±2.9	40±3	39±3	20 - 41
Total Bilirubin (µmol/L)	< 2	< 2	< 2	< 2	< 2	< 2	2-5
Alkaline Phosphate (U/L)	68.5±12	44±3	69.5±8	58±1	44±9	48±8	17-192

Table 4.10: Continued: Serum biochemical data for rabbits treated with OPG-chitosan and chitosan gels and untreated rabbits (control) at the base time and after 12 weeks of treatment.

Parameter	Pre-treatment			Posttreatment			Normal range
	Group III	Group II	Group I	Group III	Group II	Group I	
Alanine Aminotransferase (U/L)	58±6.9	60±9.7	48.7±10	53.7±15.8	67±12	54±7	38-86
G-Glutamyl Transferase (U/L)	6±1.2	7±1.5	3±1.4	4±0.6	7±1.7	5±1.2	6.00-22.00
Triglyceride (mmol/L)	0.7±0.5	0.6±0.2	0.4±0.01	1.2±0.2	0.6±0.2	0.5±0.2	-
Total Cholesterol (mmol/L)	1±0.2	1±0.2	1±0.2	1±0.2	1±0.2	1±0.2	-
HDL Cholesterol (mmol/L)	0.7±0.1	0.5±0.03	0.7±0.1	0.9±0.04	0.6±0.1	0.6±0.1	-
LDL Cholesterol (mmol/L)	0.2±0.1	0.2±0.08	0.1±0.1	0.1±0.1	0.2±0.1	0.26±0.1	-

Data are expressed as means ± SD of 3 rabbits for each group.

CHAPTER 5: DISCUSSION

There is no study yet that formulates OPG with chitosan as its matrix material so in this study, we formulated a new gel comprising OPG for bone tissue regeneration where OPG is released over a prolonged period of time to inhibit the bone resorption. The present study evaluated the biocompatibility and osteogenic potential of newly formed OPG-chitosan gel *in vitro* and *in vivo*. To date, this is the first study to apply OPG protein locally via chitosan gel.

Discussion on materials and methods
Optimization of OPG-chitosan gels formulation

Before novel material can be applied in clinical practice, tests must be undertaken to ensure that this material is non-toxic to the human tissue. *In vitro* biocompatibility test has to be conducted to ensure the material is safe for *in vivo* studies (animal/human). The materials that were selected in this study undergone the biocompatibility test that included the cytotoxicity and proliferation tests. For local delivery of OPG, chitosan was selected as it has properties that make it an ideal material for biomedical applications such as anticholesterolemic and antimicrobial activity, biocompatibility, biodegradability, fungistaticity, hemostatic potential, non-carcinogenicity, nontoxic, accentuated affinity to proteins, mucoadehesive material, as well as promotion of cell adhesion, proliferation, and differentiation (Coimbra et al., 2011b). In this biocompatibility tests, OPG, chitosan or combinations were tested on NHPL fibroblast cell line as it is one of the important cells involved in the healing process. The NHPL fibroblast cell is one the main cells that contribute to the periodontal bone regeneration as it has osteoblast-like properties such as alkaline phosphatase activity, vitamin D-dependent production of osteocalcin and initiation of mineral-like nodules in the presence of a supportive medium (Basdra & Komposch, 1997; Jönsson et al., 2011;

Scanlon et al., 2011). The water-soluble chitosan was selected to formulate the OPG-chitosan gel as it does not require an acidic vehicle to render it soluble while hydrophobic chitosan required acidic environment (at pH > 5.0), which might be harmful to tissue (Pang, et al., 2005). The using of chitosan binderin gel formulation gaves a rise to controlled drug delivery systems exhibiting sustained drug release (Nunthanid et al., 2004).

AB assay is a water-soluble dye that has been previously used for quantifying *in vitro* viability of various cells (Rampersad, 2012; Bonnier et al., 2015). AB is stable and more importantly non-toxic to the cells, continuous monitoring of cultures over time is possible (Mirmohammadsadeghi et al., 2012). Hence, in this study, cell viability and proliferation was evaluated by comparing the color change in response to the chemical reduction of growth medium immersed in a test sample versus non-exposure in the control group. A reduction of AB assay by cells indicates the presence of metabolically active cells (Kries et al., 2010; Divieto & Sassi, 2015). This reduction of the AB is theoretically proportional to the growth rate and viability of cells.

For FTIR spectroscopy, attenuated total reflectance (ATR) is an IR sampling technique that provides excellent quality data in conjunction with the best possible reproducibility of any IR sampling. The major advantages of FTIR using ATR technique adopted in this study as compared to the transmission technique because it has high quality spectrum for qualitative analysis, minimal sample preparation (nondestructive and time efficient), ability to analyze liquids, solids, gels or coating, spectra are not affected by sample thickness as the radiation penetrates only a few micrometers, provides highly reproducible results and can be used for a wide variety of sample types (Grdadolnik, 2002).

For physicochemical properties, thermal properties of the gel were evaluated by using TGA and DSC. These tests were conducted to ensure the thermal stability of the OPG-chitosan gel. The swelling test and equilibrium water content were analyzed because the water binding capacity of the grafting material plays an important role in tissue regeneration and the swelling ratio strongly depends on the hydrophilic nature (Yan, et al., 2010). A bioactive polymer 3D scaffold absorbing an adequate amount of water shows properties comparable to living tissue such as physiological stability, permeability to biomolecules and low interfacial tension. In order to ensure the OPG-chitosan gel has stable structure that stay for time enough for bone regeneration, the degradation rate of gel and protein release manner was evaluated. We selected the concentration of lysozyme correspond to the concentration in human serum (Porstmann et al., 1989; Freier, et al., 2005). It is well known that, in human serum, chitosan is mainly depolymerized enzymatically by lysozyme, and not by other enzymes or other depolymerization mechanisms (Vårum et al., 1997).

In vivo evaluation of OPG-chitosan gel

In order to have a clear understanding of the efficacy, pathophysiological interactions, and potential toxicities of novel therapies, we have to study the formulated material *in vivo*. This is especially important with "first-in-man" studies of novel therapies (Korsmeyer, 1999). We selected rabbit as animal model because it is one of the most commonly used animals for medical research and covers approximately 35 % of musculoskeletal research studies (Neyt et al., 1998). It is also one of the International Standards established regarding the species suitable for testing implantation of materials in bone for reconstruction, fracture or osteotomy, bone in-growth and bone defect repair and for evaluating the potential application of the material such as the process of material degradation and replacement by host tissue. Our study approved the potential of using the OPG-chitosan gel in aiding of bone healing in the rabbit calvaria

(International Standard ISO 10993-6, 1994). It has been shown that the animal calvaria is an accurate and reproducible mode for testing bone graft materials as it has many similarities to the maxillofacial region as acceptor site (Isaksson, 1991). It has a good size for the easier surgical procedure and specimen handling and it is a plate which permits creations of a uniform circular defect that allows appropriate radiographic and histological analysis. Also, the cranial defect does not require fixation as it is supported by dura and the overlying skin (An & Freidman, 1998). Regarding sample size, three rabbit in each group is suitable for this study according to sample size formula for animal studies published in 2013 (Charan & Biswas, 2013).

In the present study, the defects could be created safely between the frontal and interparietal skull bone without touching the coronal or lambdoid suture in order to avoid as much fibrous suture tissue within the defect as possible. In order to create a defect with the same thickness of bone on either side of the sagittal suture at the parietal bone anatomical conditions were not given. Resulting, a circular skull defect of 15 mm diameter was chosen and placed centrally within the parietal bone (Rentsch et al., 2014).

In the present study, extremeCT, a type of peripheral computed tomography, was used to evaluate the microstructure of trabecular and cortical bone of the rabbit. An automated method for microCT analysis has several advantages over manual analysis. Only an automated approach can be purely objective and handle every dataset in exactly the same manner. Additionally, an automated analysis method is much faster than any manual procedure (Baiker et al., 2012).In addition, extremeCT is considered a useful and reliable method for evaluating bone healing (Maréchal et al., 2005; Acar et al., 2016) and they reported that micro-CT is as effective as histomorphometry, yielding concordant results. Indeed, extremeCT and histological results yielded similar results in our analysis of new bone formation.

Another important point for the right interpretation of the obtained results is to understand the role of the substances associated with the process of bone growth and healing. The use of bone markers is very important for identifying the deposition of calcium during the growth of the new bone tissue (Gehrke, 2013). Three markers were used in this study that were OPN, OC and Cathepsin K. Secretion of OPN continues throughout the maturation of the new bone and the binding of extracellular OPN may activate several signalling cascades leading to increased proliferation, cell motility, and survival signals (Sodek et al., 2000), all of which may be necessary to sustain the proliferation throughout osteogenesis (Perrien et al., 2002). OC specifically interacts with hydroxyapatite and is supposed to affect the growth or maturation of calcium phosphate mineral phases and it is related to the regulation of mineralization or bone turnover (Gruber & Ingram, 2003; Bondarenko, et al., 2014; Kim et al., 2015). Cathepsin K immunohistochemistry was performed to detect active osteoclasts which is essential for bone resorption (Troen, 2004). In order to confirm *in vivo* biocompatibility of OPG-chitosan gel, the analysis of serum biochemical parameters was run which provides important information about visceral organ damage in rabbits, particularly for the liver and the kidneys.

Discussion of results

Optimization of OPG-chitosan gels formulation

In this study, the biocompatibility of OPG and chitosan raw materials was tested on NHPL fibroblasts as they are the important cells involved in the healing process. The results showed regardless of MWs, chitosan have no marked inhibition on the viability of the NHPL fibroblast cells as shown in Table 5.1. This finding supported the fact that chitosan has the ability to induce proliferation of NHPL fibroblast cells. Pang et al. (2005) reported that chitosan enhanced the type I collagen synthesis and facilitated the proliferation and differentiation of NHPL fibroblast cells into osteogenic cells. This

could be explained by the fact that chitosan acts a substrate for cell attachment and allow proliferation by mimicking the glycosaminoglycan of the extracellular matrix (Zamora et al., 2011).

With regards to OPG, Figure 5.1 displayed the viability of NHPL fibroblast cells was significantly high at 0.024 and up to 3 μg mL^{-1} concentration of OPG. However, the viability of NHPL fibroblast cells reduce at higher concentration (>3 μg mL^{-1}). This is the first study to report on the cytotoxicity evaluation of OPG in the NHPL fibroblast cells. The results demonstrated that at low concentration of OPG (0.024 mg mL^{-1}) has the greatest ability to induce proliferation of NHPL fibroblast cells compared to other concentrations. This is in agreement with previous study that has reported minimal concentrations of OPG are required to significantly inhibit TRAIL-induced apoptosis in osteoclast and human breast and overian cancer cell lines (Holen et al., 2002; Lane et al., 2012). Lane et al. (2012) revealed that recombinant OPG protected human prostate cancer cell lines from TRAIL-induced apoptosis in a dose (25 ng mL^{-1}) indicating that OPG acts as a survival factor for cells. Fu et al., (2013) reported that OPG has inhibitory effect on osteoclast in dose less than 100 ng mL^{-1}. The higher concentration of OPG reduced the viability of cells because an increase the intensity of stimulus could produce oxidative stress resulting in cell death.

Regarding the OPG combined with chitosan (Figure 5.2), the proliferation of the cells was greater when OPG (0.024 mg mL^{-1}) was combined with chitosan (low and moderate molecular weights) compared to separate treatments either with chitosan or OPG. The reason why the OPG-chitosan combination is better than chitosan alone, this is can be explained by OPG which can act as a decoy receptor for TNF-related apoptosis-inducing ligand because it is efficiently bound with TRAIL. TRAIL signaling leads to cell death by activation of caspase-8 leads to caspase cascade that culminates in

cell death (Crowder & El-Deiry, 2012; Baud'huin, et al., 2013). Previous studies reported the exogenous application of recombinant OPG has indeed been shown to be capable of inhibiting TRAIL-induced apoptosis and subsequently downregulate the caspase 8 expression and inhibit cell death (Shipman & Croucher, 2003; Miyashita et al., 2004; Lemke et al., 2014). From our result, it can be speculated that OPG may act synergistically with chitosan to increase the proliferation NHPL fibroblast cells

The results of AOPI assay were also shown in Figure 4.3 and 4.4. The results approved the biocompatibility of OPG combined with chitosan (Table 5.3). The LMW chitosan combined with OPG based on our study had the greatest ability to induce cells proliferation compared to the moderate and high MWs of chitosan. This is in accordance with Chen et al. (2002) and Nor Asiah et al. (2013) who have reported that low MW chitosan significantly promoted the growth of normal fibroblasts. Other studies also reported that fibroblasts treated with low MW chitosan stimulated fibroblasts proliferation compared to chitosan at higher MWs (Wang et al., 2007; Jensen, 2013). The LMW chitosan has more structural characteristics similar to those of the glycosaminoglycans that facilitate the migration. This study also verified that the rate of NHPL fibroblast cells proliferation increased with time exposure to the OPG-chitosan combination and did not cause toxicity effects on NHPL fibroblast cell growth. This is also in agreement with a study reported by Nor Asiah et al., (2013). Similarly, the chitosan-based biomaterials are being tested in the treatment of bone defect (Ezoddini-Ardakani, et al., 2011a; Florczyk, et al., 2013; Jung, et al., 2014).

From previous results, we formulated OPG-chitosan gel and evaluated the effect of OPG-chitosan gel with different MWs of water-soluble chitosan on osteoblasts and NHPL fibroblasts. The results of the cytotoxicity tests suggested that all different types of chitosan and OPG-chitosan gels did not affect cell viability, indicating that they are

sufficiently biocompatible (Figure 4.5 and 4.6). The OPG-chitosan gels with NH osteoblasts and NHPL fibroblasts were subjected to SEM scanning. SEM images identified the distribution of cells on the gel surface and showed that cytoplasmic attachments of fibroblast cells and filopodia extending from the osteoblast cells across the surface (Figure 4.7). This finding supported the result of the cytotoxicity, where by the scaffold was found to have a favorable surface for cell attachment.

There are two common strategies used for chemical modification of the chitosan that leads to bioactive chitosan derivatives for tissue engineering applications. The first approach involves chemical modification to alter chitosan physiochemical properties through the introduction of the certain structural moieties to the polymer chain. For example, chitosan can be converted to the water-soluble form by introducing acidic functionalities via modification with lactobionic acid. In the second approach, chemical modification is conducted by covalently binding of specific biomolecules such as proteins to chitosan via reaction of carboxyl groups on the peptide and amine groups in chitosan forming imide bonds (Ho et al., 2005; Kumbar et al., 2014) that was similar to our study.

The physicochemical properties of OPG-chitosan gel were determined. The interactions between chitosan and proteins were confirmed by using FTIR. The interactions between chitosan and proteins are represented by amide I band, amide II and by NH and CO deformations (Pranoto et al., 2005; Silva et al., 2007). The FTIR spectra for the gels (Figure 4.9 and Table 4.3) were performed in order to achieve a complete comparison of the interaction between chitosan matrix and the bioactive compounds. Results showed that the shift of the bands corresponding to the interactions between chitosan and proteins. This is in agreement with previous studies that reported incorporation of bioactive compounds with chitosan is associated with amide I band the,

which affected the hydrophilicity of the samples (Silva, et al., 2007; Cai et al., 2010; Bourbon et al., 2011).

Thermal properties of the gel were evaluated by using TGA and DSC. It appeared that gels could withstand temperatures up to 200°C before it starts decomposing. Thus the finding suggested that all different types of chitosan and OPG-chitosan gels used in this study could be safely used in the clinical setting as its decomposition temperature is way above the normal body temperature (37 °C) (Figure 4.10). The first stage started at 50 °C with a weight loss of chitosan due to the loss of water. As the amine group present in chitosan increase, the water content increase. Therefore, in the first stage chitosan losses most of its weight and as the thermal analysis moves ahead it lost most of its weight. After 400 °C the remaining weight of the chitosan goes down substantially. This analysis confirmed structural changes which occur during depolymerisation of chitosan (Dhawade & Jagtap, 2012).Therefore, the thermal analysis of the gels showed thermal stability and the decomposition of the polymer appears in the temperature range between 200 and 400 °C. Other studies also reported that the thermal degradation of chitosan begins at about 250 °C (Sakurai et al., 2000; EL-Haflan et al., 2010). DSC analysis of chitosan and OPG-chitosan gels showed an endothermic transition centered between 100 to160 as in Figure 4.11: this peak was due to an order-disorder transition of ionic clusters due to the loss of water as describe in Scipioni et al. (2014). In fact, larger amount of water adsorbed into the composite membrane are expected to increase the free volume facilitating the chain mobility and the larger energy required to overcome the bonding interaction within highly hydrated hydrophilic domains. The broad endothermic peaks observed are referred to quite complex phenomena and could be deconvoluted in at least two overlapped Lorentzian functions and could be related to structural reorganization due to the water loss (Sgambetterra et al., 2016).

Figure 4.12 showed an increase in MW resulted in a decrease in water uptake. This was due to the permeability increased with the increasing swelling ratio, so chitosan with a higher MW which had a less porous structure has lower water-uptake ability while LMW chitosan had higher permeability and higher water uptake ability (Huei & Hwa, 1996). The swelling ratio of the chitosan and OPG-chitosan gels strongly depended on the hydrophilic nature and microstructure of the gels. Since water-soluble chitosan was hydrophilic materials, the ability to retain the gel structure seemed to be the main explanation for the differences observed in the swelling ratio between the different MWs of chitosan (Yan, et al., 2010). Also, one of the important properties of the biomaterial was simulated physiological fluids. Thus, the chitosan and OPG-chitosan gels were exhibited similarity of the fluid contents with those of living tissues as EWC of gels are more than 60 % and the percent water content values of the body about 60 %. A hydrogel with high water content was generally more advantageous for medical applications because of its permeability and biocompatibility (Katime & Mendizábal, 2010). The best swelling ability could facilitate not only cell attachment but also penetration of cells inside gels. These blends were considered to have a high surface area and, thus, the cells could attach and grow in a three-dimensional fashion (Jensen, 2013).

The previous investigations revealed that the initial degradation rate of a chitosan sample was dependent on its molecular weight (Zhang & Neau, 2001; Li et al., 2007). Based on this study, the results showed that chitosan with a lower MW are a more susceptible substrate to degrade (Figure 4.13). In order to distinguish between enzymatic degradation and simple dissolution, we compared the mass loss of samples after 28 days that had been stored in PBS with lysozyme to those that had been stored in PBS without lysozyme so the results of solubility indicated enzymatic degradation (Figure 4.14). The lowest MW chitosan displayed the highest mass loss which almost

dissolved after 28 days of enzyme addition. This could be due to low crystallinity and relatively weak intermolecular forces. Lower MW chitosan proved to be more susceptible to lysozyme than the higher MW counterparts. The degradation and solubility of water-soluble chitosan (LMW) were more than other MWs chitosan, the presence of binder (HMW chitosan) could prolong the biodegradation of scaffolds (Jensen, 2013). The results proved to be a vital characteristic of gels as the degradation rate of a graft must be optimal to maintain a stable structure long enough to obtain cell layers on graft.

The *in vitro* release profiles of OPG protein demonstrated that the release of OPG from OPG-chitosan gels was sustained for 28 days (Figure 4.15). The results of our present study are in consistent with previous studies, for example, the heparin-based chitosan delivery systems prevented the high initial burst, and they also demonstrated a sustained or extended release pattern of growth factors (Ishibe et al., 2009; Kim et al., 2011; Yun et al., 2013).

In vivo evaluation of OPG-chitosan gel

The osteogenic potential of OPG-chitosan gel was evaluated in rabbit. The clinical result showed the healing of the surgical defects treated with OPG-chitosan gel was uneventful. No signs of inflammation or infection were encountered (Figures 4.16 and 4.17). This is one of the hallmarks of biocompatibility for the newly OPG-chitosan gel.

Radiographically, the healing of the part-comparison analysis (Figure 4.18, 4.19 and 4.20) 3D model constructed by extremeCT confirmed the results of the clinical evaluation and showed that OPG-chitosan gel defect is almost completely closed after 12 weeks. The healing of defects treated with OPG-chitosan gel and chitosan gel is better than the healing in the control group. The results also showed that the OPG-chitosan and chitosan gels have the highest bone volume and density compared to other

groups at different time points (Table 4.4 and Figure 4.21 to Figure 4.25). The ExtemeCT is useful and used previously to evaluate bone regeneration. Baek et al. (2016) used microCT to evaluate chitin based membrane and from results, they concluded that the membrane had significant effect on the new bone formation and has the potential to be applied for guided bone regeneration. The same finding was observed in study by He et al. study (2015).

Histologically, hematoxylin and eosin stain results of the defects in this study revealed that chitosan gel induced a limited amount of new bone formation. In contrast, the application of OPG-chitosan gel showed better effects in inducing the bone formation at 6 weeks and the defect was almost completely healed after 12 weeks. In the control group, the amount of bone formation is less compared to chitosan gel and OPG-chitosan gel groups at 6 and 12 weeks (Figure 4.26 to figure 4.30). These results revealed that the chitosan enhances the bone formation but it is not enough to regenerate the defect completely. This finding supported that OPG protein is an active component that contributes to better bone regeneration. One other important observation was a large number of osteons found in bone tissue at 6 and 12 weeks in the OPG-chitosan groups. These results are in agreement with previous studies that the amount of new bone formation in the chitosan alone are more than the control groups but less when compared with the chitosan combined with other active components (Oktay et al., 2010; Yasmeen et al., 2014; Bush et al., 2016).

The compatibility and osteoconductivity of the OPG-chitosan gel could be seen by the presence of progressive bone neoformation and bone remodeling throughout the experimental site. Moreover, cortical organization, seen as the presence trabecular projections with the maturation of lamellar bone, showed thickness at the margin of the defect that was compatible with the original bone structure of the region. Other

important observations were the presence of osteocytes and many numbers of osteons in new bone tissue in the implanted area. These observations are in agreement with an earlier study (Allegrini et al., 2006).

In a bony defect, the most intense cellular reaction occurs during the first 6 weeks and in another word, the defect is first bridged by a trabecular framework consisting of primitive woven bone. In the following, there is a reduction in the numbers of cells in these areas, as well as increased in calcium deposition and this is in agreement with Gehrke (2013) who reported the same findings. Other studies reported that bone remodeling was very active after eight weeks of healing and was presented with diverse degrees of bone maturation and also an irregular new bone formation in the marrow cavity (Jansen et al., 1991).

The osteoinductive effect of treatment was strongly reinforced *in vivo* by the increased expression of osteopontin and collagen type I in lesioned bone treated with the bioconstruct (Arrigoni et al., 2013). Immunohistochemistry results (Figure 4.31 to 4.36 and Table 4.5 and 4.6) exhibited there was a significantly stronger expression of OPN in OPG-chitosan gel compared to control. The high expression of bone formation marker in OPG-chitosan gel group compared to other groups confirmed the osteogenic potential of gel Regarding OC, OC expression is presented as a late marker of osteogenesis and consistent with mature bone (Gruber & Ingram, 2003; Freire et al., 2015). OC showed staining of the newly formed bone matrix revealing characteristics of the mature bone. It is localized beside osteoblasts, osteoid and the mineralized bone also in the osteocyte lacunes and the cement lines. OC is specific also for both osteoblasts and osteocytes (Wittenburg et al., 2009). Tera et al. (2014) observed OC staining of the newly formed bone in experiments on guided bone regeneration in rats; Controversial results were obtained by Luvizuto, et al. (2000) after analyzing alveolar bone repair in

ovariectomized rats. In that study, the results showed that OC staining was relatively weaker in the regenerating bone compared to the mature bone. In this study, there were no similar dynamics of OC expression in all groups. For all, an increase in the OC expression was connected with an increased level of new bone formation. The increase of the OC expression in OPG-chitosan group overlapped with an increase of bone formation. Conversely, the chitosan gel and control groups demonstrated a less expression of OC. Obviously, the expression level of OC is directly related to the activity of bone formation, which also approved statistically.

The results obtained from this study confirm the important role of OC and OPN in bone healing that is an agreement with Bondarenko et al. study (2014). The evaluation of biocompatibility and osteoconductivity of OPG-chitosan gel showed the superiority of the latter in term of biocompatibility (no adverse reactions were observed), osteoconductivity and continuation of osteogenesis process throughout the entire period of bone healing. Complete wound closure of critical size bone defect filled with OPG-chitosan gel as compared to chitosan gel and the control further supported the favorable biological properties displayed by this biomaterial in a clinical situation.

The expressions of OPN and OC in all groups were higher at 6 weeks compared to 12 weeks except OC expression in OPG-chitosan gel group, there was no significant difference. This is agreement with other studies that found OPN is expressed throughout matrix maturation and OC seems to have a role in the early stages of bone formation and it shows positive expression and at area of bone formation at 6 weeks (Al-Hijazi et al.; Al-Ghani et al., 2011; Kim, et al., 2015).

Cathepsin K is expressed by osteoclasts and a small number of osteoclast precursors but is absent in osteoblasts and osteocytes making its expression in bone-specific for the resorption phase of bone metabolism (Drake et al., 1996). Osteoblasts control the

formation and activity of osteoclasts and, therefore, the resorption of bone through coupling mechanisms such as RANK, RANKL, and OPG (Pederson et al., 2008; Teti, 2013; Jeon et al., 2016). From the results (Figure 4.37), the number of osteoclast in the OPG-chitosan gel was less than other groups. This may be due to the action of OPG that block the activation and maturation of osteoclast.

The *in vivo* results of this study were in agreement in pervious with many studies that chitosan has been shown to improve hemostasis and to enhance wound healing in animal models demonstrated enhanced bone growth using chitosan in critical size defects in rabbit and sheep models (Pang et al., 2005). Previous studies also showed a significant increase of bone formation in the osseous healing area where the OPG or chitosan-based biomaterials was applied (Ezoddini-Ardakani, et al., 2011a; Florczyk, et al., 2013; Lamoureux, et al., 2007; Jung, et al., 2014; Jung et al., 2000a; Yao, et al., 2011).

Serum levels of the liver, kidney functional tests yielded no signs of harmful systemic effect of treatment (Table 4.7 to 4.10). There were no significant differences between the serum biochemical level before and after treatment in all groups. Therefore, OPG-chitosan gel was considered as biocompatible material and it will be save to use in bone regeneration.

CHAPTER 6: CONCLUSION

> ## Conclusion

A unique candidate material with reliable properties for use as an OPG-chitosan gel in bone repair and reconstruction has been produced. In our study, OPG-chitosan gel was formulated from natural materials for bone tissue regeneration comprising OPG wherein OPG was released from the gel over a prolonged period of time. The OPG-chitosan gel enhance the NHPL fibroblast and osteoblast cells growth. The gel surface was appropriate for the bone cells to adhere, proliferate and form an extracellular matrix on its surface. It has specific degradation by lysozyme and was able to degrade with time *in vivo* and it also has the ability for sustained release property. Owing to this fact it is preferably at a controlled rate, and eventually creating space for the new bone tissue to grow. The OPG-chitosan gel is biocompatible, biodegradable, and capable of supporting new bone growth *in vivo*. The osteoconductivity of the OPG-chitosan gel have been proven in this study and it showed the bone healing and formation in the OPG-chitosan gel filled critical size cranial defects of New Zeland white rabbits without toxicity effects. In conclusion, that the OPG-chitosan gel has many characteristics suitable for bone repair and regeneration and thus may be beneficial to tissue engineering applications.

> **Limitation**

1. There is no standard control (commercial cytotoxic drug).

2. Mechanical properties of gels were not evaluated as facilities for gel were not available.

3. The scanning of the rabbits' calvaria during the bone healing period was not done as facilities for extremeCT scan were limited.

4. Rabbit was the only animal available as the animal model instead of larger animals such as monkey, due to the high cost incurred for the purchase and maintenance, and limited facilities to house these bigger animals.

5. As the rabbits' mouth accessibility was small, it was only possible to perform the experiment extra-orally, hence limiting study intra-orally i.e. the alveolar process.

➢ **Recommendation of the present study**

A detail study on the gel formulation is needed to incorporate the use of modification polymer and nanotechnology. In addition, it would be interesting to study the effect of OPG-chitosan gel on cell genetic mutation and its potential use as a carrier for stem cell in a large animal model.

REFERENCES

Abbas, A. K., Kumar, V., & Fausto, N. (2005). *Robbins & Cotran-Patologia*: Elsevier.

Acar, A. H., Yolcu, Ü., Altındiş, S., Gül, M., Alan, H., & Malkoç, S. (2016). Bone regeneration by low-level laser therapy and low-intensity pulsed ultrasound therapy in the rabbit calvarium. *Archives of Oral Biology, 61*, 60-65.

Al-Bayaty, F. H., Kamaruddin, A. A., Ismail, M. A., & Abdulla, M. A. (2013). Formulation and evaluation of a new biodegradable periodontal chip containing thymoquinone in a chitosan base for the management of chronic periodontitis. *Journal of Nanomaterials, 2013*, 16.

Al-Ghani, B., Al-Hijazi, A., & AL-Zubaydi, T. (2011). In vivo immunohistochemical investegation of bone deposition at collagen coated Ti implant surface. *J Bagh College Dentistry, 23*.

Al-Hijazi, A. Y., Thair, L., & Mahdi, E. I. Immunohistochemical detection to evaluate the biological role of Ti implants coated by a combination of fibronectin protein and hydroxyapitate (EPD)(in vivo study). *Scientific Journal Published by the College of Dentistry–University of Baghdad*, 31.

Allegrini, S., Rumpel, E., Kauschke, E., Fanghänel, J., & König, B. (2006). Hydroxyapatite grafting promotes new bone formation and osseointegration of smooth titanium implants. *Annals of Anatomy-Anatomischer Anzeiger, 188*(2), 143-151.

An, Y. H., & Freidman, R. J. (1998). *Animal models in orthopaedic research*: CRC Press.

Anal, A. K., & Stevens, W. F. (2005). Chitosan–alginate multilayer beads for controlled release of ampicillin. *International Journal of Pharmaceutics, 290*(1), 45-54.

Anderson, D. M., Maraskovsky, E., Billingsley, W. L., Dougall, W. C., Tometsko, M. E., Roux, E. R., Teepe, M. C., DuBose, R. F., Cosman, D., & Galibert, L. (1997). A homologue of the TNF receptor and its ligand enhance T-cell growth and dendritic-cell function. *Nature, 390*(6656), 175-179.

Arica, B., Calis, S., Atilla, P., Durlu, N., Cakar, N., Kas, H., & Hincal, A. (2005). In vitro and in vivo studies of ibuprofen-loaded biodegradable alginate beads. *Journal of Microencapsulation, 22*(2), 153-165.

Arrigoni, E., de Girolamo, L., Di Giancamillo, A., Stanco, D., Dellavia, C., Carnelli, D., Campagnol, M., Domeneghini, C., & Brini, A. T. (2013). Adipose-derived stem cells and rabbit bone regeneration: histomorphometric, immunohistochemical and mechanical characterization. *Journal of Orthopaedic Science, 18*(2), 331-339.

Baek, Y. J., Kim, J. H., Song, J. M., Yoon, S. Y., Kim, H. S., & Shin, S. H. (2016). Chitin-fibroin-hydroxyapatite membrane for guided bone regeneration: micro-

computed tomography evaluation in a rat model. *Maxillofacial Plastic and Reconstructive Surgery*, 38(1), 1.

Baiker, M., Snoeks, T. J., Kaijzel, E. L., Que, I., Dijkstra, J., Lelieveldt, B. P., & Löwik, C. W. (2012). Automated bone volume and thickness measurements in small animal whole-body MicroCT data. *Molecular Imaging and Biology, 14*(4), 420-430.

Baldock, P. A., Thomas, G. P., Hodge, J. M., Baker, S. U., Dressel, U., O'Loughlin, P. D., Nicholson, G. C., Briffa, K. H., Eisman, J. A., & Gardiner, E. M. (2006). Vitamin D action and regulation of bone remodeling: suppression of osteoclastogenesis by the mature osteoblast. *Journal of Bone and Mineral Research, 21*(10), 1618-1626.

Balli, U., Aydogdu, A., Dede, F. O., Turer, C. C., & Guven, B. (2015). Gingival Crevicular Fluid Levels of Sclerostin, Osteoprotegerin, and Receptor Activator of Nuclear Factor-κB Ligand in Periodontitis. *Journal of Periodontology, 86*(12), 1396-1404.

Banerjee, I., Mishra, D., & Maiti, T. K. (2009). PLGA microspheres incorporated gelatin scaffold: microspheres modulate scaffold properties. *International Journal of Biomaterials, 2009*.

Basdra, E. K., & Komposch, G. (1997). Osteoblast-like properties of human periodontal ligament cells: an in vitro analysis. *The European Journal of Orthodontics, 19*(6), 615-621.

Baud'huin, M., Duplomb, L., Teletchea, S., Lamoureux, F., Ruiz-Velasco, C., Maillasson, M., Redini, F., Heymann, M.-F., & Heymann, D. (2013). Osteoprotegerin: Multiple partners for multiple functions. *Cytokine & Growth Factor Reviews*.

Bekker PJ, H. D., Nakanishi A, Arrighi HM, Dunstan CR. (1999). Osteoprotegerin (OPG) has potent and sustained anti-resorptive activity in postmenopausal women. *J Bone Miner Res., 14*((Suppl 1)), 1190.

Bekker, P. J., Holloway, D., Nakanishi, A., Arrighi, M., Leese, P. T., & Dunstan, C. R. (2001). The effect of a single dose of osteoprotegerin in postmenopausal women. *Journal of Bone and Mineral Research, 16*(2), 348-360.

Bellido, T., Jilka, R., Boyce, B., Girasole, G., Broxmeyer, H., Dalrymple, S., Murray, R., & Manolagas, S. (1995). Regulation of interleukin-6, osteoclastogenesis, and bone mass by androgens. The role of the androgen receptor. *Journal of Clinical Investigation, 95*(6), 2886.

Body, J. J., Greipp, P., Coleman, R. E., Facon, T., Geurs, F., Fermand, J. P., Harousseau, J. L., Lipton, A., Mariette, X., & Williams, C. D. (2003). A Phase I study of AMGN-0007, a recombinant osteoprotegerin construct, in patients with multiple myeloma or breast carcinoma related bone metastases. *Cancer, 97*(S3), 887-892.

Bojar, W., Kucharska, M., Ciach, T., Koperski, Ł., Jastrzębski, Z., & Szałwiński, M. (2014). Bone regeneration potential of the new chitosan-based alloplastic biomaterial. *Journal of Biomaterials Applications, 28*(7), 1060-1068.

Bolon, B., Carter, C., Daris, M., Morony, S., Capparelli, C., Hsieh, A., Mao, M., Kostenuik, P., Dunstan, C. R., & Lacey, D. L. (2001). Adenoviral Delivery of Osteoprotegerin Ameliorates Bone Resorption in a Mouse Ovariectomy Model of Osteoporosis&ast. *Molecular therapy, 3*(2), 197-205.

Bondarenko, A., Angrisani, N., Meyer-Lindenberg, A., Seitz, J., Waizy, H., & Reifenrath, J. (2014). Magnesium-based bone implants: Immunohistochemical analysis of peri-implant osteogenesis by evaluation of osteopontin and osteocalcin expression. *Journal of Biomedical Materials Research Part A, 102*(5), 1449-1457.

Bonnier, F., Keating, M., Wrobel, T. P., Majzner, K., Baranska, M., Garcia-Munoz, A., Blanco, A., & Byrne, H. J. (2015). Cell viability assessment using the Alamar blue assay: A comparison of 2D and 3D cell culture models. *Toxicology in Vitro, 29*(1), 124-131.

Bord, S.-., Ireland, D., Beavan, S., & Compston, J. (2003). The effects of estrogen on osteoprotegerin, RANKL, and estrogen receptor expression in human osteoblasts. *Bone, 32*(2), 136-141.

Bostanci, N., İlgenli, T., Emingil, G., Afacan, B., Han, B., Töz, H., Atilla, G., Hughes, F. J., & Belibasakis, G. N. (2007). Gingival crevicular fluid levels of RANKL and OPG in periodontal diseases: implications of their relative ratio. *Journal of Clinical Periodontology, 34*(5), 370-376.

Bostanci, N., Ilgenli, T., Emingil, G., Afacan, B., Han, B., Töz, H., Berdeli, A., Atilla, G., McKay, I., & Hughes, F. (2007). Differential expression of receptor activator of nuclear factor-κB ligand and osteoprotegerin mRNA in periodontal diseases. *Journal of Periodontal Research, 42*(4), 287-293.

Bourbon, A. I., Pinheiro, A. C., Cerqueira, M. A., Rocha, C. M., Avides, M. C., Quintas, M. A., & Vicente, A. A. (2011). Physico-chemical characterization of chitosan-based edible films incorporating bioactive compounds of different molecular weight. *Journal of Food Engineering, 106*(2), 111-118.

Bronner, F., Farach-Carson, M. C., & Rubin, J. E. (2005). *Bone resorption* (Vol. 2): Springer.

Bush, J. R., Liang, H., Dickinson, M., & Botchwey, E. A. (2016). Xylan hemicellulose improves chitosan hydrogel for bone tissue regeneration. *Polymers for Advanced Technologies*.

Cacchioli, A., Spaggiari, B., Ravanetti, F., Martini, F., Borghetti, P., & Gabbi, C. (2007). The critical sized bony defect: morphological study of bone healing. *Annali della facoltà di medicina veterinaria. Università di Parma, 26*, 97-110.

Cai, J., Yang, J., Wang, C., Hu, Y., Lin, J., & Fan, L. (2010). Structural characterization and antimicrobial activity of chitosan (CS-40)/nisin complexes. *Journal of Applied Polymer Science, 116*(6), 3702-3707.

Calasans-Maia, M., Rossi, A. M., Dias, E. P., Santos, S. R., Áscoli, F., & Granjeiro, J. M. (2008). Stimulatory effect on osseous repair of zinc-substituted hydroxyapatite: Histological study in rabbit's tibia. *Key Engineering Materials, 361*, 1269-1272.

Calasans-Maia, M. D., Monteiro, M. L., Áscoli, F. O., & Granjeiro, J. M. (2009). The rabbit as an animal model for experimental surgery. *Acta Cirurgica Brasileira, 24*(4), 325-328.

Cama, G., Tardajos, M., & Dubruel, P. (2015). *PCL/chitosan scaffolds for bone tissue regeneration: fabrication and characterization.* Paper presented at the Seminar on Nano-biomaterials: What challenges are we facing?

Canon, J., Bryant, R., Roudier, M., Branstetter, D. G., & Dougall, W. C. (2012). RANKL inhibition combined with tamoxifen treatment increases anti-tumor efficacy and prevents tumor-induced bone destruction in an estrogen receptor-positive breast cancer bone metastasis model. *Breast Cancer Research And Treatment, 135*(3), 771-780.

Canon, J. R., Roudier, M., Bryant, R., Morony, S., Stolina, M., Kostenuik, P. J., & Dougall, W. C. (2008). Inhibition of RANKL blocks skeletal tumor progression and improves survival in a mouse model of breast cancer bone metastasis. *Clinical & Experimental Metastasis, 25*(2), 119-129.

Capparelli, C., Morony, S., Warmington, K., Adamu, S., Lacey, D., Dunstan, C. R., Stouch, B., Martin, S., & Kostenuik, P. J. (2003). Sustained antiresorptive effects after a single treatment with human recombinant osteoprotegerin (OPG): a pharmacodynamic and pharmacokinetic analysis in rats. *Journal of Bone and Mineral Research, 18*(5), 852-858.

Carter, P. H., & Schipani, E. (2006). The roles of parathyroid hormone and calcitonin in bone remodeling: prospects for novel therapeutics. *Endocrine, Metabolic & Immune Disorders-Drug Targets (Formerly Current Drug Targets-Immune, Endocrine & Metabolic Disorders), 6*(1), 59-76.

Castaneda, S., Largo, R., Calvo, E., Rodriguez-Salvanes, F., Marcos, M., Diaz-Curiel, M., & Herrero-Beaumont, G. (2006). Bone mineral measurements of subchondral and trabecular bone in healthy and osteoporotic rabbits. *Skeletal Radiology, 35*(1), 34-41.

Catanzariti, A., & Karlock, L. (1996). The application of allograft bone in foot and ankle surgery. *The Journal Of Foot And Ankle Surgery, 35*(5), 440-451.

Chang, C.-H., Lin, Y.-H., Yeh, C.-L., Chen, Y.-C., Chiou, S.-F., Hsu, Y.-M., Chen, Y.-S., & Wang, C.-C. (2009). Nanoparticles incorporated in pH-sensitive hydrogels as amoxicillin delivery for eradication of Helicobacter pylori. *Biomacromolecules, 11*(1), 133-142.

Charan, J., & Biswas, T. (2013). How to calculate sample size for different study designs in medical research? *Indian Journal Of Psychological Medicine, 35*(2), 121.

Chen, X.-G., Wang, Z., Liu, W.-S., & Park, H.-J. (2002). The effect of carboxymethyl-chitosan on proliferation and collagen secretion of normal and keloid skin fibroblasts. *Biomaterials, 23*(23), 4609-4614.

Chien, H.-F., Chen, C.-P., Chen, Y.-C., Chang, P.-H., Tsai, T., & Chen, C.-T. (2013). The use of chitosan to enhance photodynamic inactivation against Candida albicans and its drug-resistant clinical isolates. *International Journal Of Molecular Sciences, 14*(4), 7445-7456.

Choi, B.-K., Moon, S.-Y., Cha, J.-H., Kim, K.-W., & Yoo, Y.-J. (2005). Prostaglandin E2 is a main mediator in receptor activator of nuclear factor-κB ligand-dependent osteoclastogenesis induced by Porphyromonas gingivalis, Treponema denticola, and Treponema socranskii. *Journal of Periodontology, 76*(5), 813-820.

Chung, P. Y. J., & Van Hul, W. (2012). Paget's disease of bone: evidence for complex pathogenetic interactions. *In Seminars in arthritis and rheumatism*, *41*(5), 619-641).

Clézardin, P. (2011). The role of RANK/RANKL/osteoprotegerin (OPG) triad in cancer-induced bone diseases: physiopathology and clinical implications]. *Bulletin du Cancer, 7*, 98

Clezardin, P., & Teti, A. (2007). Bone metastasis: pathogenesis and therapeutic implications. *Clinical & Experimental Metastasis, 24*(8), 599-608.

Coimbra, P., Alves, P., Valente, T., Santos, R., Correia, I., & Ferreira, P. (2011a). Sodium hyaluronate/chitosan polyelectrolyte complex scaffolds for dental pulp regeneration: synthesis and characterization. *International Journal Of Biological Macromolecules, 49*(4), 573-579.

Coimbra, P., Alves, P., Valente, T. A. M., Santos, R., Correia, I. J., & Ferreira, P. (2011b). Sodium hyaluronate/chitosan polyelectrolyte complex scaffolds for dental pulp regeneration: Synthesis and characterization. *International Journal of Biological Macromolecules, 49*(4), 573-579.

Cooper, G. M., Mooney, M. P., Gosain, A. K., Campbell, P. G., Losee, J. E., & Huard, J. (2010). Testing the "critical-size" in calvarial bone defects: revisiting the concept of a critical-sized defect (CSD). *Plastic And Reconstructive Surgery*, 125(6), 1685.

Crotti, T., Smith, M. D., Hirsch, R., Soukoulis, S., Weedon, H., Capone, M., Ahern, M. J., & Haynes, D. (2003). Receptor activator NF κB ligand (RANKL) and osteoprotegerin (OPG) protein expression in periodontitis. *Journal of Periodontal Research, 38*(4), 380-387.

Crowder, R., & El-Deiry, W. (2012). Caspase-8 regulation of TRAIL-mediated cell death. *Exp Oncol, 34*(3), 160-164.

Cundy, T., Davidson, J., Rutland, M. D., Stewart, C., & DePaoli, A. M. (2005). Recombinant osteoprotegerin for juvenile Paget's disease. *New England Journal of Medicine, 353*(9), 918-923.

Dai, T., Tanaka, M., Huang, Y.-Y., & Hamblin, M. R. (2011). Chitosan preparations for wounds and burns: antimicrobial and wound-healing effects. *Expert Review of Anti-Infective Therapy, 9(7), 857-879.*

Di Bella, C., Farlie, P., & Penington, A. J. (2008). Bone regeneration in a rabbit critical-sized skull defect using autologous adipose-derived cells. *Tissue Engineering Part A, 14*(4), 483-490.

Divieto, C., & Sassi, M. P. (2015). A first approach to evaluate the cell dose in highly porous scaffolds by using a nondestructive metabolic method. *Future Science OA, 1*(4).

Drake, F. H., Dodds, R. A., James, I. E., Connor, J. R., Debouck, C., Richardson, S., Lee-Rykaczewski, E., Coleman, L., Rieman, D., & Barthlow, R. (1996). Cathepsin K, but not cathepsins B, L, or S, is abundantly expressed in human osteoclasts. *Journal of Biological Chemistry, 271*(21), 12511-12516.

Drugarin, D., Drugarin, M., Negru, S., & Cioaca, R. (2003). Rankl-Rank/Opg Molecular Complex-Control Factors in Bone Remodeling. *TMJ, 53*(3-4), 297-302.

Duceppe, N., & Tabrizian, M. (2010). Advances in using chitosan-based nanoparticles for in vitro and in vivo drug and gene delivery. *Expert Opinion on Drug Delivery, 7*(10), 1191-1207.

Egerbacher, M., Moussa, E., Helmreich, M., Böck, P., & Schuh, M. (2006). Mammary Gland Secretory Concretions Contain Non-Collagenous Bone Matrix Proteins. *Anatomia, Histologia, Embryologia, 35*(5), 343-348.

EL-Haflan, E., Elgannoudi, E. S., Mainal, A., & Yahaya, A. H. (2010). Characterization of chitosan in acetic acid: Rheological and thermal studies. *Turkish Journal of Chemistry, 34*(1), 47-56.

El-Sherbiny, I. M., El-Baz, N. M., & Yacoub, M. H. (2015). Inhaled nano-and microparticles for drug delivery. *Global Cardiology Science & Practice, 2015*.

El Hadrami, A., Adam, L. R., El Hadrami, I., & Daayf, F. (2010). Chitosan in plant protection. *Marine Drugs, 8*(4), 968-987.

Emery, J. G., McDonnell, P., Burke, M. B., Deen, K. C., Lyn, S., Silverman, C., Dul, E., Appelbaum, E. R., Eichman, C., & DiPrinzio, R. (1998). Osteoprotegerin is a receptor for the cytotoxic ligand TRAIL. *Journal of Biological Chemistry, 273*(23), 14363-14367.

Ezoddini-Ardakani, F., Azam, A. N., Yassaei, S., Fatehi, F., & Rouhi, G. (2011a). Effects of chitosan on dental bone repair. *Health, 3*(04), 200.

Ezoddini-Ardakani, F., Azam, A. N., Yassaei, S., Fatehi, F., & Rouhi, G. (2011b). Effects of chitosan on dental bone repair. *Health (1949-4998), 3*(4).

Fan, R., Sun, B., Zhang, C.-f., Lu, Y.-l., Xuan, W., Wang, Q.-q., & Yin, X. (2011). Receptor activator of nuclear factor kappa B ligand and osteoprotegerin expression in chronic apical periodontitis: possible association with inflammatory cells. *Chinese Medical Journal-Beijing, 124*(14), 2162.

Fata, J. E., Kong, Y.-Y., Li, J., Sasaki, T., Irie-Sasaki, J., Moorehead, R. A., Elliott, R., Scully, S., Voura, E. B., & Lacey, D. L. (2000). The osteoclast differentiation factor osteoprotegerin-ligand is essential for mammary gland development. *Cell, 103*(1), 41-50.

Felix, R., Hofstetter, W., & Cecchini, M. G. (1996). Recent developments in the understanding of the pathophysiology of osteopetrosis. *European Journal of Endocrinology, 134*(2), 143-156.

Fili, S., Karalaki, M., & Schaller, B. (2009). Therapeutic implications of osteoprotegerin. *Cancer Cell International, 9*(1), 1.

Florczyk, S. J., Leung, M., Li, Z., Huang, J. I., Hopper, R. A., & Zhang, M. (2013). Evaluation of three-dimensional porous chitosan–alginate scaffolds in rat calvarial defects for bone regeneration applications. *Journal of Biomedical Materials Research Part A, 101*(10), 2974-2983.

Florencio-Silva, R., Sasso, G. R. d. S., Sasso-Cerri, E., Simões, M. J., & Cerri, P. S. (2015). Biology of bone tissue: structure, function, and factors that influence bone cells. *BioMed research international, 2015*.

Freier, T., Koh, H. S., Kazazian, K., & Shoichet, M. S. (2005). Controlling cell adhesion and degradation of chitosan films by N-acetylation. *Biomaterials, 26*(29), 5872-5878.

Freire, M., Choi, J.-H., Nguyen, A., Chee, Y. D., Kook, J.-K., You, H.-K., & Zadeh, H. H. (2015). Application of AMOR in craniofacial rabbit bone bioengineering. *BioMed Research International, 2015*.

Frost, H. (1990). Skeletal structural adaptations to mechanical usage (SATMU): 2. Redefining Wolff's law: the remodeling problem. *The Anatomical Record, 226*(4), 414-422.

Fu, Y. X., Gu, J. H., Zhang, Y. R., Tong, X. S., Zhao, H. Y., Yuan, Y., ... & Liu, Z. P. (2013). Inhibitory effects of osteoprotegerin on osteoclast formation and function under serum-free conditions. *Journal of Veterinary Science*, 14(4), 405-412.

Galea, G. L., Meakin, L. B., Sugiyama, T., Zebda, N., Sunters, A., Taipaleenmaki, H., Stein, G. S., van Wijnen, A. J., Lanyon, L. E., & Price, J. S. (2013). Estrogen Receptor α Mediates Proliferation of Osteoblastic Cells Stimulated by Estrogen and Mechanical Strain, but Their Acute Down-regulation of the Wnt Antagonist Sost Is Mediated by Estrogen Receptor β. *Journal of Biological Chemistry, 288*(13), 9035-9048.

Galli, D., Vitale, M., & Vaccarezza, M. (2014). Bone marrow-derived mesenchymal cell differentiation toward myogenic lineages: facts and perspectives. *BioMed Research International, 2014*.

Gartner, L. P., & Hiatt, J. L. (2012). *Color Atlas and Text of Histology*: Wolters Kluwer Health.

Gehrke, S. A. (2013). Analysis of Bone Tissue Healing around Titanium Implant Surface Treated with Tio Sandblasted after Three and Six Weeks Used Different Histological Methods-a Study in Rabbits. *Science Journal of Medicine and Clinical Trials, 2013*.

Gentile, P., Nandagiri, V. K., Daly, J., Chiono, V., Mattu, C., Tonda-Turo, C., Ciardelli, G., & Ramtoola, Z. (2016). Localised controlled release of simvastatin from porous chitosan–gelatin scaffolds engrafted with simvastatin loaded PLGA-microparticles for bone tissue engineering application. *Materials Science and Engineering: C, 59*, 249-257.

Gentile, P., Nandagiri, V. K., Pabari, R., Daly, J., Tonda-Turo, C., Ciardelli, G., & Ramtoola, Z. (2015). Influence of parathyroid hormone-loaded PLGA nanoparticles in porous scaffolds for bone regeneration. *International Journal of Molecular Sciences, 16*(9), 20492-20510.

Grdadolnik, J. (2002). ATR-FTIR spectroscopy: Its advantage and limitations. *Acta Chimica Slovenica, 49*(3), 631-642.

Grimaud, E., Soubigou, L., Couillaud, S., Coipeau, P., Moreau, A., Passuti, N., Gouin, F., Redini, F., & Heymann, D. (2003). Receptor activator of nuclear factor κB ligand (RANKL)/osteoprotegerin (OPG) ratio is increased in severe osteolysis. *The American Journal of Pathology, 163*(5), 2021-2031.

Gruber, H. E., & Ingram, J. A. (2003). Basic Staining and Histochemical Techniques and Immunohistochemical Localizations Using Bone Sections *Handbook of Histology Methods for Bone and Cartilage* (pp. 281-286): Springer.

Hadjidakis, D. J., & Androulakis, I. I. (2006). Bone remodeling. *Annals of the New York Academy of Sciences, 1092*(1), 385-396.

Hage, I. S., & Hamade, R. F. (2015). Distribution of Porosity in Cortical (Bovine) Bone. Paper in ASME 2015 International Mechanical Engineering Congress and Exposition.

Harcourt-Brown, F., & Harcourt-Brown, N. H. (2002). Textbook of rabbit medicine. *Elsevier*.

Hassan, S. H., El-Refai, M. I., Ghallab, N. A., Kasem, R. F., & Shaker, O. G. (2015). Effect of periodontal surgery on osteoprotegerin levels in gingival crevicular fluid, saliva, and gingival tissues of chronic periodontitis patients. *Disease markers, 2015*.

He, Y., Dong, Y., Cui, F., Chen, X., & Lin, R. (2015). Ectopic Osteogenesis and Scaffold Biodegradation of Nano-Hydroxyapatite-Chitosan in a Rat Model. *PloS one*, 10(8), 0135366.

Hillier, M. L., & Bell, L. S. (2007). Differentiating human bone from animal bone: a review of histological methods. *Journal of Forensic Sciences, 52*(2), 249-263.

Ho, M.-H., Wang, D.-M., Hsieh, H.-J., Liu, H.-C., Hsien, T.-Y., Lai, J.-Y., & Hou, L.-T. (2005). Preparation and characterization of RGD-immobilized chitosan scaffolds. *Biomaterials, 26*(16), 3197-3206.

Hofbauer, L., Kuhne, C., & Viereck, V. (2004). The OPG/RANKL/RANK system in metabolic bone diseases. *Journal of Musculoskeletal and Neuronal Interactions, 4*(3), 268.

Hofbauer, L. C., & Heufelder, A. E. (2000). The role of receptor activator of nuclear factor-κB ligand and osteoprotegerin in the pathogenesis and treatment of metabolic bone diseases. *Journal of Clinical Endocrinology & Metabolism, 85*(7), 2355-2363.

Hofbauer, L. C., Khosla, S., Dunstan, C. R., Lacey, D. L., Spelsberg, T. C., & Riggs, B. L. (1999). Estrogen Stimulates Gene Expression and Protein Production of Osteoprotegerin in Human Osteoblastic Cells*. *Endocrinology, 140*(9), 4367-4370.

Hofbauer, L. C., Neubauer, A., & Heufelder, A. E. (2001). Receptor activator of nuclear factor-κB ligand and osteoprotegerin. *Cancer, 92*(3), 460-470.

Holen, I., Croucher, P. I., Hamdy, F. C., & Eaton, C. L. (2002). Osteoprotegerin (OPG) is a survival factor for human prostate cancer cells. *Cancer Research, 62*(6), 1619-1623.

Holen, I., & Shipman, C. (2006). Role of osteoprotegerin (OPG) in cancer. *Clinical Science, 110*, 279-291.

Hsu, H., Lacey, D. L., Dunstan, C. R., Solovyev, I., Colombero, A., Timms, E., Tan, H.-L., Elliott, G., Kelley, M. J., & Sarosi, I. (1999). Tumor necrosis factor receptor family member RANK mediates osteoclast differentiation and activation induced by osteoprotegerin ligand. *Proceedings of the National Academy of Sciences, 96*(7), 3540-3545.

Hu, C.-Y., Lo, S.-L., Chang, C.-L., Chen, F.-L., Wu, Y.-D., & Ma, J.-l. (2013). Treatment of highly turbid water using chitosan and aluminum salts. *Separation and Purification Technology, 104*, 322-326.

Huang, J. C., Sakata, T., Pfleger, L. L., Bencsik, M., Halloran, B. P., Bikle, D. D., & Nissenson, R. A. (2004). PTH differentially regulates expression of RANKL and OPG. *Journal of Bone and Mineral Research, 19*(2), 235-244.

Huei, C. R., & Hwa, H.-D. (1996). Effect of molecular weight of chitosan with the same degree of deacetylation on the thermal, mechanical, and permeability properties of the prepared membrane. *Carbohydrate Polymers, 29*(4), 353-358.

Humber, C. C. (2010). *Evaluation of an in situ formed Bioresorbable Membrane and Hyperbaric Oxygen on Bone Regeneration using Alloplastic Bone Substitutes in Critical Sized Rabbit Calvarial Defects.* University of Toronto.

Ilium, L. (1998). Chitosan and its use as a pharmaceutical excipient. *Pharmaceutical Research, 15*(9), 1326-1331.

Isaksson, S. (1991). Aspects of bone healing and bone substitute incorporation. An experimental study in rabbit skull bone defects. *Swedish dental journal. Supplement, 84*, 1-46.

Ishibe, T., Goto, T., Kodama, T., Miyazaki, T., Kobayashi, S., & Takahashi, T. (2009). Bone formation on apatite-coated titanium with incorporated BMP-2/heparin in vivo. *Oral Surgery, Oral Medicine, Oral Pathology, Oral Radiology, and Endodontology, 108*(6), 867-875.

Ivanovski, S., Li, H., Daley, T., & Bartold, P. (2000). An immunohistochemical study of matrix molecules associated with barrier membrane-mediated periodontal wound healing. *Journal of Periodontal Research, 35*(3), 115-126.

Jahromi, M. Z., Ranjbarian, P., & Shiravi, S. (2014). Cytotoxicity evaluation of Iranian propolis and calcium hydroxide on dental pulp fibroblasts. *Journal of Dental Research, Dental Clinics, Dental Prospects, 8*(3), 130.

Jansen, J., Van De Waerden, J., Wolke, J., & De Groot, K. (1991). Histologic evaluation of the osseous adaptation to titanium and hydroxyapatite-coated titanium implants. *Journal of biomedical materials research, 25*(8), 973-989.

Jayakumar, R., Prabaharan, M., Sudheesh Kumar, P., Nair, S., & Tamura, H. (2011). Biomaterials based on chitin and chitosan in wound dressing applications. *Biotechnology advances, 29*(3), 322-337.

Jensen, E. C. (2013). Quantitative analysis of histological staining and fluorescence using ImageJ. *The Anatomical Record, 296*(3), 378-381.

Jeon, O. H., Panicker, L. M., Lu, Q., Chae, J. J., Feldman, R. A., & Elisseeff, J. H. (2016). Human iPSC-derived osteoblasts and osteoclasts together promote bone regeneration in 3D biomaterials. *Scientific Reports, 6*.

Ji, Q., Deng, J., Yu, X., Xu, Q., & Xu, X. (2009). [An in vitro evaluation of the antibacterial activity of chitosan-based thermosensitive hydrogel against periodontal pathogens]. *Shanghai Journal of Stomatology, 18*(4), 397-400.

Jimtaisong, A., & Saewan, N. (2014). Utilization of carboxymethyl chitosan in cosmetics. *International Journal of Cosmetic Science, 36*(1), 12-21.

Jin, Q., Cirelli, J. A., Park, C. H., Sugai, J. V., Taba Jr, M., Kostenuik, P. J., & Giannobile, W. V. (2007). RANKL inhibition through osteoprotegerin blocks bone loss in experimental periodontitis. *Journal of Periodontology, 78*(7), 1300-1308.

Jönsson, D., Nebel, D., Bratthall, G., & Nilsson, B. O. (2011). The human periodontal ligament cell: a fibroblast-like cell acting as an immune cell. *Journal of Periodontal Research, 46*(2), 153-157.

Jothi, M., Bhat, K., Pratibha, P., & Bhat, G. (2009). The evaluation of a biodegradable dental chip containing chlorhexidine in chitosan base as a targeted drug delivery in the management of chronic periodontitis in patients. *Drug Development Research, 70*(5), 395-401.

Junbo, B., & Cunxian, S. (2009). Chitosan chip and application to evaluate DNA loading on the surface of the metal. *Biomedical Materials, 4*(1), 011002.

Jung, H. D., Yook, S. W., Han, C. M., Jang, T. S., Kim, H. E., Koh, Y. H., & Estrin, Y. (2013). Highly aligned porous Ti scaffold coated with bone morphogenetic protein-loaded silica/chitosan hybrid for enhanced bone regeneration. *Journal of Biomedical Materials Research Part B: Applied Biomaterials*.

Jung, H. D., Yook, S. W., Han, C. M., Jang, T. S., Kim, H. E., Koh, Y. H., & Estrin, Y. (2014). Highly aligned porous Ti scaffold coated with bone morphogenetic protein-loaded silica/chitosan hybrid for enhanced bone regeneration. *Journal of Biomedical Materials Research Part B: Applied Biomaterials, 102*(5), 913-921.

Jung, U. W., Suh, J.-J., Choi, S.-H., Cho, K.-S., Chai, J.-K., & Kim, C.-K. (2000a). The Bone Regenerative Effects of Chitosan on the Calvarial Critical Size Defectin Sprague Dawley Rats. *The Journal of the Korean Academy of Periodontology, 30*(4), 851-868.

Jung, U. W., Suh, J. J., Choi, S. H., Cho, K. S., Chai, J. K., & Kim, C. K. (2000b). The Bone Regenerative Effects of Chitosan on the Calvarial Critical Size Defectin Sprague Dawley Rats. *The Journal of the Korean Academy of Periodontology, 30*(4), 851-868.

Karunanithy, P., Prasad, R., Jakka, V. S., Aparna, R., Phani, A., Prabhakara, G., & Ahmed, S. A. (2013). Enhanced Antimicrobial Activity of Polyaniline Grafted Chitosan. *Advanced Science, Engineering and Medicine, 5*(5), 420-426.

Katime, I., & Mendizábal, E. (2010). Swelling properties of new hydrogels based on the dimethyl amino ethyl acrylate methyl chloride quaternary salt with acrylic acid and 2-methylene butane-1, 4-dioic acid monomers in aqueous solutions. *Materials Sciences and Applications, 1*(03), 162.

Kim, C. H., Takai, E., Zhou, H., Von Stechow, D., Müller, R., Dempster, D. W., & Guo, X. E. (2003). Trabecular bone response to mechanical and parathyroid hormone stimulation: the role of mechanical microenvironment. *Journal of Bone and Mineral Research, 18*(12), 2116-2125.

Kim, H.-J., Zhao, H., Kitaura, H., Bhattacharyya, S., Brewer, J. A., Muglia, L. J., Ross, F. P., & Teitelbaum, S. L. (2006). Glucocorticoids suppress bone formation via the osteoclast. *Journal of Clinical Investigation, 116*(8), 2152-2160.

Kim, M.-O., Jung, H., Kim, S.-C., Park, J.-K., & Seo, Y.-K. (2015). Electromagnetic fields and nanomagnetic particles increase the osteogenic differentiation of

human bone marrow-derived mesenchymal stem cells. *International Journal of Molecular Medicine, 35*(1), 153-160.

Kim, S. E., Song, S.-H., Yun, Y. P., Choi, B.-J., Kwon, I. K., Bae, M. S., Moon, H.-J., & Kwon, Y.-D. (2011). The effect of immobilization of heparin and bone morphogenic protein-2 (BMP-2) to titanium surfaces on inflammation and osteoblast function. *Biomaterials, 32*(2), 366-373.

Kobayashi-Sakamoto, M., Hirose, K., Isogai, E., & Chiba, I. (2004). NF-κB-dependent induction of osteoprotegerin by Porphyromonas gingivalis in endothelial cells. *Biochemical and Biophysical Research Communications, 315*(1), 107-112.

Kohli, S. S., & Kohli, V. S. (2011). Role of RANKL–RANK/osteoprotegerin molecular complex in bone remodeling and its immunopathologic implications. *Indian Journal of Endocrinology and Metabolism, 15*(3), 175.

Koide, M., Kobayashi, Y., Ninomiya, T., Nakamura, M., Yasuda, H., Arai, Y., Okahashi, N., Yoshinari, N., Takahashi, N., & Udagawa, N. (2013). Osteoprotegerin-Deficient Male Mice as a Model for Severe Alveolar Bone Loss: Comparison With RANKL-Overexpressing Transgenic Male Mice. *Endocrinology, 154*(2), 773-782.

Kong, Y.-Y., Feige, U., Sarosi, I., Bolon, B., Tafuri, A., Morony, S., Capparelli, C., Li, J., Elliott, R., & McCabe, S. (1999a). Activated T cells regulate bone loss and joint destruction in adjuvant arthritis through osteoprotegerin ligand. *Nature, 402*, 43-47.

Kong, Y.-Y., Yoshida, H., Sarosi, I., Tan, H.-L., Timms, E., Capparelli, C., Morony, S., Oliveira-dos-Santos, A. J., Van, G., & Itie, A. (1999b). OPGL is a key regulator of osteoclastogenesis, lymphocyte development and lymph-node organogenesis. *Nature, 397*(6717), 315-323.

Korsmeyer, S. J. (1999). BCL-2 gene family and the regulation of programmed cell death. *Cancer Research, 59*(7), 1693s-1700s.

Kostenuik, P. J., Capparelli, C., Morony, S., Adamu, S., Shimamoto, G., Shen, V., Lacey, D. L., & Dunstan, C. R. (2001). OPG and PTH-(1–34) have additive effects on bone density and mechanical strength in osteopenic ovariectomized rats. *Endocrinology, 142*(10), 4295-4304.

Kries, J. P., Warrier, T., & Podust, L. M. (2010). Identification of Small-Molecule Scaffolds for P450 Inhibitors. *Current Protocols in Microbiology*, 17.14. 11-17.14. 25.

Kumbar, S., Laurencin, C., & Deng, M. (2014). *Natural and Synthetic Biomedical Polymers*: Newnes.

Kuo, S.-M., Niu, G., Lan, C.-W., Cheng, M.-F., Chiang, M.-Y., & Chang, S.-J. (2009). Guided tissue regeneration with use of CaSO4-Chitosan composite membrane. *Journal of Medical and Biological Engineering, 29*(6).

Lamoureux, F., Richard, P., Wittrant, Y., Battaglia, S., Pilet, P., Trichet, V., Blanchard, F., Gouin, F., Pitard, B., Heymann, D., & Redini, F. (2007). Therapeutic Relevance of Osteoprotegerin Gene Therapy in Osteosarcoma: Blockade of the Vicious Cycle between Tumor Cell Proliferation and Bone Resorption. *Cancer Research, 67*(15), 7308-7318.

Lane, D., Matte, I., Rancourt, C., & Piché, A. (2012). Osteoprotegerin (OPG) protects ovarian cancer cells from TRAIL-induced apoptosis but does not contribute to malignant ascites-mediated attenuation of TRAIL-induced apoptosis. *J Ovarian Res, 5*(1), 34.

Lee, S.-K., & Lorenzo, J. A. (1999). Parathyroid hormone stimulates TRANCE and inhibits osteoprotegerin messenger ribonucleic acid expression in murine bone marrow cultures: correlation with osteoclast-like cell formation. *Endocrinology, 140*(8), 3552-3561.

Lee, Y.-M., Park, Y.-J., Lee, S.-J., Ku, Y., Han, S.-B., Klokkevold, P. R., & Chung, C.-P. (2000). The bone regenerative effect of platelet-derived growth factor-BB delivered with a chitosan/tricalcium phosphate sponge carrier. *Journal of Periodontology, 71*(3), 418-424.

LeHoux, J., & Grondin, F. (1993). Some effects of chitosan on liver function in the rat. *Endocrinology, 132*(3), 1078-1084.

Lemke, J. v., Von Karstedt, S., Zinngrebe, J., & Walczak, H. (2014). Getting TRAIL back on track for cancer therapy. *Cell Death & Differentiation, 21*(9), 1350-1364.

Levengood, S. K. L., & Zhang, M. (2014). Chitosan-based scaffolds for bone tissue engineering. *Journal of Materials Chemistry B, 2*(21), 3161-3184.

Li, J., Du, Y., & Liang, H. (2007). Influence of molecular parameters on the degradation of chitosan by a commercial enzyme. *Polymer Degradation and Stability, 92*(3), 515-524.

Lienemann, P. S., Lutolf, M. P., & Ehrbar, M. (2012). Biomimetic hydrogels for controlled biomolecule delivery to augment bone regeneration. *Advanced Drug Delivery Reviews, 64*(12), 1078-1089.

Liebschner, M. A. (2004). Biomechanical considerations of animal models used in tissue engineering of bone. *Biomaterials, 25*(9), 1697-1714.

Liu, W., & Zhang, X. (2015). Receptor activator of nuclear factor-κB ligand (RANKL)/RANK/osteoprotegerin system in bone and other tissues (Review). *Molecular Medicine Reports, 11*(5), 3212-3218.

Lubberts, E., van den Bersselaar, L., Oppers-Walgreen, B., Schwarzenberger, P., Coenen-de Roo, C. J., Kolls, J. K., Joosten, L. A., & van den Berg, W. B. (2003). IL-17 promotes bone erosion in murine collagen-induced arthritis through loss of the receptor activator of NF-κB ligand/osteoprotegerin balance. *The Journal of Immunology, 170*(5), 2655-2662.

Lum, L., Wong, B. R., Josien, R., Becherer, J. D., Erdjument-Bromage, H., Schlöndorff, J., Tempst, P., Choi, Y., & Blobel, C. P. (1999). Evidence for a role of a tumor necrosis factor-α (TNF-α)-converting enzyme-like protease in shedding of TRANCE, a TNF family member involved in osteoclastogenesis and dendritic cell survival. *Journal of Biological Chemistry, 274*(19), 13613-13618.

Ma, L., Gao, C., Mao, Z., Zhou, J., Shen, J., Hu, X., & Han, C. (2003). Collagen/chitosan porous scaffolds with improved biostability for skin tissue engineering. *Biomaterials, 24*(26), 4833-4841.

Maréchal, M., Luyten, F., Nijs, J., Postnov, A., Schepers, E., & Steenberghe, D. (2005). Histomorphometry and micro-computed tomography of bone augmentation under a titanium membrane. *Clinical Oral Implants Research, 16*(6), 708-714.

Matassi, F., Nistri, L., Paez, D. C., & Innocenti, M. (2011). New biomaterials for bone regeneration. *Clinical Cases in Mineral and Bone Metabolism, 8*(1), 21.

Meihua, Z., Yunzhi, Y., & Yu, M. (2012). The expression and significance of receptor activator of nuclear factor κB ligand and osteoprotegerin in periapical cyst and periapical granuloma. *West China Journal of Stomatology, 30*(4).

Mendes, S. C., Reis, R., Bovell, Y. P., Cunha, A., van Blitterswijk, C. A., & de Bruijn, J. D. (2001). Biocompatibility testing of novel starch-based materials with potential application in orthopaedic surgery: a preliminary study. *Biomaterials, 22*(14), 2057-2064.

Mennini, N., Furlanetto, S., Maestrelli, F., Pinzauti, S., & Mura, P. (2008). Response surface methodology in the optimization of chitosan–Ca pectinate bead formulations. *European journal of pharmaceutical sciences, 35*(4), 318-325.

Mescher, A. L. (2013). *Junqueira's basic histology: text and atlas*: Mcgraw-hill.

Mhurchu, C. N., Dunshea-Mooij, C., Bennett, D., & Rodgers, A. (2005). Effect of chitosan on weight loss in overweight and obese individuals: a systematic review of randomized controlled trials. *Obesity Reviews, 6*(1), 35-42.

Milone, F., Pivonello, C., Cariati, F., Sarnataro, M., Ramundo, V., Marotta, V., Jann, H., Pape, U.-F., Wiedenmann, B., & Colao, A. (2013). Assessment and clinical implications of RANK/RANKL/OPG pathway as markers of bone tumor progression in patients with NET harboring bone metastases. *Biomarkers, 18*(2), 121-125.

Mirmohammadsadeghi, H., Sabzghabaee, A., Javanmard, S. H., Moshayedi, M., & Barneh, F. (2012). Set-up an alamarblue based viability assay as an alternative method to routine MTT tests. *Research in Pharmaceutical Sciences, 7*(5), S491.

Miyashita, T., Kawakami, A., Nakashima, T., Yamasaki, S., Tamai, M., Tanaka, F., Kamachi, M., Ida, H., Migita, K., & Origuchi, T. (2004). Osteoprotegerin (OPG) acts as an endogenous decoy receptor in tumour necrosis factor-related apoptosis-inducing ligand (TRAIL)-mediated apoptosis of fibroblast-like synovial cells. *Clinical & Experimental Immunology, 137*(2), 430-436.

Mogi, M., Otogoto, J., Ota, N., & Togari, A. (2004). Differential expression of RANKL and osteoprotegerin in gingival crevicular fluid of patients with periodontitis. *Journal of Dental Research, 83*(2), 166-169.

Monfoulet, L. E., Rabier, B., Dacquin, R., Anginot, A., Photsavang, J., Jurdic, P., Vico, L., Malaval, L., & Chassande, O. (2011). Thyroid hormone receptor β mediates thyroid hormone effects on bone remodeling and bone mass. *Journal of Bone and Mineral Research, 26*(9), 2036-2044.

Moreira, M. d. R., Pereda, M., Marcovich, N. E., & Roura, S. I. (2011). Antimicrobial effectiveness of bioactive packaging materials from edible chitosan and casein polymers: assessment on carrot, cheese, and salami. *Journal of Food Science, 76*(1), M54-M63.

Mouriño, V., Cattalini, J. P., Roether, J. A., Dubey, P., Roy, I., & Boccaccini, A. R. (2013). Composite polymer-bioceramic scaffolds with drug delivery capability for bone tissue engineering. *Expert Opinion on Drug Delivery, 10*(10), 1353-1365.

Mundy, G. R. (2002). Metastasis: Metastasis to bone: causes, consequences and therapeutic opportunities. *Nature Reviews Cancer, 2*(8), 584-593.

Muzzarelli, R., Mattioli-Belmonte, M., Tietz, C., Biagini, R., Ferioli, G., Brunelli, M., Fini, M., Giardino, R., Ilari, P., & Biagini, G. (1994). Stimulatory effect on bone formation exerted by a modified chitosan. *Biomaterials, 15*(13), 1075-1081.

Nagasawa, T., Kobayashi, H., Kiji, M., Aramaki, M., Mahanonda, R., Kojima, T., Murakami, Y., Saito, M., Morotome, Y., & Ishikawa, I. (2002). LPS-stimulated human gingival fibroblasts inhibit the differentiation of monocytes into osteoclasts through the production of osteoprotegerin. *Clinical & Experimental Immunology, 130*(2), 338-344.

Nair, R., Reddy, B. H., Kumar, C. A., & Kumar, K. J. (2009). Application of Chitosan microspheres as drug carriers: A Review. *Journal of Pharmaceutical Sciences and Research, 1*(2), 1-12.

Nakamura, T., Imai, Y., Matsumoto, T., Sato, S., Takeuchi, K., Igarashi, K., Harada, Y., Azuma, Y., Krust, A., & Yamamoto, Y. (2007). Estrogen prevents bone loss via estrogen receptor α and induction of Fas ligand in osteoclasts. *Cell, 130*(5), 811-823.

Nakashima, T., & Penninger, J. M. (2003). RANKL and RANK as novel therapeutic targets for arthritis. *Current Opinion in Rheumatology, 15*(3), 280-287.

Neumann, E., Gay, S., & Müller-Ladner, U. (2005). The RANK/RANKL/osteoprotegerin system in rheumatoid arthritis: new insights from animal models. *Arthritis & Rheumatism, 52*(10), 2960-2967.

Neville-Webbe, H., Cross, N., Eaton, C., Nyambo, R., Evans, C., Coleman, R., & Holen, I. (2004). Osteoprotegerin (OPG) produced by bone marrow stromal cells protects breast cancer cells from TRAIL-induced apoptosis. *Breast Cancer Research and Treatment, 86*(3), 271-282.

Neyt, J., Buckwalter, J. A., & Carroll, N. (1998). Use of animal models in musculoskeletal research. *The Iowa Orthopaedic Journal, 18*, 118.

Noel, S. P., Courtney, H., Bumgardner, J. D., & Haggard, W. O. (2008). Chitosan Films: A Potential Local Drug Delivery System for Antibiotics. *Clinical Orthopaedics and Related Research, 466*(6), 1377-1382.

Nor Asiah, M., Halim, A. S., Shamsuddin, S., Hussin, C. M. C., Ujang, Z., & Rashid, A. H. A. (2013). The effect of chitosan derivatives film on the proliferation of human skin fibroblast: an-in vitro study. *Journal of Sustainability Science and Management, 8*(2), 212-219.

Nor, N. A. M., Halim, A. S., Shamsuddin, S., Hussin, C. M. C., Ujang, Z., & Rashid, A. H. A. (2013). The effect of chitosan derivatives film on the proliferation of human skin fibroblast: an-in vitro study. *Journal of Sustainability Science and Management, 8*(2), 212-219.

Nunthanid, J., Laungtana-Anan, M., Sriamornsak, P., Limmatvapirat, S., Puttipipatkhachorn, S., Lim, L., & Khor, E. (2004). Characterization of chitosan acetate as a binder for sustained release tablets. *Journal of Controlled Release, 99*(1), 15-26.

Nwe, N., Furuike, T., & Tamura, H. (2009). The mechanical and biological properties of chitosan scaffolds for tissue regeneration templates are significantly enhanced by chitosan from Gongronella butleri. *Materials, 2*(2), 374-398.

Oktay, E., Demiralp, B., Demiralp, B., Senel, S., Cevdet Akman, A., Eratalay, K., & Akincibay, H. (2010). Effects of platelet-rich plasma and chitosan combination on bone regeneration in experimental rabbit cranial defects. *Journal of Oral Implantology, 36*(3), 175-184.

Onyia, J., Miles, R., Yang, X., Halladay, D., Hale, J., Glasebrook, A., McClure, D., Seno, G., Churgay, L., & Chandrasekhar, S. (2000). In vivo demonstration that human parathyroid hormone 1–38 inhibits the expression of osteoprotegerin in bone with the kinetics of an immediate early gene. *Journal of Bone and Mineral Research, 15*(5), 863-871.

Oyajobi, B. O. (2007). Multiple myeloma/hypercalcemia. *Arthritis research and therapy, 9*, S4.

Pang, E.-K., Paik, J.-W., Kim, S.-K., Jung, U.-W., Kim, C.-S., Cho, K.-S., Kim, C.-K., & Choi, S.-H. (2005). Effects of chitosan on human periodontal ligament fibroblasts in vitro and on bone formation in rat calvarial defects. *Journal of periodontology, 76*(9), 1526-1533.

Park, H., Min, C., Kwak, H., Youn, K., Choi, S., & Kim, H. (2004). Topography of the outer mandibular symphyseal region with reference to the autogenous bone graft. *International Journal of Oral and Maxillofacial Surgery, 33*(8), 781-785.

Pearce, A., Richards, R., Milz, S., Schneider, E., & Pearce, S. (2007). Animal models for implant biomaterial research in bone: a review. *Eur Cell Mater, 13*(1), 1-10.

Pederson, L., Kremer, M., Judd, J., Pascoe, D., Spelsberg, T. C., Riggs, B. L., & Oursler, M. J. (1999). Androgens regulate bone resorption activity of isolated osteoclasts in vitro. *Proceedings of the National Academy of Sciences, 96*(2), 505-510.

Pederson, L., Ruan, M., Westendorf, J. J., Khosla, S., & Oursler, M. J. (2008). Regulation of bone formation by osteoclasts involves Wnt/BMP signaling and the chemokine sphingosine-1-phosphate. *Proceedings of the National Academy of Sciences, 105*(52), 20764-20769.

Perrien, D. S., Brown, E. C., Aronson, J., Skinner, R. A., Montague, D. C., Badger, T. M., & Lumpkin, C. K. (2002). Immunohistochemical study of osteopontin expression during distraction osteogenesis in the rat. *Journal of Histochemistry & Cytochemistry, 50*(4), 567-574.

Perrini, S., Laviola, L., Carreira, M. C., Cignarelli, A., Natalicchio, A., & Giorgino, F. (2010). The GH/IGF1 axis and signaling pathways in the muscle and bone: mechanisms underlying age-related skeletal muscle wasting and osteoporosis. *Journal of Endocrinology, 205*(3), 201-210.

Porstmann, B., Jung, K., Schmechta, H., Evers, U., Pergande, M., Porstmann, T., Kramm, H.-J., & Krause, H. (1989). Measurement of lysozyme in human body fluids: comparison of various enzyme immunoassay techniques and their diagnostic application. *Clinical Biochemistry, 22*(5), 349-355.

Pranoto, Y., Rakshit, S., & Salokhe, V. (2005). Enhancing antimicrobial activity of chitosan films by incorporating garlic oil, potassium sorbate and nisin. *LWT-Food Science and Technology, 38*(8), 859-865.

Pritzker, L. B. (2004). The Role of Osteoprotegerin and Tumor Necrosis Factor-related Apoptosis-inducing Ligand in Human Microvascular Endothelial Cell Survival. *Molecular Biology of the Cell, 15*(6), 2834-2841.

Qian, Y., & Huang, H. Z. (2010). The role of RANKL and MMP-9 in the bone resorption caused by ameloblastoma. *Journal of Oral Pathology & Medicine, 39*(8), 592-598.

Rampersad, S. N. (2012). Multiple applications of Alamar Blue as an indicator of metabolic function and cellular health in cell viability bioassays. *Sensors, 12*(9), 12347-12360.

Reid, P. E., Brown, N. J., & Holen, I. (2009). Breast cancer cells stimulate osteoprotegerin (OPG) production by endothelial cells through direct cell contact. *Molecular cancer, 8*(1), 49.

Rentsch, C., Rentsch, B., Heinemann, S., Bernhardt, R., Bischoff, B., Förster, Y., Scharnweber, D., & Rammelt, S. (2014). ECM inspired coating of embroidered 3D scaffolds enhances calvaria bone regeneration. *BioMed research international, 2014*.

Rodrigues, J. C., Hegde, M. N., & Kumari, S. (2012). A comparative evaluation of root canal sealers on human gingival fibroblasts-A cell culture study. *Thermal Behavior of Conventional and Thermoplastic Gutta-percha Cones, 24*(1), 48.

Rogers, G. F., & Greene, A. K. (2012). Autogenous bone graft: basic science and clinical implications. *Journal of Craniofacial Surgery, 23*(1), 323-327.

Ross, M. H., & Pawlina, W. (Eds.). (2011). *Histology: a text and atlas: with correlated cell and molecular biology* (sixth edition ed.): Lippincott Wiliams & Wilkins, a Wolters Kluwer business.

Ruhl, S., Berlenbach, P., Langenfelder, S., Hörl, D., Lehn, N., Hiller, K. A., & Durchschlag, H. (2011). Integrity of proteins in human saliva after sterilization by gamma irradiation. Applied and environmental microbiology, 77(3), 749-755.

Sakata, M., Shiba, H., Komatsuzawa, H., Fujita, T., Ohta, K., Sugai, M., Suginaka, H., & Kurihara, H. (1999). Expression of osteoprotegerin (osteoclastogenesis inhibitory factor) in cultures of human dental mesenchymal cells and epithelial cells. *Journal of Bone and Mineral Research, 14*(9), 1486-1492.

Sakurai, K., Maegawa, T., & Takahashi, T. (2000). Glass transition temperature of chitosan and miscibility of chitosan/poly (N-vinyl pyrrolidone) blends. *Polymer, 41*(19), 7051-7056.

Sato, T., Tominaga, Y., Iwasaki, Y., Kazama, J. J., Shigematsu, T., Inagaki, H., Watanabe, I., Katayama, A., Haba, T., & Uchida, K. (2001). Osteoprotegerin levels before and after renal transplantation. *American journal of kidney diseases, 38*(4), S175-S177.

Scanlon, C. S., Marchesan, J. T., Soehren, S., Matsuo, M., & Kapila, Y. L. (2011). Capturing the regenerative potential of periodontal ligament fibroblasts. *Journal of Stem cells & Regenerative medicine, 7*(1), 54.

Schimandle, J. H., & Boden, S. D. (1994). Spine update the use of animal models to study spinal fusion. *Spine, 19*(17), 1998-2006.

Schneeweis, L. A., Willard, D., & Milla, M. E. (2005). Functional dissection of osteoprotegerin and its interaction with receptor activator of NF-κB ligand. *Journal of Biological Chemistry, 280*(50), 41155-41164.

Schwach-Abdellaoui, K., Vivien-Castioni, N., & Gurny, R. (2000). Local delivery of antimicrobial agents for the treatment of periodontal diseases. *European Journal of Pharmaceutics and Biopharmaceutics, 50*(1), 83-99.

Scipioni, R., Gazzoli, D., Teocoli, F., Palumbo, O., Paolone, A., Ibris, N., Brutti, S., & Navarra, M. A. (2014). Preparation and characterization of nanocomposite polymer membranes containing functionalized SnO2 additives. *Membranes, 4*(1), 123-142.

Sgambetterra, M., Brutti, S., Allodi, V., Mariotto, G., Panero, S., & Navarra, M. A. (2016). Critical Filler Concentration in Sulfated Titania-Added Nafion™ Membranes for Fuel Cell Applications. *Energies, 9*(4), 272.

Shipman, C. M., & Croucher, P. I. (2003). Osteoprotegerin is a soluble decoy receptor for tumor necrosis factor-related apoptosis-inducing ligand/Apo2 ligand and can function as a paracrine survival factor for human myeloma cells. *Cancer Research, 63*(5), 912-916.

Silva, S., Goodfellow, B. J., Benesch, J., Rocha, J., Mano, J., & Reis, R. (2007). Morphology and miscibility of chitosan/soy protein blended membranes. *Carbohydrate Polymers, 70*(1), 25-31.

Simonet, W., Lacey, D., Dunstan, C., Kelley, M., Chang, M.-S., Lüthy, R., Nguyen, H., Wooden, S., Bennett, L., & Boone, T. (1997). Osteoprotegerin: a novel secreted protein involved in the regulation of bone density. *Cell, 89*(2), 309-319.

Sodek, J., Ganss, B., & McKee, M. (2000). Osteopontin. *Critical Reviews in Oral Biology & Medicine, 11*(3), 279-303.

Soysa, N. S., Alles, N., Aoki, K., & Ohya, K. (2012). Osteoclast formation and differentiation: an overview. *J Med Dent Sci, 59*(3), 65-74.

Spicer, P. P., Kretlow, J. D., Young, S., Jansen, J. A., Kasper, F. K., & Mikos, A. G. (2012). Evaluation of bone regeneration using the rat critical size calvarial defect. *Nature protocols, 7*(10), 1918-1929.

Spin-Neto, R., Coletti, F. L., Freitas, R. M. d., Pavone, C., Campana-Filho, S. P., & Marcantonio, R. A. C. (2012). Chitosan-based biomaterials used in critical-size bone defects: radiographic study in rat's calvaria. *Revista de Odontologia da UNESP, 41*(5), 312-317.

Spin-Neto, R., De Freitas, R. M., Pavone, C., Cardoso, M. B., Campana-Filho, S. P., Marcantonio, R. A. C., & Marcantonio, E. (2010). Histological evaluation of chitosan-based biomaterials used for the correction of critical size defects in rat's calvaria. *Journal of Biomedical Materials Research Part A, 93*(1), 107-114.

Srinatha, A., Pandit, J., & Singh, S. (2008). Ionic cross-linked chitosan beads for extended release of ciprofloxacin: in vitro characterization. *Indian Journal of Pharmaceutical Sciences, 70*(1), 16.

Stein, E., Ebeling, P., & Shane, E. (2007). Post-transplantation osteoporosis. *Endocrinology and metabolism clinics of North America, 36*(4), 937-963.

Stilgren, L., Hegedüs, L., Beck-Nielsen, H., & Abrahamsen, B. (2003). Osteoprotegerin levels in primary hyperparathyroidism: effect of parathyroidectomy and association with bone metabolism. *Calcified tissue international, 73*(3), 210-216.

Struillou, X., Boutigny, H., Soueidan, A., & Layrolle, P. (2010). Experimental animal models in periodontology: a review. *The Open Dentistry Journal, 4*, 37.

Suda, T., Takahashi, N., Udagawa, N., Jimi, E., Gillespie, M. T., & Martin, T. J. (1999). Modulation of osteoclast differentiation and function by the new members of the tumor necrosis factor receptor and ligand families. *Endocrine Reviews, 20*(3), 345-357.

Szymczak, J., & Bohdanowicz-Pawlak, A. (2013). Osteoprotegerin, RANKL, and Bone Turnover in Primary Hyperparathyroidism: The Effect of Parathyroidectomy and Treatment with Alendronate. *Hormone and Metabolic Research*(EFirst).

Tanaka, H., Mine, T., Ogasa, H., Taguchi, T., & Liang, C. T. (2011). Expression of RANKL/OPG during bone remodeling in vivo. *Biochemical and Biophysical Research Communications, 411*(4), 690-694.

Tangsadthakun, C., Kanokpanont, S., Sanchavanakit, N., Banaprasert, T., & Damrongsakkul, S. (2017). Properties of collagen/chitosan scaffolds for skin tissue engineering. *Journal of Metals, Materials and Minerals, 16(1)*.

Taubman, M., & Kawai, T. (2001). Involvement of T-lymphocytes in periodontal disease and in direct and indirect induction of bone resorption. *Critical Reviews in Oral Biology & Medicine, 12*(2), 125-135.

Tera, T. d. M., Nascimento, R. D., Prado, R. F. d., Santamaria, M. P., & JARDINI, M. A. N. (2014). Immunolocalization of markers for bone formation during guided bone regeneration in osteopenic rats. *Journal of Applied Oral Science, 22*(6), 541-553.

Teti, A. (2013). Mechanisms of osteoclast-dependent bone formation. *BoneKEy reports,2*.

Theoleyre, S., Kwan Tat, S., Vusio, P., Blanchard, F., Gallagher, J., Ricard-Blum, S., Fortun, Y., Padrines, M., Redini, F., & Heymann, D. (2006). Characterization of osteoprotegerin binding to glycosaminoglycans by surface plasmon resonance: Role in the interactions with receptor activator of nuclear factor κB ligand (RANKL) and RANK. *Biochemical and biophysical research communications, 347*(2), 460-467.

Thirunavukkarasu, K., Miles, R. R., Halladay, D. L., Yang, X., Galvin, R. J., Chandrasekhar, S., Martin, T. J., & Onyia, J. E. (2001). Stimulation of Osteoprotegerin (OPG) Gene Expression by Transforming Growth Factor-β (TGF-β) mapping of the opg promoter region that mediates TGF-β effects. *Journal of Biological Chemistry, 276*(39), 36241-36250.

Thompson, W. R., Uzer, G., Brobst, K. E., Xie, Z., Sen, B., Yen, S. S., Styner, M., & Rubin, J. (2015). Osteocyte specific responses to soluble and mechanical stimuli in a stem cell derived culture model. *Scientific Reports, 5*.

Tiranathanagul, S., Yongchaitrakul, T., Pattamapun, K., & Pavasant, P. (2004). Actinobacillus actinomycetemcomitans lipopolysaccharide activates matrix metalloproteinase-2 and increases receptor activator of nuclear factor-κB ligand expression in human periodontal ligament cells. *Journal of Periodontology, 75*(12), 1647-1654.

Tiyaboonchai, W. (2003). Chitosan nanoparticles: a promising system for drug delivery. *Naresuan University Journal, 11*(3), 51-66.

Tiyaboonchai, W. (2013). Chitosan nanoparticles: a promising system for drug delivery. *Naresuan University Journal, 11*(3), 51-66.

Tobón-Arroyave, S. I., Franco-González, L. M., Isaza-Guzmán, D. M., Floréz-Moreno, G. A., Bravo-Vásquez, T., Castañeda-Peláez, D. A., & Vieco-Durán, B. (2005). Immunohistochemical expression of RANK, GRα and CTR in central giant cell granuloma of the jaws. *Oral Oncology, 41*(5), 480-488.

Tomoyasu, A., Goto, M., Fujise, N., Mochizuki, S.-i., Yasuda, H., Morinaga, T., Tsuda, E., & Higashio, K. (1998). Characterization of monomeric and homodimeric forms of osteoclastogenesis inhibitory factor. *Biochemical and Biophysical Research Communications, 245*(2), 382-387.

Troen, B. R. (2004). The role of cathepsin K in normal bone resorption. *Drug News Perspect, 17*(1), 19-28.

Tsukii, K., Shima, N., Mochizuki, S.-i., Yamaguchi, K., Kinosaki, M., Yano, K., Shibata, O., Udagawa, N., Yasuda, H., & Suda, T. (1998). Osteoclast Differentiation Factor Mediates an Essential Signal for Bone Resorption Induced by 1α, 25-Dihydroxyvitamin D$_3$, Prostaglandin E$_2$, or Parathyroid Hormone in the Microenvironment of Bone. *Biochemical and Biophysical Research Communications, 246*(2), 337-341.

Tunyogi-Csapo, M., Kis-Toth, K., Radacs, M., Farkas, B., Jacobs, J. J., Finnegan, A., Mikecz, K., & Glant, T. T. (2008). Cytokine-controlled RANKL and osteoprotegerin expression by human and mouse synovial fibroblasts: Fibroblast-mediated pathologic bone resorption. *Arthritis & Rheumatism, 58*(8), 2397-2408.

Turner, P. V., Kerr, C. L., Healy, A. J., & Taylor, W. M. (2006). Effect of meloxicam and butorphanol on minimum alveolar concentration of isoflurane in rabbits. *American Journal of Veterinary Research, 67*(5), 770-774.

Ueland, T., Bollerslev, J., Godang, K., Muller, F., Froland, S. S., & Aukrust, P. (2001). Increased serum osteoprotegerin in disorders characterized by persistent immune activation or glucocorticoid excess--possible role in bone homeostasis. *European Journal of Endocrinology, 145*(6), 685-690.

Vårum, K. M., Myhr, M. M., Hjerde, R. J., & Smidsrød, O. (1997). In vitro degradation rates of partially N-acetylated chitosans in human serum. *Carbohydrate Research, 299*(1), 99-101.

Vega, D., Maalouf, N. M., & Sakhaee, K. (2007). The role of receptor activator of nuclear factor-κB (RANK)/RANK ligand/osteoprotegerin: clinical implications. *Journal of Clinical Endocrinology & Metabolism, 92*(12), 4514-4521.

von Tirpitz, C., Epp, S., Klaus, J., Mason, R., Hawa, G., Brinskelle-Schmal, N., Hofbauer, L. C., Adler, G., Kratzer, W., & Reinshagen, M. (2003). Effect of systemic glucocorticoid therapy on bone metabolism and the osteoprotegerin system in patients with active Crohn's disease. *European Journal of Gastroenterology & Hepatology, 15*(11), 1165-1170.

Wang, J., Gao, H., Wang, K., Zhou, R., Li, X., Guo, J., & Lv, H. (2011). Effect of epimedium extract on osteoprotegerin and RANKL mRNA expressions in

glucocorticoid-induced femoral head necrosis in rats]. *Nan fang yi ke da xue xue bao= Journal of Southern Medical University, 31*(10), 1714.

Wang, Q., Zhang, J., & Wang, A. (2009). Preparation and characterization of a novel pH-sensitive chitosan-g-poly (acrylic acid)/attapulgite/sodium alginate composite hydrogel bead for controlled release of diclofenac sodium. *Carbohydrate Polymers, 78*(4), 731-737.

Wang, Z., Liu, W., Han, B., Yao, R., & Wei, C. (2007). [Preparation of carboxymethyl-chitosan with different molecular weight and its effects on proliferation of skin fibroblasts and keratinocytes]. *Journal of Biomedical Engineering, 24*(2), 340-344.

Whyte, M. P., Obrecht, S. E., Finnegan, P. M., Jones, J. L., Podgornik, M. N., McAlister, W. H., & Mumm, S. (2002). Osteoprotegerin deficiency and juvenile Paget's disease. *New England Journal of Medicine, 347*(3), 175-184.

Wiley, S. R., Schooley, K., Smolak, P. J., Din, W. S., Huang, C.-P., Nicholl, J. K., Sutherland, G. R., Smith, T. D., Rauch, C., & Smith, C. A. (1995). Identification and characterization of a new member of the TNF family that induces apoptosis. *Immunity, 3*(6), 673-682.

Wiren, K. M., Toombs, A. R., Semirale, A. A., & Zhang, X. (2006). Osteoblast and osteocyte apoptosis associated with androgen action in bone: requirement of increased Bax/Bcl-2 ratio. *Bone, 38*(5), 637-651.

Wittenburg, G., Volkel, C., Mai, R., & Lauer, G. (2009). Immunohistochemical comparison of differentiation markers on paraffin and plastic embedded human bone samples. *J Physiol Pharmacol, 60*(Suppl 8), 43-49.

Yamaguchi, K., Kinosaki, M., Goto, M., Kobayashi, F., Tsuda, E., Morinaga, T., & Higashio, K. (1998). Characterization of structural domains of human osteoclastogenesis inhibitory factor. *Journal of Biological Chemistry, 273*(9), 5117-5123.

Yan, L. P., Wang, Y. J., Ren, L., Wu, G., Caridade, S. G., Fan, J. B., Wang, L. Y., Ji, P. H., Oliveira, J. M., & Oliveira, J. T. (2010). Genipin-cross-linked collagen/chitosan biomimetic scaffolds for articular cartilage tissue engineering applications. *Journal of Biomedical Materials Research Part A, 95*(2), 465-475.

Yao, Y., Wang, G., Wang, Z., Wang, C., Zhang, H., & Liu, C. (2011). Synergistic enhancement of new bone formation by recombinant human bone morphogenetic protein-2 and osteoprotegerin in trans-sutural distraction osteogenesis: a pilot study in dogs. *Journal of Oral and Maxillofacial Surgery, 69*(11), e446-e455.

Yasmeen, S., Lo, M. K., Bajracharya, S., & Roldo, M. (2014). Injectable scaffolds for bone regeneration. *Langmuir, 30*(43), 12977-12985.

Yasuda, H., Shima, N., Nakagawa, N., Mochizuki, S.-I., Yano, K., Fujise, N., Sato, Y., Goto, M., Yamaguchi, K., & Kuriyama, M. (1998). Identity of osteoclastogenesis inhibitory factor (OCIF) and osteoprotegerin (OPG): a

mechanism by which OPG/OCIF inhibits osteoclastogenesis in vitro. *Endocrinology, 139*(3), 1329-1337.

Yeung, R. S. (2004). The osteoprotegerin/osteoprotegerin ligand family: role in inflammation and bone loss. *The Journal of rheumatology, 31*(5), 844-846.

Yun, Y.-P., Lee, S.-Y., Kim, H.-J., Song, J.-J., & Kim, S. E. (2013). Improvement of osteoblast functions by sustained release of bone morphogenetic protein-2 (BMP-2) from heparin-coated chitosan scaffold. *Tissue Engineering and Regenerative Medicine, 10*(4), 183-191.

Zamora, D. O., Natesan, S., & Christy, R. J. (2012). Constructing a collagen hydrogel for the delivery of stem cell-loaded chitosan microspheres. *JoVE (Journal of Visualized Experiments)*, (64), 3624-3624.

Zeng, D., Luo, X., & Tu, R. (2012). Application of bioactive coatings based on chitosan for soybean seed protection. *International Journal of Carbohydrate Chemistry, 2012*.

Zhang, H., & Neau, S. H. (2001). In vitro degradation of chitosan by a commercial enzyme preparation: effect of molecular weight and degree of deacetylation. *Biomaterials, 22*(12), 1653-1658.

Zhao, L., Chen, J., Cheng, L., Wang, X., Du, J., Wang, F., & Peng, Z. (2014). Effects of Enterococcus faecalis lipoteichoic acid on receptor activator of nuclear factor-κB ligand and osteoprotegerin expression in periodontal ligament fibroblasts. *International Endodontic Journal, 47*(2), 163-172.

Ziani, K., Ursúa, B., & Maté, J. I. (2010). Application of bioactive coatings based on chitosan for artichoke seed protection. *Crop protection, 29*(8), 853-859.

Zou, W., Amcheslavsky, A., & Bar-Shavit, Z. (2003). CpG oligodeoxynucleotides modulate the osteoclastogenic activity of osteoblasts via Toll-like receptor 9. *Journal of Biological Chemistry, 278*(19), 16732-16740.

LIST OF PUBLICATIONS AND PAPERS PRESENTED

PUBLICATIONS

- Soher Nagi Jayash *, Najihah M Hashim, Misni Misran and NA Baharuddin. *In vitro* evaluation of osteoprotegerin in chitosan for potential bone defect applications. PeerJ (Accepted) (ISI)

- Soher Nagi Jayash *, Najihah M Hashim, Misni Misran and NA Baharuddin. Formulation and *in vitro* & *in vivo* evaluation of a new osteoprotegerin-chitosan gel for bone tissue regeneration. Biomedical Materials Research Part A (Accepted) (ISI)

CONFERENCES

- International Conference on Innovative Dentistry 2015

- Annual Colloquium on Drug Development from Natural Products 2015 (Best poster presentation prize)

- International Conference of Natural Products 2014

PATENT

- An osteoprotegerin-chitosan gel for bone tissue regeneration. PI 2016701598, UM, in 4th May 2016.

In vitro evaluation of osteoprotegerin in chitosan for potential bone defect applications

Soher Nagi Jayash[1], Najihah M. Hashim[2,3], Misni Misran[4] and NA Baharuddin[1]

[1] Department of Restorative Dentistry, Faculty of Dentistry, University of Malaya, Kuala Lumpur, Malaysia
[2] Department of Pharmacy, Faculty of Medicine, University of Malaya, Kuala Lumpur, Malaysia
[3] Centre For Natural Products And Drug Discovery (CENAR), Department of Chemistry, Faculty of Science, University of Malaya, Kuala Lumpur, Malaysia
[4] Department of Chemistry, Faculty of Science, University of Malaya, Kuala Lumpur, Malaysia

ABSTRACT

Background. The receptor activator of nuclear factor kappa-B (RANK)/RANK ligand/osteoprotegerin (OPG) system plays a critical role in bone remodelling by regulating osteoclast formation and activity. OPG has been used systemically in the treatment of bone diseases. In searching for more effective and safer treatment for bone diseases, we investigated newly formulated OPG-chitosan complexes, which is prepared as a local application for its osteogenic potential to remediate bone defects. **Methods.** We examined high, medium and low molecular weights of chitosan combined with OPG. The cytotoxicity of OPG in chitosan and its proliferation *in vitro* was evaluated using normal, human periodontal ligament (NHPL) fibroblasts in 2D and 3D cell culture. The cytotoxicity of these combinations was compared by measuring cell survival with a tetrazolium salt reduction (MTT) assay and AlamarBlue assay. The cellular morphological changes were observed under an inverted microscope. A propidium iodide and acridine orange double-staining assay was used to evaluate the morphology and quantify the viable and nonviable cells. The expression level of osteopontin and osteocalcin protein in treated normal human osteoblast cells was evaluated by using Western blot. **Results.** The results demonstrated that OPG in combination with chitosan was nontoxic, and OPG combined with low molecular weight chitosan has the most significant effect on NHPL fibroblasts and stimulates proliferation of cells over the period of treatment.

Subjects Bioengineering, Orthopedics, Pharmacology
Keywords Chitosan, Osteoproteogerin, Bone, Normal human periodontal ligament fibroblast, Normal human osteoblast

INTRODUCTION

Osteoprotegerin (OPG) is a secretory glycoprotein of the tumour necrosis factor (TNF) receptor, which is highly expressed in adult bone, lung, heart, kidney and placenta (*Nagasawa et al., 2002*; *Baharuddin et al., 2015*). The role of OPG in the pathological aspects of bone diseases, such as osteoporosis associated with estrogen deficiency and

Formulation and *in vitro* & *in vivo* evaluation of a new osteoprotegerin-chitosan gel for bone tissue regeneration

Soher Nagi Jayash *[1], Najihah Mohd Hashim *[2,3], Misni Misran [4] and NA Baharuddin [1]

[1] Department of Restorative Dentistry, Faculty of Dentistry, University of Malaya, 30603 Kuala Lumpur, Malaysia

[2] Department of Pharmacy, Faculty of Medicine, University of Malaya, 50603 Kuala Lumpur, Malaysia

[3] Centre For Natural Products And Drug Discovery (CENAR), Department of Chemistry, Faculty of Science, University of Malaya, 50603 Kuala Lumpur, Malaysia

[4] Department of Chemistry, Faculty of Science, University of Malaya, 50603 Kuala Lumpur, Malaysia

* Corresponding author:

E-mail: soheernagi20@yahoo.com

najihahmh@gmail.com

Abstract

The osteoprotegerin (OPG) system plays a critical role in bone remodelling by regulating osteoclast formation and activity. The study aimed to determine the physicochemical properties and biocompatibility of a newly formulated OPG-chitosan gel. The OPG-chitosan gel was formulated using human OPG protein and water-soluble chitosan. The physicochemical properties were determined using Fourier transform infrared (FTIR) spectroscopy, thermogravimetric analysis (TGA) and differential scanning calorimetry (DSC).

APPENDIX

APPENDIX A : ETHICAL APPROVAL OF *IN VIVO* STUDY

UNIVERSITY OF MALAYA
KUALA LUMPUR

23rd January 2015

Dr. Nor Adinar binti Baharuddin
Department of Restorative Dentistry
Faculty of Dentistry

Dear Researcher,

Evaluation of osteogenic potential and systemic effects of newly formed OPG-chitosan gel in rabbit model

This is to inform you that the FOM Institutional Animal Care and Use Committee, University of Malaya (FOM IACUC) has approved your Animal Use Protocol with the above mentioned title for a duration of three (3) years until **January 2018.**

Please be advised that should you require changes to be made to the approved protocol, you are responsible to submit an application for amendments. Failure to do so may result in the Approval of your Animal Use Protocol be withdrawn by FOM IACUC.

Your Ethics Reference no. : **20150115/DENT/R/NAB**

Thank you.

Yours sincerely,

Professor Dr. Sim Si Mui
Chairperson
Faculty of Medicine Institutional Animal Care and Use Committee (FOM IACUC)

Faculty of Medicine Institutional Animal Care and Use Committee (FOM IACUC)
Deputy Dean (Research), Faculty of Medicine, University of Malaya, 50603, Kuala Lumpur, MALAYSIA
Tel: (603) 7967 7515 • Fax: (603) 7956 8841• E-mail: fom-iacuc@ummc.edu.my
• Website: http://www.resfom.um.edu.my

157

APPENDIX C: REAGENTS PREPARATION AND PROTOCOLS

- **Human Osteoprotegerin (OPG) ELISA Kit**

Detection range: 0.312 ng ml-1-20 ng/ml.

Materials provided

Assay plate (12 x 8 coated Microwells), Standard (Freeze dried), Biotin-antibody (100 x concentrate), HRP-avidin (100 x concentrate), Biotin-antibody Diluent, HRP-avidin Diluent, Sample Diluent, Wash Buffer (25 x concentrate), TMB Substrate, Stop Solution, Adhesive Strip (For 96 wells).

Reagent preparation

1- Biotin-antibody (1x) - Centrifuge the vial before opening. Biotin-antibody requires a 100-fold dilution. A suggested 100-fold dilution is 10 μl of Biotin-antibody + 990 μl of Biotin-antibody Diluent.

2. HRP-avidin (1x) - Centrifuge the vial before opening. HRP-avidin requires a 100-fold dilution. A suggested 100-fold dilution is 10 μl of HRP-avidin + 990 μl of HRP-avidin Diluent.

3. Wash Buffer(1x)- If crystals have formed in the concentrate, warm up to room temperature and mix gently until the crystals have completely dissolved. Dilute 20 ml of Wash Buffer Concentrate (25 x) into deionized or distilled water to prepare 500 ml of Wash Buffer (1 x).

4. Standard: Centrifuge the standard vial at 6000-10000rpm for 30s. Reconstitute the Standard with 1.0 ml of Sample Diluent. Do not substitute other diluents. This reconstitution produces a stock solution of 20 ng/ml. Mix the standard to ensure complete reconstitution and allow the standard to sit for a minimum of 15 minutes with gentle agitation prior to making dilutions. Pipette 250 μl of Sample Diluent into each tube (S0-S6). Use the stock solution to produce a 2-fold dilution series (below). Mix each tube thoroughly before the next transfer. The undiluted Standard serves as the high standard (20 ng/ml). Sample Diluent serves as the zero standard (0 ng/ml).

Tube	S7	S6	S5	S4	S3	S2	S1	S0
ng ml^{-1}	20	10	5	2.5	1.25	0.625	0.312	0

Assay procedure

Bring all reagents and samples to room temperature before use. Centrifuge the sample again after thawing before the assay. It is recommended that all samples and standards be assayed in duplicate.

1. Prepare all reagents, working standards, and samples as directed in the previous sections.

2. Refer to the Assay Layout Sheet to determine the number of wells to be used and put any remaining wells and the desiccant back into the pouch and seal the ziploc, store unused wells at 4°C.

3. Add 100µl of standard and sample per well. Cover with the adhesive strip provided. Incubate for 2 hours at 37°C. A plate layout is provided to record standards and samples assayed.

4. Remove the liquid of each well, don't wash.

5. Add 100µl of Biotin-antibody (1x) to each well. Cover with a new adhesive strip. Incubate for 1 hour at 37°C. (Biotin-antibody (1x) may appear cloudy. Warm up to room temperature and mix gently until solution appears uniform.)

6. Aspirate each well and wash, repeating the process two times for a total of three washes. Wash by filling each well with Wash Buffer (200µl) using a squirt bottle, multi-channel pipette, manifold dispenser, or autowasher, and let it stand for 2 minutes, complete removal of liquid at each step is essential to good performance. After the last wash, remove any remaining wash Buffer by aspirating ordecanting. Invert the plate and blot it against clean paper towels.

7. Add 100µl of HRP-avidin (1x) to each well. Cover the microtiter plate with a new adhesive strip. Incubate for 1 hour at 37°C.

8. Repeat the aspiration/wash process for five times as in step 6.

9. Add 90µl of TMB Substrate to each well. Incubate for 15-30 minutes at 37°C. Protect from light.

10. Add 50µl of Stop Solution to each well, gently tap the plate to ensure thorough mixing.

11. Determine the optical density of each well within 5 minutes, using a microplate reader set to 450 nm. If wavelength correction is available, set to 540 nm or 570 nm.

Subtract readings at 540 nm or 570 nm from the readings at 450 nm. This subtraction will correct for optical imperfections in the plate. Readings made directly at 450 nm without correction may be higher and less accurate.

ASSAY PROCEDURE SUMMARY

① Prepare reagents, samples and standards as instructed.

⬇

② Add 100µl standard or sample to each well. Incubate 2 hours at 37°C.

⬇

③ Remove the liquid of each well, don't wash.

⬇

④ Add 100µl Biotin-antibody(1x) to each well. Incubate 1 hour at 37°C.

⬇

⑤ Aspirate and wash 3 times.

⬇

⑥ Add 100µl HRP-avidin (1x) to each well. Incubate 1 hour at 37°C.

⬇

⑦ Aspirate and wash 5 times.

⬇
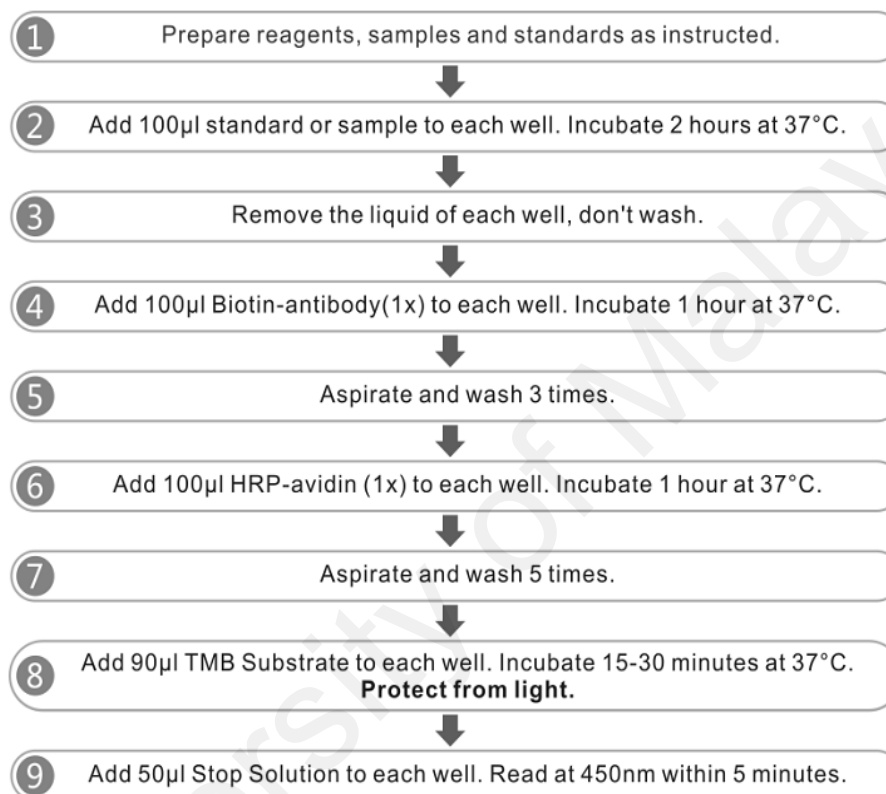
⑧ Add 90µl TMB Substrate to each well. Incubate 15-30 minutes at 37°C. **Protect from light.**

⬇

⑨ Add 50µl Stop Solution to each well. Read at 450nm within 5 minutes.

*Samples may require dilution. Please refer to Sample Preparation section.

- **NanoOrange® Protein Quantitation Kit**

Experimental Protocol

This section describes the protocol for 2 mL assays. For 200 μL microplate assays, adjust all volumes accordingly.

Reagent Preparation

1.1 **Prepare 1X protein quantitation diluent:** Mix the concentrated NanoOrange® protein quantitation diluent and dilute 10-fold in distilled water. For each assay, 2.5 mL of 1X protein quantitation diluent will be required.

1.2 **Prepare 1X NanoOrange® reagent working solution:** Dilute the NanoOrange® protein quantitation reagent (Component A) 500-fold into the 1X protein quantitation diluent from step 1.1.

For example, to prepare 50 mL of 1X NanoOrange® working solution (enough for 20 assays), first prepare the 1X diluent by mixing 5 mL of the 10X diluent stock with 45 mL of distilled water; next add 100 μL of the NanoOrange® reagent and mix thoroughly. Protect the 1X NanoOrange® working solution from light to prevent photodegradation of the NanoOrange® dye. For best results, use the working solution within a few hours of its preparation.

Notes About Heating Solutions in Microplates

This assay requires heating the sample to 90°C for 10 minutes to denature the protein. When samples are heated in a microplate, cover the plate must with a plastic cover or heat-resistant film to prevent evaporation. During the heating and cooling steps, water may condense on the cover, unless a special heater cover is used. To achieve accurate results, collect these water droplets by centrifuging the microplate briefly in a centrifuge. Alternatively, samples may be processed in microcentrifuge tubes, centrifuged in a microcentrifuge, and then transferred to microplate wells for reading. If transferring samples, we recommend transferring only 200 μL of the 250 μL sample, as it is difficult to retrieve all 250 μL using a pipette.

Protein Standard Curve

The reference standard curve is used to convert fluorescence to μg/mL protein, and also to control for variation between fluorometers and for day-to-day variation in the performance of a single fluorometer.

Ideally, the protein type used for the standard curve should be the same as the protein that is used in the experiment; however, as with other protein assays, bovine serum albumin (BSA) serves as a convenient reference standard. The NanoOrange® Kit includes a 2 mg/mL sample of BSA (Component B) that can be used to prepare a standard curve.

The standard curve may be generated to cover the full assay range, 0–10 μg/mL, or to cover a selected range. This section describes how to generate a simple standard curve with points corresponding to 0, 1, 3, 6, and 10 μg BSA per mL. If desired, serial dilutions can be made to create additional standards ranging from 0.01 to 0.6 μg/mL, to fill out the standard curve in the low range.

2.1 **Prepare a 10 μg/mL solution of BSA:** Dilute the 2 mg/mL BSA standard (Component B) 1:200 into the 1X NanoOrange® working solution. For example, dilute 30 μL of BSA standard into 5.97 mL of 1X NanoOrange® working solution (prepared in step 1.2).

2.2 Dilute the 10 μg/mL BSA solution to make 0, 1, 3, 6, and 10 μg/mL standards, as described in Table 3.

2.3 If desired, prepare 0.1, 0.3, and 0.6 μg/mL standards, as described in Table 3, by diluting a

Table 3. Protocol for preparing a standard curve using BSA.

Volume (µL) of BSA Solution*	Volume of 1X NanoOrange® Working Solution	Final BSA Concentration
0 mL	2.50 mL	0 µg/mL
2.50 mL of 10 µg/mL	0 mL	10 µg/mL
1.50 mL of 10 µg/mL	1.00 mL	6 µg/mL
0.75 mL of 10 µg/mL	1.75 mL	3 µg/mL
0.25 mL of 10 µg/mL	2.25 mL	1 µg/mL
1.50 mL of 1 µg/mL	1.00 mL	0.6 µg/mL
0.75 mL of 1 µg/mL	1.75 mL	0.3 µg/mL
0.25 mL of 1 µg/mL	2.25 mL	0.1 µg/mL
1.50 mL of 0.1 µg/mL	1.00 mL	0.06 µg/mL
0.75 mL of 0.1 µg/mL	1.75 mL	0.03 µg/mL
0.25 mL of 0.1 µg/mL	2.25 mL	0.01 µg/mL

* The BSA solutions must be made up in 1X NanoOrange® working solution, as described in the text.

1 µg/mL BSA solution. Prepare the 1 µg/mL BSA solution by diluting 300 µL of 10 µg/mL BSA (made in step 2.2) into 2.70 mL of 1X NanoOrange® working solution.

2.4 If desired, prepare 0.01, 0.03, and 0.06 µg/mL standards, as described in Table 3, by diluting a 0.1 µg/mL BSA solution. Prepare the 0.1 µg/mL BSA solution by diluting 300 µL of 1 µg/mL BSA (made in step 2.3) into 2.70 mL of 1X NanoOrange® working solution.

2.5 Incubate samples at 90°C to 96°C for 10 minutes, **protected from light**.

2.6 Cool to room temperature for 20 minutes, **protected from light**.

2.7 **Measure the fluorescence:** Transfer 2.0 mL of the sample to a standard disposable fluorescence cuvette and measure the fluorescence using a fluorometer equipped with filters or settings capable of allowing excitation at about 485 nm and capturing the emission at about 590 nm. To ensure that the sample readings remain in the detection range of the fluorometer, set the instrument's gain so that the 10 µg/mL sample yields a fluorescence intensity near the maximum. To minimize photobleaching effects, keep the time for fluorescence measurement as short as possible and constant for all samples.

2.8 **Generate a standard curve:** Subtract the fluorescence value of the reagent blank (0 µg/mL) from that of each sample. Use these corrected values to generate a standard curve of fluorescence versus protein concentration (for example, see Figure 1).

Sample Analysis

3.1 Dilute the experimental protein solution in 1X NanoOrange® working solution (prepared in step 1.2) to achieve a final volume of 2.5 mL. It is best if the sample volume is no more than ~4% of the total volume. If higher volumes must be used, we recommend performing a standard curve using similar volumes. You may wish to use two or three different dilution factors for a given sample. Higher dilution factors may dilute contaminants to acceptable levels (see Table 4 for contaminant tolerance limits in the final assay solution); however, avoid extremely small sample volumes as they are difficult to pipet accurately.

3.2 Incubate samples at 90°C to 96°C for 10 minutes, **protected from light**.

3.3 Cool to room temperature for at least 20 minutes, **protected from light**.

3.4 **Measure the fluorescence:** Transfer 2.0 mL of the sample to a standard disposable fluorescence cuvette and measure the fluorescence using instrument parameters identical to those used in

Table 4. Tolerance levels for contaminants in the NanoOrange® protein quantitation assay.

Contaminating Compound	Maximum Tolerable Concentration*
DTT	100 mM
β-mercaptoethanol	100 mM
urea	1 M
sodium chloride	20 mM
potassium chloride	20 mM
magnesium chloride	1 mM
calcium chloride	1 mM
zinc chloride	0.5 mM
sodium acetate	20 mM
sodium phosphate	20 mM
ammonium sulfate	10 mM
HEPES	10 mM
sodium azide	10 mM
EDTA	5 mM
sodium hydroxide	10 mM
hydrochloric acid	10 mM
ascorbic acid	10 mM
sucrose	10 mM
glycerol	10%
PEG	1%
DNA	100 ng/mL
amino acids	10 µg/mL
Tween® 20	below 0.001%
SDS	0.01%
Triton® X-100	0.001%

* Compounds present in the final assay solution at or below the indicated concentration do not appreciably interfere with the NanoOrange® protein quantitation assay. Whenever feasible, the blank and protein standards should be prepared in a solution closely matching that of the experimental samples.

generating the standard curve (step 2.6). To minimize photobleaching effects, keep the time for fluorescence measurement as short as possible and the same as that used for the standard curve.

3.5 Determine the protein concentration: Subtract the fluorescence value of the reagent blank from that of the sample and use the standard curve generated in step 2.7 to determine the protein concentration of the sample.

References

1. Anal Biochem 150, 76 (1985); 2. Anal Biochem 72, 248 (1976); 3. J Biol Chem 193, 265 (1951); 4. Scopes, R.K., *Protein Purification, Principles and Practice*, 2nd Edition, Springer-Verlag (1987).

- **Substrate Working Solution (CHROM)**

The DAB-containing Substrate Working Solution (CHROM) is prepared by mixing thoroughly 20 µL Dako REAL™ DAB+ Chromogen (Bottle C) and 1 mL Dako REAL™ Substrate Buffer (Bottle B). Prepare only the volume required for the number of slides that shall be stained. Use CHROM within 5 days (store in darkness at 2–8 °C). For preparation of reagents not provided with the kit, please see the package insert included with the individual reagent.

Dako
Proteinase K

ENGLISH	**Code S3004**
Intended use	For In Vitro diagnostic use.
	Proteinase K is used for the proteolytic digestion of paraffin-embedded, formalin-fixed tissues prior to immunohistochemical (IHC) or *in situ* hybridization (ISH) procedures.
Summary and explanation	Proteolytic digestion of formalin-fixed tissues improves accessibility of antibodies and DNA probes to target sites within tissue. In the case of IHC, proteolytic digestion exposes certain epitopes which have been masked during fixation. In ISH procedures, accessibility of tissue DNA sequences is enhanced allowing better probe penetration and hybridization.
Reagent provided	**Code S3004**
	Each vial consists of 2 mL concentrated proteolytic enzyme solution, diluted in 0.01 mol/L Tris-HCl pH 8.0, sufficient for preparing 100 mL (for IHC), or 50 mL (for ISH) of enzyme solution. These volumes are sufficient for 1000 or 500 tests depending on the chosen method.
Materials required, but not supplied	0.05 mol/L Tris-HCl buffer pH 7.5 to 7.7.
Precautions	1. For professional users.
	2. As with any product derived from biological sources, proper handling procedures should be used.
	3. Wear appropriate Personal Protective Equipment to avoid contact with eyes and skin.
	4. Unused solution should be disposed of according to local, State and Federal regulations.
	5. Safety Data Sheet available for professional users on request.
Storage	Store vial at 2–8 °C. Store diluted enzyme solution at –20 °C. For convenience, aliquots may be frozen at –20 °C and thawed prior to use.
Staining preparation	1. IHC procedure:
	Mix one drop (40 µL) in 2 mL 0.05 mol/L Tris-HCl pH 7.5 to 7.7.
	2. General ISH procedure:
	Mix two drops (80 µL) in 2 mL 0.05 mol/L Tris-HCl pH 7.5 to 7.7.
	The resulting enzyme solutions should not be diluted further.
Staining procedure	The times required for optimal digestion of formalin-fixed tissues will vary with the extent of fixation. Generally, digestion of tissues for three to six minutes at room temperature is sufficient. Digestion time may be extended up to 15 minutes, if necessary.
Product specific limitations	Over-digestion of tissue sections may result in the loss of tissue morphology or cause sections to detach from the slides. The use of silanized slides is recommended for any *in situ* hybridization procedure requiring digestion. For IHC, either silanized slides or poly-L-lysine coated slides are recommended.

166

Anti-Osteocalcin antibody [OCG3] ab13420

abcam®
discover more

⭐⭐⭐⭐⭐ 2 Abreviews | 📖 14 References | 1 Image

Overview

Product name	Anti-Osteocalcin antibody [OCG3]
Description	Mouse monoclonal [OCG3] to Osteocalcin
Tested applications	WB, IHC-Fr, IHC-P, ICC/IF
Species reactivity	**Reacts with:** Rat, Sheep, Rabbit, Goat, Chicken, Cow, Dog, Human, Pig
	Does not react with
	Mouse
Immunogen	Full length protein (Cow).
Epitope	Residues 21-31
Positive control	Normal bovine bone tissue
General notes	Though we have tested ab13420 does not react with mouse sample in our lab, there is a report from a reviewer that it got positive result with mouse sample in IHC-Fr. This information need to be confirmed further.

Properties

Form	Liquid
Storage instructions	Store at +4°C short term (1-2 weeks). Aliquot and store at -20°C or -80°C. Avoid repeated freeze / thaw cycles.
Storage buffer	Preservative: 0.1% Sodium Azide
	Constituents: 1% BSA, 10mM PBS, pH 7.4
Purity	Protein A purified
Clonality	Monoclonal
Clone number	OCG3
Isotype	IgG3

Applications

Our Abpromise guarantee covers the use of ab13420 in the following tested applications.

The application notes include recommended starting dilutions; optimal dilutions/concentrations should be determined by the end user.

Application	Abreviews	Notes
WB		Use at an assay dependent dilution. Predicted molecular weight: 12 kDa. Use under reducing or non-reducing conditions.
IHC-Fr	⭐⭐⭐⭐	Use a concentration of 10 µg/ml.
IHC-P	⭐⭐⭐⭐	Use a concentration of 10 µg/ml. Enzymatic retrieval with Proteinase K is recommended.
ICC/IF		Use at an assay dependent concentration. PubMed: 21396708

Target

Function	Constitutes 1-2% of the total bone protein. It binds strongly to apatite and calcium.
Sequence similarities	Belongs to the osteocalcin/matrix Gla protein family.
	Contains 1 Gla (gamma-carboxy-glutamate) domain.
Post-translational modifications	Gamma-carboxyglutamate residues are formed by vitamin K dependent carboxylation. These residues are essential for the binding of calcium.
Cellular localization	Secreted.

Anti-Osteocalcin antibody [OCG3] images

NB110-89062
Osteopontin/OPN Antibody (1B20)

Product Information

Unit Size	0.1 ml
Concentration	1 mg/ml
Storage	Store at 4C short term. Aliquot and store at -20C long term. Avoid freeze-thaw cycles.
Clonality	Monoclonal
Clone	1B20
Preservative	0.05% Sodium Azide
Isotype	IgG1
Purity	Protein A purified
Buffer	Tris-glycine, 150 mM NaCl

Product Description

Host	Mouse
Gene ID	6696
Gene Symbol	SPP1
Species	Human, Rat, Rabbit
Species Reactivity	Human, Rat and Rabbit.
Immunogen	A synthetic peptide corresponding to the C-terminus of human Osteopontin [Swiss-Prot# P10451].

## Product Application Details

|	
Applications	Western Blot, Simple Western, Immunocytochemistry/Immunofluorescence, Immunohistochemistry, Immunohistochemistry-Frozen, Immunohistochemistry-Paraffin, Immunoprecipitation
Recommended Dilutions	Western Blot 1:1000, Simple Western 1:20, Immunohistochemistry 1:100, Immunocytochemistry/Immunofluorescence 1:50, Immunoprecipitation 1:10-1:500, Immunohistochemistry-Paraffin 1:100, Immunohistochemistry-Frozen
Application Notes	This Osteopontin (1B20) antibody is useful for Western blot, Immunohistochemistry on paraffin-embedded sections, Immunocytochemistry/Immunofluorescence and Immunoprecipitation. In Western blot multiple bands can be seen due to glycosylation and phosphorylation of the protein. Use in Immunohistochemistry-Frozen reported in scientific literature (PMID 24269728)In Simple Western only 10-15 uL of the recommended dilution is used per data point.

www.novusbio.com

support@novusbio.com

168

Cathepsin K Polyclonal Antibody

CATALOG #:	3588-100
AMOUNT:	100 µg
HOST:	Rabbit
IMMUNOGEN:	Synthetic peptide surrounding amino acid 321 of rat cathepsin K (ID# BV-88).
SPECIES REACTIVITY:	Human, Mouse, Rat, Chicken, Rabbit, Pig
FORMULATION:	100 µg (0.5 mg/ml) protein A purified rabbit anti-cathepsin K polyclonal antibody in phosphate buffered saline (PBS), pH 7.2, containing 30% glycerol, 0.5% BSA, 0.01% thimerosal.
BACKGROUND:	Cathepsin family of proteases contains several diverse classes of enzymes. The cysteine protease class comprises cathepsin B, H, K, L, O, and S. The aspartyl protease class contains cathepsin D and E. Cathepsin G belongs to the serine protease class. Cathepsins are involved in various cellular events such as peptide biosynthesis, protein degradation, and apoptosis. Cathepsin K expression is highest in bone, cartilage, and skeletal muscle.
SPECIFICITY:	The antibody detects proform (43 kDa) and the mature form (29 kDa) of cathepsin K.
APPLICATION AND USAGE:	The antibody can be used for Western blotting (0.5-4 µg/ml), and in Immunohistochemistry (2.5 µg/ml). From customer's feedback, the antibody can also be used in Immunoprecipitation. However, the optimal conditions should be determined individually. Blocking peptide is available separately (Cat. # 3588BP-50).
STORAGE CONDITIONS:	Store at -20°C. For long-term storage, aliquot and freeze at -70°C. Avoid repeated freeze/defrost cycles.
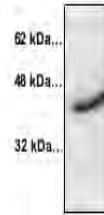
Western blot with Cathepsin K Polyclonal Antibody – Cat # 3588-100
Rat kidney tissue lysate (200 ng) loaded
Blocking/Dilution buffer: 5% NFDM (1 hr at RT) /TBST
Cathepsin K Polyclonal Antibody used at 1:1000 dilution - O/N at 4°C.
Goat Anti-Rabbit IgG peroxidase conjugated used at 1:10,000 dilution – 1 hr at RT

Predicted band size of proform : 43 kDa.
Observed band size: 43 kDa.
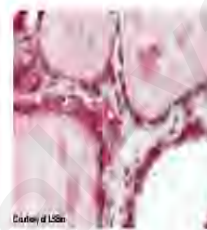
IHC staining of human thyroid tissue with Cathepsin K Polyclonal antibody: Immunohistochemistry of formalin fixed, paraffin-embedded tissue after heat-induced antigen retrieval. 2.5 µg/ml of antibody used for staining. After incubation with the primary antibody, slides were incubated with biotinylated secondary antibody, followed by alkaline phosphatase-streptavidin and chromogen.

RELATED PRODUCTS:

- Cathepsin B Antibody (Cat # 3190-100)
- Cathepsin B Blocking Peptide (Cat # 3190BP-50)
- Cathepsin D Antibody (Cat # 3191R-100)
- Cathepsin F Antibody (Cat # 3371-100)
- Cathepsin K Blocking Peptide (Cat # 3368BP-50)
- Cathepsin K Blocking Peptide (Cat # 3588BP-50)